**SOAH DOCKET NO. 582-22-0844**
**TCEQ DOCKET NO: 2021-1000-MSW**

| | | |
|---|---|---|
| **IN THE MATTER OF THE APPLICATION BY DIAMOND BACK RECYCLING AND SANITARY LANDFILL, LP FOR NEW MSW PERMIT NO. 2404** | **§** | **BEFORE THE STATE OFFICE OF ADMINISTRATIVE HEARINGS** |

# EXHIBIT KNOX-115

# PROJECT LOCATION

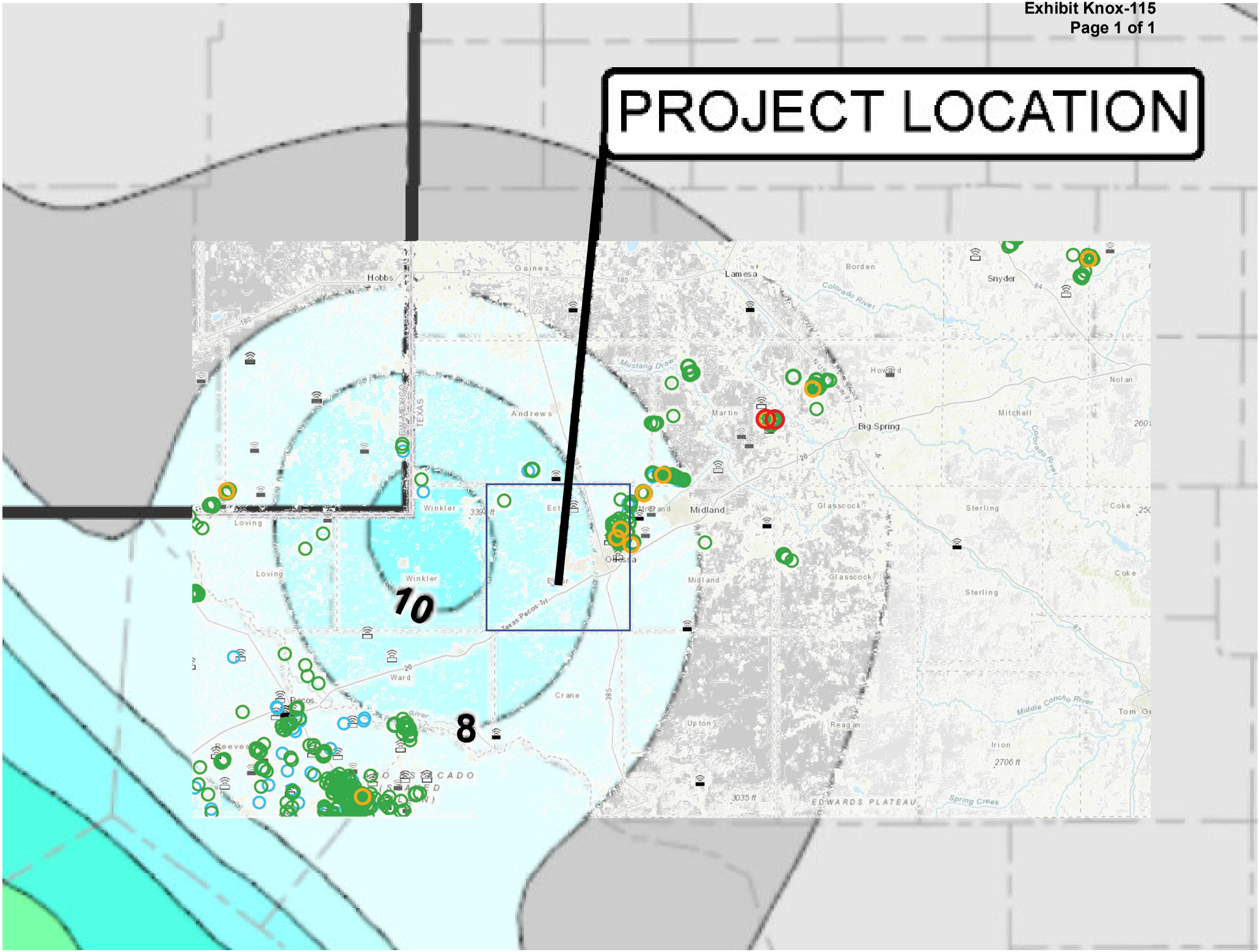

**SOAH DOCKET NO. 582-22-0844**
**TCEQ DOCKET NO: 2021-1000-MSW**

| | | |
|---|---|---|
| **IN THE MATTER OF THE** | **§** | **BEFORE THE STATE OFFICE** |
| **APPLICATION BY DIAMOND BACK** | **§** | |
| **RECYCLING AND SANITARY** | **§** | **OF** |
| **LANDFILL, LP FOR NEW MSW** | **§** | |
| **PERMIT NO. 2404** | **§** | **ADMINISTRATIVE HEARINGS** |

# EXHIBIT KNOX-116

# Analysis of a Large Database of GCL Internal Shear Strength Results

Jorge G. Zornberg, M.ASCE[1]; John S. McCartney, S.M.ASCE[2]; and Robert H. Swan Jr.[3]

**Abstract:** A database of 414 large-scale direct shear test results was assembled to evaluate variables governing geosynthetic clay liner (GCL) internal shear strength. The tests were conducted by a single independent laboratory over 12 years using procedures consistent with current testing standards. A wide range of GCL types, normal stresses, and shear displacement rates allowed investigation of the effect of reinforcement, pore water pressure generation, and sources of shear strength variability. Reinforced GCLs showed higher strength than unreinforced GCLs, with needle-punched GCLs performing better than stitch-bonded GCLs. Thermal locking of needle-punched GCLs was found to be effective at high normal stress, but hydration using low hydration normal stress was found to decrease the effectiveness of thermal locking. Shear-induced pore water pressures were indirectly evaluated using shear strength results from tests conducted using normal stresses above and below that corresponding to the GCL swell pressure. The peak shear strength was found to increase with decreasing shear displacement rates for high normal stresses, while the opposite trend was observed for low normal stresses. Shear strength envelopes showed a bilinear response, with a break at normal stresses consistent with the GCL swell pressure. Good repeatability of test results was obtained using the same-manufacturing-lot GCL specimens, while comparatively high variability was obtained using different-lot specimens. Peak shear strength variability was found to increase linearly with normal stress, but to be insensitive to specimen conditioning procedures. Evaluation of reinforced and unreinforced GCL test results indicates that, in addition to reinforcement variability, bentonite variability contributes to the shear strength variability of reinforced GCLs. Peel strength was found not to be a good indicator of the contribution of fibers to the GCL peak shear strength.

**DOI:** 10.1061/(ASCE)1090-0241(2005)131:3(367)

**CE Database subject headings:** Databases; Shear strength; Data analysis; Shear tests; Geosynthetic; Clay liners.

## Introduction

Geosynthetic clay liners (GCLs) are prefabricated geocomposite materials used in hydraulic barriers as an alternative to compacted clay liners. They consist of sodium bentonite clay bonded to one or two layers of geosynthetic backing materials (carrier geosynthetics). Advantages of GCLs include their limited thickness, good compliance with differential settlements of underlying soil or waste, easy installation, and low cost. Stability is a major concern for side slopes in bottom liner or cover systems that include GCLs because of the very low shear strength of hydrated sodium bentonite (Mesri and Olson 1970). Proper shear strength characterization is needed for the different materials and interfaces in hydraulic barriers. In particular, the failure surface of a liner system may develop internally (within the GCL), either through its bentonite core or along the bentonite/carrier geosynthetic interface. The internal shear strength of GCLs is the focus of the study presented in this paper.

Several investigators have evaluated the GCL internal shear strength using direct shear and ring shear tests (Gilbert et al. 1996, 1997; Stark et al. 1996; Eid and Stark 1997; Fox et al. 1998; Eid et al. 1999). These experimental studies have provided invaluable insight into the significance of parameters that govern the shear behavior of GCLs. However, available information on GCL internal shear strength is still limited to specific ranges of normal stresses, GCL types, and test conditions. There are three primary reasons why a comprehensive evaluation of GCL internal shear strength is still needed. First, the use of tests from different laboratories may have masked sources of variability, as was the case in a shear strength database assembled by Stoewahse et al. (2002) using results from European laboratories. Second, the current standard for internal and interface GCL shear strength testing (ASTM D6243) has only been available since 1998 (ASTM 1998), so tests conducted before the approval of this standard may have not been consistent with current procedures. Third, significant costs (large-scale direct shear devices, long time for conditioning and testing) have limited the number of available test results and precluded evaluations of variability.

A database of 414 large-scale direct shear tests conducted by a single laboratory was assembled and evaluated in this study to identify and quantify the variables governing the internal shear strength of GCLs. This database, referred to as the GCL shear strength (GCLSS) database, is used to define upper and lower bounds on peak and large-displacement GCL internal shear strength. In addition, an analysis of the results in the GCLSS database allows evaluation of: (1) The performance of GCLs

[1]Clyde E. Lee Assistant Professor, Dept. of Civil Engineering, Univ. of Texas at Austin, 1 University Stn., C1792, Austin TX 98712-0280.

[2]Graduate Student, Dept. of Civil Engineering, Univ. of Texas at Austin, 1 University Stn., C1792, Austin TX 98712-0280.

[3]President and CEO, SGI Testing Services, Atlanta, GA.

Note. Discussion open until August 1, 2005. Separate discussions must be submitted for individual papers. To extend the closing date by one month, a written request must be filed with the ASCE Managing Editor. The manuscript for this paper was submitted for review and possible publication on October 31, 2002; approved on April 23, 2004. This paper is part of the ***Journal of Geotechnical and Geoenvironmental Engineering***, Vol. 131, No. 3, March 1, 2005. ©ASCE, ISSN 1090-0241/2005/3-367–380/$25.00.

**Table 1.** Summary of GCLs in the GCLSS Database

| GCL label | GCL product | Description[a] | No. of tests reaching $\tau_p$ | No. of tests reaching $\tau_{ld}$ |
|---|---|---|---|---|
| A | Bentomat ST | Needle-punched W-NW | 270 | 203 |
| B | Claymax 500SP | Stitch-bonded W-W | 48 | 5 |
| C | Bentofix NS | Thermal-locked, needle-punched W-NW | 26 | 26 |
| D | Bentofix NW | Thermal-locked, needle-punched NW-NW | 16 | 13 |
| E | Bentofix NWL | GCL *D* with lower mass of sodium bentonite per unit area | 8 | 8 |
| F | Claymax 200R | Unreinforced W-W | 13 | 13 |
| G | Not Marketed | GCL *A* with additives to the sodium bentonite | 3 | 0 |
| H | Bentomat DN | Needle-punched NW-NW | 18 | 6 |
| I | Not Marketed | GCL *A* with adhesive strengthened reinforcements | 8 | 0 |
| J | Geobent | Needle-punched W-NW | 4 | 4 |

[a]W=Woven carrier geotextile, NW=Nonwoven carrier geotexile.

manufactured using different types of reinforcement, (2) pore water pressures during shearing (indirect evaluation), and (3) the GCL internal shear strength variability.

## Database

### Data Source

The large-scale direct shear tests in the GCLSS database were performed between 1992 and 2003 by the Soil-Geosynthetic Interaction laboratory of GeoSyntec Consultants, currently operated by SGI Testing Services (SGI). SGI is an accredited testing facility with significant consistency in its testing procedures. It should be noted that procedures used for GCL direct shear tests conducted by SGI over the period 1992 to 2003 are consistent with ASTM D6243 (ASTM 1998), even though this standard was only approved in 1998. Most tests in the GCLSS database were conducted for commercial purposes and, consequently, the testing characteristics and scope was defined by project-specific requirements. A few additional tests were conducted specifically for this investigation in order to complement tests conducted using different shear displacement rates and to incorporate peel strength results in variability analyses. Test conditions reported for each series in the GCLSS database include specimen preparation and conditioning procedures, hydration time ($t_h$), consolidation time ($t_c$), normal stress during hydration ($\sigma_h$), normal stress during shearing ($\sigma_n$), and shear displacement rate (SDR).

### Materials

Direct shear tests in the GCLSS database were conducted using ten commercial GCL products (nine reinforced, one unreinforced). Table 1 provides the designation of the GCLs used in this study (GCL *A* to *J*), the product name, and a short description of the reinforcement characteristics and carrier geotextiles. An important objective of this study is the comparison of shear strength results among different types of GCLs. Unreinforced GCLs are used in applications where high shear strength is not required, while reinforced GCLs (e.g., stitch-bonded needle-punched GCLs) are used otherwise. The unreinforced GCL investigated in this study (GCL *F*) consists of an adhesive-bonded bentonite layer held between two woven polypropylene geotextiles. The stitch-bonded GCL investigated in this study (GCL *B*) consists of a bentonite layer stitched using synthetic yarns between two woven polypropylene carrier geotextiles. The needle-punched GCLs investigated in this study (GCLs *A*, *C*, *D*, *E*, *G*, *H*, *I*, and *J*) consist of a bentonite layer between two (woven or nonwoven) carrier geotextiles that is reinforced by pulling fibers through using a needling board. The fiber reinforcements are typically left entangled on the surface of the top carrier geotextile. Since pullout of the needle-punched fibers from the top carrier geotextile may occur during shearing (Gilbert et al. 1996), some needle-punched GCL products (GCLs *C*, *D*, and *E*) were thermal locked to minimize fiber pullout. Thermal locking involves heating the GCL surface to induce bonding between individual reinforcing fibers as well as between the fibers and the carrier geotextiles (Lake and Rowe 2000). For simplicity, thermal-locked needle-punched GCLs will be referred to simply as thermal-locked GCLs in this paper.

### Testing Equipment and Procedures

The large-scale direct shear tests conducted in this study used large direct shear devices each containing a top and bottom shear box. Typically, the top shear box measured 305 mm by 305 mm in plan and 75 mm in depth. The bottom shear box measured 305 mm by 355 mm in plan and 75 mm in depth. For the GCL internal direct shear tests, the bottom shear box was sectioned down to plan dimensions of 305 mm by 305 mm. A constant SDR was applied to the bottom shear box using a mechanical screw drive system and the resultant shear load was measured on the top shear box using a load cell. The direct shear devices used in this study were capable of applying normal stresses from 2.4 to 3,000 kPa during shearing. Dead weights were placed above the GCL in tests conducted under low normal stresses, while an air bladder or a hydraulic cylinder were used to exert a normal force between the GCL and a reaction frame in tests conducted under relatively high normal stress. A load cell was used to measure the normal load. The accuracy of the normal stress application device and calibration of the load cells were verified at least every year as a part of a laboratory accreditation program.

A detail of the specimen configuration for GCL internal shear strength testing is shown in Fig. 1(a). A water bath may be used for testing GCLs under submerged conditions, although most tests in the GCLSS database were conducted without a water bath. For each test, a fresh GCL specimen was trimmed from the bulk GCL sample. The internal strength testing of the GCL specimen involved constraining the GCL specimen so that shearing could only occur within the bentonite component of the GCL. The specimen was constrained by bonding the two carrier geotextiles to porous rigid substrates using textured steel gripping surfaces. Extensions of each carrier geotextile were secured using a second

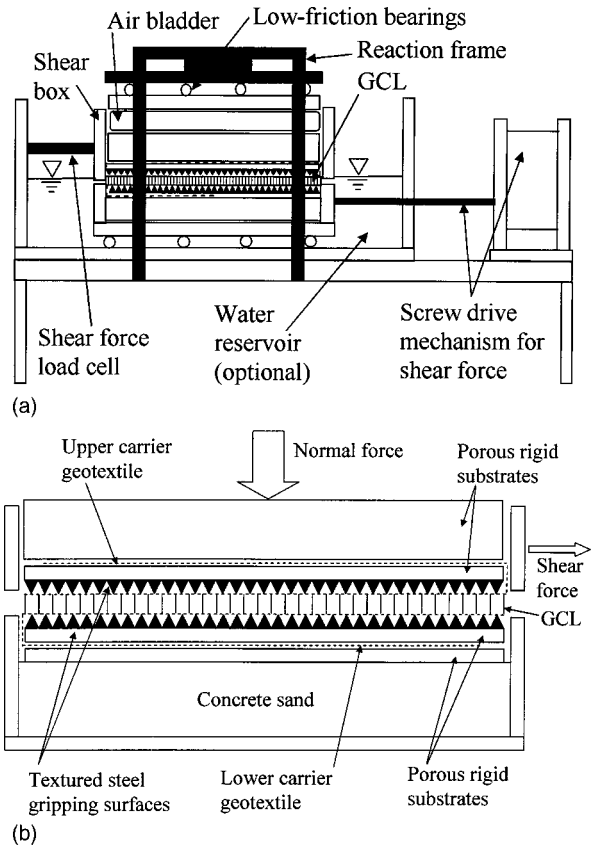


**Fig. 1.** Direct shear device: (a) Load application configuration; and (b) specimen detail

porous rigid substrate as shown in Fig. 1(b). The textured steel gripping surfaces were employed to minimize slippage between each carrier geotextile and the porous rigid substrate. Post-test examination of the sheared GCLs indicated that slippage did not occur between the GCL and the grips, suggesting a uniform shear stress transfer onto the GCL specimens.

Conditioning of specimens plays an important role in GCL internal shear strength testing as moisture interactions should simulate correctly those anticipated in the field. GCL conditioning involves hydration and (in some cases) subsequent consolidation of the sodium bentonite. Pore water pressures in the sodium bentonite of the GCLs tested in this study are negative for typical initial (as received) moisture conditions. Hydration of the sodium bentonite leads to reduction of the negative pore water pressures and vertical swelling. Changes in pore pressures and vertical deformations were not measured during GCL conditioning or shearing. Although this is consistent with the current state of the practice and ASTM (1998), measurements of vertical deformation during specimen conditioning and shearing would have allowed assessment of bentonite hydration by using conventional methods to estimate the degree of consolidation (Gilbert et al. 1997). Consequently, hydration of the bentonite was only assessed in this study by the reported hydration time. Although hydration times as high as 250 hs may be required to reach full hydration, hydration times beyond 72 hs have been reported not to significantly increase the GCL water content, especially under high $\sigma_n$ (Stark and Eid 1996). The hydration process used in this study involved typically a two-stage procedure similar to that reported by Fox et al. (1998). The specimen and rigid substrates were placed under a specified $\sigma_h$ outside the direct shear device and soaked in tap water during the specified $t_h$. This assembly was then transferred to the direct shear device. $\sigma_h$ was often specified to equal the shearing normal stress ($\sigma_n$). However, if $\sigma_h$ was less than $\sigma_n$ (e.g., to simulate field conditions representative of bottom liners), the normal stress was slowly ramped up to $\sigma_n$, and pore pressures were allowed to dissipate during a consolidation period ($t_c$).

Shearing was conducted after GCL conditioning by applying the shear load under a constant SDR. The shear force was recorded for increasing shear displacement. The maximum shear stress was identified as the peak shear strength ($\tau_p$), and the shear stress at the end of testing was identified as the large-displacement shear strength ($\tau_{ld}$). Table 1 shows the number of tests used to define $\tau_p$ and $\tau_{ld}$ of each GCL. $\tau_{ld}$ was reported only when the post-peak shear stress reached an approximately constant value within the maximum displacement of the test device (75 mm). In some cases, shearing was discontinued after reaching the peak value because the test, conducted for commercial purposes, did not require post-peak assessment. In other cases, a peak shear strength value was reached, but partial separation of the reinforcements from the carrier geotextiles after reaching the peak led to an unrealistically high $\tau_{ld}$, especially at low normal stress. As will be discussed below, the particular mode of shear failure of stitch-bonded GCL *B* generally did not allow shearing beyond the peak value.

SDR in the field is anticipated to occur slowly, which is consistent with drained conditions (Gilbert et al. 1997). The SDR used for most tests in the GCLSS database is 1.0 mm/min. While relatively fast for guaranteeing drained conditions, a SDR of 1.0 mm/min is typically used in engineering practice because of time and cost considerations. Additional tests were sheared using slower rates (as low as 0.0015 mm/min). Shearing was typically terminated when a displacement of 75 mm, or an approximately constant $\tau_{ld}$ value, was reached. Consistent with observations reported by Gilbert et al. (1996) and Fox et al. (1998), dismantling of the needle-punched thermal-bonded and unreinforced GCL specimens indicated that failure occurred typically through the interface between the bentonite and the carrier geotextile. The carrier geotextiles were always found to contain extruded bentonite. In the stitch-bonded GCL *B* specimens, the continuous fibers stretched during initial shearing. However, once the continuous fibers became fully stretched, continued shear displacement often led to rupture of the fibers or tearing of the carrier geotextiles at the threaded connections. Despite the particular arrangement of fiber reinforcements in stitch-bonded GCLs, observation of the specimens after testing did not show slippage of the woven geotextiles at the interface with the gripping system.

## Analysis of Results from Different GCL Materials

A total of 32 failure envelopes (FEs) were defined considering the different GCL types and test conditions used in this investigation. A total of 385 of the 414 test results were used, while 29 test results did not have similar conditioning procedures to any of the 32 defined failure envelopes. Table 2 summarizes the test conditions, the approximate range of $\sigma_n$, and the friction angle and cohesion intercept defining the $\tau_p$ and $\tau_{ld}$ envelopes. In some cases, the internal shear strength was also characterized using a bilinear FE. The square root of the mean-squared error of the linear regression, which is considered the standard deviation of the linear regression (Helsel and Hirsh 1991), was calculated as a measure of the spread of data around the best-fit lines:

**Table 2.** Summary of Failure Envelopes in the Geosynthetic Clay Liner Shear Strength (GCLSS) Database

| | | | Test conditions | | | | | Peak | | | | Large-displacement[b] | | | |
|---|---|---|---|---|---|---|---|---|---|---|---|---|---|---|---|
| Failure envelope[a] | GCL label | Number of tests | SDR (mm/min) | $\sigma_h$ (kPa)[c] | $t_h$ (hs) | $t_c$ (hs) | $\sigma_n$ range (kPa) | $c_p$ (kPa) | $\phi_p$ (Degrees) | $R^2$ | $s$ (kPa) | $c_{ld}$ (kPa) | $\phi_{ld}$ (Degrees) | $R^2$ | $s$ (kPa) |
| **FE 1** | *A* | 27 | 1.0 | $\sigma_n$ | 24 | 0 | 3.4–72 | 13.5 | 46.6 | 0.987 | 3.11 | 2.1 | 8.6 | 0.842 | 1.25 |
| **FE 2** | *A* | 2 | 1.0 | 4.8 | 24 | 0 | 14–24 | 10.7 | 37.1 | 1.000 | N/A | 3.3 | 4.0 | 1.000 | N/A |
| **FE 3** | *A* | 12 | 0.5 | $\sigma_n$ | 24 | 0 | 48–386 | 42.8 | 24.6 | 0.975 | 11.00 | 9.4 | 9.8 | 0.968 | 4.78 |
| **FE 4** | *A* | 40 | 1.0 | $\sigma_n$ | 48 | 0 | 2.4–2759 | 42.4 | 14.0 | 0.966 | 25.36 | 16.2 | 6.3 | 0.983 | 12.49 |
| **FE 4 (Low $\sigma_n$)** | *A* | 31 | 1.0 | $\sigma_n$ | 48 | 0 | 2.4–97 | 14.4 | 35.4 | 0.948 | 13.04 | N/A | N/A | N/A | N/A |
| **FE 4 (High $\sigma_n$)** | *A* | 9 | 1.0 | $\sigma_n$ | 48 | 0 | 97–2759 | 102.4 | 11.9 | 0.987 | 52.78 | N/A | N/A | N/A | N/A |
| **FE 5** | *A* | 5 | 1.0 | 4.8 | 48 | 0 | 14–276 | 35.9 | 29.9 | 0.991 | 6.79 | 2.0 | 4.4 | 0.996 | N/A |
| **FE 6** | *A* | 8 | 1.0 | $\sigma_n$ | 72 | 0 | 2.4–103 | 17.4 | 34.7 | 0.840 | 10.80 | 2.8 | 8.5 | 0.943 | 1.93 |
| **FE 7** | *A* | 141 | 0.1 | 20.7 | 168 | 48 | 35–310 | 20.6 | 25.2 | 0.999 | 23.88 | 15.5 | 9.4 | 0.999 | 10.65 |
| **FE 8a** | *A* | 1 | 0.0015 | 8.0 | 144 | 1,476 | 248 | | | | | | | | |
| **FE 8b** | *A* | 1 | 0.0015 | 63.0 | 48 | 540 | 520 | 74.3 | 21.9 | 0.988 | 23.38 | 35.0 | 5.8 | 0.991 | 5.22 |
| **FE 8c** | *A* | 1 | 0.0015 | 8.0 | 144 | 2,328 | 993 | | | | | | | | |
| **FE 9** | *A* | 3 | 1.0 | 68.9 | 24 | 12 | 138–552 | 37.9 | 22.7 | 0.998 | 5.53 | 2.8 | 11.2 | 0.918 | 17.69 |
| **FE 10** | *A* | 3 | 1.0 | 6.9 | 60 | 24 | 4.8–29 | 12.4 | 50.1 | 0.991 | 1.98 | N/A | N/A | N/A | N/A |
| **FE 11** | *A* | 7 | 1.0 | 0.0 | 0 | 0 | 2.4–35 | 12.9 | 60.1 | 0.921 | 4.64 | N/A | N/A | N/A | N/A |
| **FE 12** | *B* | 7 | 1.0 | $\sigma_n$ | 24 | 0 | 24–690 | 53.4 | 7.3 | 0.818 | 16.93 | N/A | N/A | N/A | N/A |
| **FE 13** | *B* | 25 | 1.0 | 4.8 | 48 | 0 | 2.4–982 | 24.3 | 4.4 | 0.949 | 3.87 | N/A | N/A | N/A | N/A |
| **FE 14** | *B* | 10 | 1.0 | 7.2 | 96 | 0 | 10–1000 | 24.1 | 4.6 | 0.976 | 5.21 | N/A | N/A | N/A | N/A |
| **FE 15** | *B* | 3 | 0.1 | 20.7 | 168 | 48 | 35–310 | 32.4 | 7.3 | 0.994 | 1.95 | N/A | N/A | N/A | N/A |
| **FE 16** | *C* | 13 | 0.5 | $\sigma_n$ | 24 | 0 | 7.2–575 | 23.3 | 23.8 | 0.959 | 13.08 | 12.3 | 9.8 | 0.951 | 11.12 |
| **FE 16 (Low $\sigma_n$)** | *C* | 6 | 0.5 | $\sigma_n$ | 24 | 0 | 7.2–103 | 17.2 | 28.3 | 0.999 | 12.07 | N/A | N/A | N/A | N/A |
| **FE 16 (High $\sigma_n$)** | *C* | 7 | 0.5 | $\sigma_n$ | 24 | 0 | 103–575 | 9.7 | 14.9 | 0.950 | 14.41 | N/A | N/A | N/A | N/A |
| **FE 17** | *C* | 10 | 0.2 | 55.2 | 24 | 0 | 10–290 | 22.0 | 29.3 | 0.993 | 5.17 | 8.0 | 12.0 | 0.975 | 3.86 |
| **FE 18** | *C* | 3 | 0.1 | 20.7 | 168 | 48 | 35–310 | 22.3 | 16.6 | 1.000 | 0.21 | 0.9 | 8.3 | 0.974 | 4.67 |
| **FE 19** | *D* | 6 | 1.0 | $\sigma_n$ | 72 | 0 | 6.9–552 | 5.7 | 18.6 | 1.000 | 5.28 | 0.1 | 8.4 | 0.985 | 5.21 |
| **FE 20** | *D* | 3 | 0.5 | $\sigma_n$ | 24 | 0 | 98–380 | 75.3 | 25.1 | 0.997 | 0.20 | 21.3 | 9.6 | 0.982 | 5.43 |
| **FE 21** | *D* | 6 | 0.1 | 3.4 | 24 | 24 | 6.9–690 | 40.9 | 27.1 | 0.972 | 27.40 | 15.5 | 8.0 | 1.000 | 0.18 |
| **FE 21 (Low $\sigma_n$)** | *D* | 3 | 0.1 | 3.4 | 24 | 24 | 6.9–28 | 22.4 | 38.9 | 0.972 | 2.03 | N/A | N/A | N/A | N/A |
| **FE 21 (High $\sigma_n$)** | *D* | 3 | 0.1 | 3.4 | 24 | 24 | 172–690 | 101.0 | 21.6 | 1.000 | 2.03 | N/A | N/A | N/A | N/A |
| **FE 22** | *E* | 4 | 1.0 | $\sigma_n$ | 336 | 0 | 14–58 | 32.7 | 31.8 | 0.993 | 1.20 | 7.3 | 11.3 | 0.994 | 0.37 |
| **FE 23** | *E* | 4 | 1.0 | $\sigma_n$ | 48 | 0 | 14–58 | 30.6 | 38.9 | 0.993 | 1.57 | 6.8 | 13.7 | 0.993 | 0.46 |
| **FE 24** | *F* | 3 | 1.0 | $\sigma_n$ | 168 | 0 | 14–55 | 1.7 | 12.3 | 0.999 | 0.18 | 2.1 | 8.5 | 1.000 | 0.00 |
| **FE 25** | *F* | 3 | 1.0 | 0.0 | 0 | 0 | 69–483 | 16.1 | 3.7 | 1.000 | 0.28 | 10.1 | 4.0 | 1.000 | 1.13 |
| **FE 26** | *G* | 4 | 1.0 | $\sigma_n$ | 24 | 0 | 2.4–19 | 4.8 | 30.4 | 1.000 | 0.11 | N/A | N/A | N/A | N/A |
| **FE 27** | *H* | 6 | 1.0 | $\sigma_n$ | 24 | 0 | 4.8–483 | 19.7 | 33.8 | 0.997 | 8.29 | 23.8 | 5.3 | 0.997 | 1.56 |
| **FE 27 (Low $\sigma_n$)** | *H* | 4 | 1.0 | $\sigma_n$ | 24 | 0 | 4.8–48 | 5.3 | 47.0 | 0.998 | 1.60 | N/A | N/A | N/A | N/A |
| **FE 27 (High $\sigma_n$)** | *H* | 2 | 1.0 | $\sigma_n$ | 24 | 0 | 241–483 | 8.5 | 31.7 | 1.000 | N/A | N/A | N/A | N/A | N/A |
| **FE 28** | *H* | 6 | 1.0 | 3.4 | 24 | 24 | 6.9–690 | 33.0 | 32.1 | 0.988 | 21.12 | 29.9 | 8.5 | 0.996 | 3.46 |
| **FE 28 (Low $\sigma_n$)** | *H* | 3 | 1.0 | 3.4 | 24 | 24 | 6.9–28 | 16.5 | 45.0 | 0.971 | 2.58 | N/A | N/A | N/A | N/A |
| **FE 28 (High $\sigma_n$)** | *H* | 3 | 1.0 | 3.4 | 24 | 24 | 172–690 | 78.9 | 28.4 | 1.000 | 3.13 | N/A | N/A | N/A | N/A |
| **FE 29** | *H* | 6 | 0.25 | 0.0 | 96 | 24 | 4.8–10 | 12.1 | 46.3 | 1.000 | 1.63 | N/A | N/A | N/A | N/A |
| **FE 30** | *I* | 4 | 1.0 | 0.0 | 0 | 0 | 2.4–24 | 19.3 | 58.2 | 0.988 | 5.01 | N/A | N/A | N/A | N/A |
| **FE 31** | *I* | 4 | 1.0 | 2.4 | 72 | 0 | 2.4–24 | 21.9 | 51.1 | 0.932 | 1.56 | N/A | N/A | N/A | N/A |
| **FE 32** | *J* | 4 | 1.0 | $\sigma_n$ | 24 | 0 | 24–193 | 5.5 | 9.1 | 1.000 | 0.31 | 0.4 | 6.9 | 0.982 | 1.51 |

[a]FE 4, 16, 21, 27, and 28 represented using both linear and bilinear envelopes.

[b]N/A=Not applicable.

[c]$\sigma_h=\sigma_n$ means that the normal stress used during hydration is the same as the normal stress used during shearing.

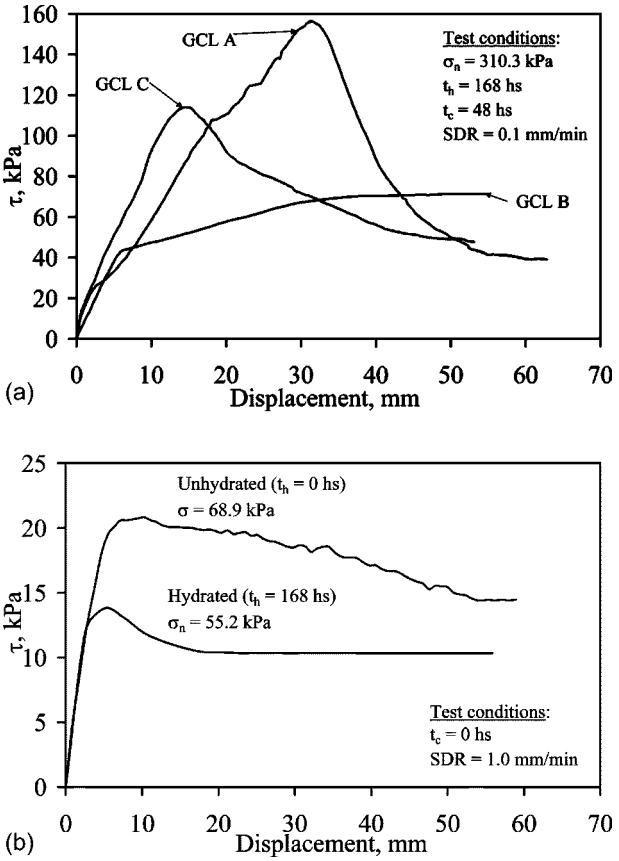


**Fig. 2.** Shear stress-displacement curves for different GCLs: (a) GCLs *A* (needle punched), *B* (stitch bonded), and *C* (thermally locked); and (b) GCL *F* (unreinforced)

$$s = \sqrt{\frac{\sum_{i=1}^{n} e_i^2}{n-2}} \tag{1}$$

where $s$=standard deviation of the linear regression; $e_i$=difference between the shear strength value and the value on the best-fit line at the same normal stress; and $n$=number of data points in the regression. Since the data summarized in Table 2 follow approximately a normal distribution around the FEs, a bound of one standard deviation contains 84% of the likely shear strength values (Helsel and Hirsh 1991).

The effect on the GCL internal shear strength of the type of internal reinforcements is investigated in this section in order to provide: (1) An evaluation of the shear stress-displacement behavior of the different GCL types, (2) a preliminary overview of GCL internal shear strength, and (3) a comparison of GCLs tested under similar conditioning procedures.

### *Shear Stress-Displacement Behavior*

Fig. 2(a) shows shear stress-displacement curves for GCLs *A* (needle punched), *B* (stitch bonded), and *C* (thermal locked). The three GCL types were tested using the same $\sigma_n$ (310.3 kPa), same $t_h$ (168 h), same $t_c$ (48 h), and same SDR (0.1 mm/min.). GCL *A* shows a well-defined $\tau_p$ and a marked post-peak shear strength loss. Unlike GCL *A*, GCL *B* shows a rapid initial mobilization of shear strength until reaching a "yield" stress level, beyond which a less pronounced hardening takes place until reaching $\tau_p$. The

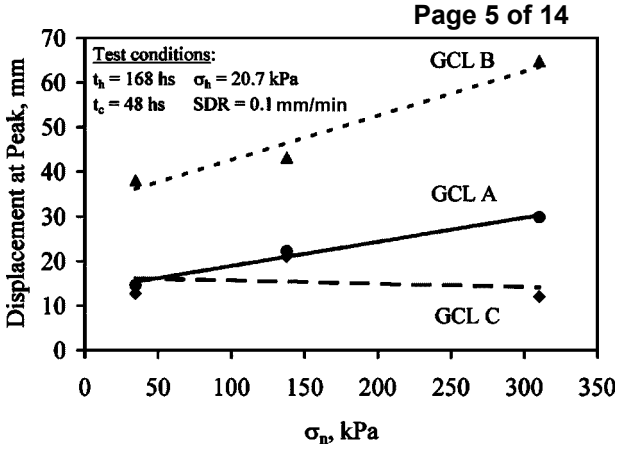


**Fig. 3.** Displacement at peak shear strength as a function of $\sigma_n$ for GCLs *A*, *B*, and *C*

displacement at peak for GCL *B* is significantly larger than that observed for GCL *A*. The post-peak behavior of GCL *B* could not be evaluated since this GCL did not reach a steady large-displacement strength value at the maximum displacement of the device. Thermal-locked GCL *C* shows a behavior similar to that of needle-punched GCL *A*, although the $\tau_p$ value is below that obtained for GCL *A*. GCLs *A* and *C* were reinforced using similar needle-punching techniques and have the same specified peel strength (6.5 N/m). Consequently, differences in their behavior are attributed to the effect of thermal locking. Comparison of the response of the two GCLs, tested under identical conditions, suggests that thermal locking did not lead to the expected increase in shear strength.

Fig. 2(b) shows shear stress-displacement curves for GCL *F* (unreinforced) tested under hydrated and unhydrated conditions. Although a direct comparison of $\tau_p$ is not possible as the specimens were tested using different $\sigma_n$, the results indicate that the hydrated GCL has lower $\tau_p$ and $\tau_{ld}$ than the unhydrated GCL. Both specimens, however, show a significantly lower $\tau_p$ than that obtained for reinforced GCLs. The displacement at peak of unreinforced GCLs is consistent with displacement at the yield stress observed for GCL *B*. However, the displacement at peak of unreinforced GCLs is significantly lower than the one obtained for the reinforced GCLs. While both hydrated and unhydrated unreinforced GCLs show post-peak shear strength loss, the hydrated GCL appears to reach residual conditions at lower shear displacement than the unhydrated GCL.

Fig. 3 summarizes the displacement at peak for the three tests shown in Fig. 2(a) along with results from additional tests conducted under two additional $\sigma_n$ values (34.5 and 137.9 kPa). GCLs *A* and *B* show increasing displacement at peak with increasing $\sigma_n$, while the displacement at peak for GCL *C* is apparently insensitive to $\sigma_n$. GCL *B* shows significantly larger displacement at peak than the other GCL types, which may be particularly relevant for displacement-based stability analyses (e.g., for seismic design). For example, if the design criterion requires a maximum shear displacement of 50 mm for a $\sigma_n$=310.3 kPa, the results in Fig. 2(a) indicate that $\tau_p$ would govern the design if GCL *B* is selected, but $\tau_{ld}$ would need to be considered if GCLs *A* or *C* are used.

### *Overall Internal Strength Assessment*

Fig. 4(a) shows the $\tau_p$ data for all GCLs in the GCLSS database, illustrating the wide range of normal stresses at which the GCLs

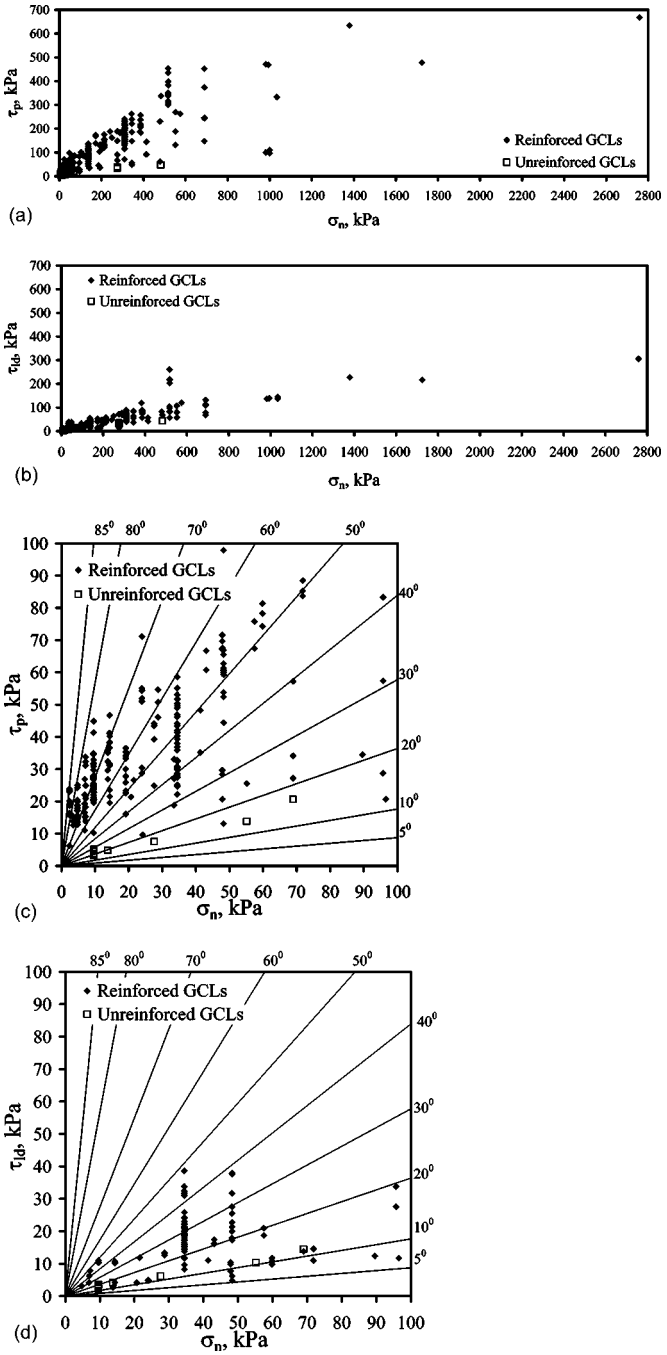


**Fig. 4.** Shear strength results for all geosynthetic clay liners: (a) peak shear strength values; (b) large-displacement shear strength values; (c) peak shear strength (scaled); and (d) large-displacement shear strength (scaled)

were tested and the significant scatter in the data. Similarly, Fig. 4(b) shows the $\tau_{ld}$ data for all GCLs in the GCLSS database, illustrating that the range of $\tau_{ld}$ values is significantly narrower than the range of $\tau_p$ values. As most data points shown in Figs. 4(a and b) correspond to comparatively low $\sigma_n$, Figs. 4(c and d) show a detail for $\sigma_n$ values below 100 kPa. The results shown in Fig. 4(c) reflect the relevance of using a cohesion intercept to characterize $\tau_p$ at low $\sigma_n$. Inspection of the standard deviation $s$ values in Table 2 indicates that the $s(\tau_p)$ for unreinforced GCLs (FE 24 and 25) is less than that for reinforced GCLs. Fig. 4(d) shows that the trend in $\tau_{ld}$ for low $\sigma_n$ is consistent with the trend observed for higher $\sigma_n$. Inspection of the results in Figs. 4(b and d), as well as the information presented in Table 2 indicates that large-displacement shear strength is approximately independent of the GCL type. Reinforced GCLs tend to show a higher large-displacement shear strength value than the unreinforced GCLs, with stitch-bonded GCLs having the lowest large-displacement shear strength among all reinforced GCLs.

The test results for all GCLs were grouped into ten data sets based on reinforcement type. Table 3 summarizes the information for each data set, and provides the parameters for the shear strength envelopes $(c,\phi)$ of each data set. The GCL data sets are used only for preliminary database analysis, as they do not account for the effect of specimen conditioning on shear strength. Comparisons of $\tau_p$ values among the ten GCL data sets is aided by defining the shear strength values calculated using the GCL data set envelopes at given reference normal stresses. Table 3 includes the values of $\tau_{50}$ and $\tau_{300}$ for each data set, which are the average shear strength values at $\sigma_n=50$ and 300 kPa, respectively. These reference normal stresses are representative of normal stress values for landfill cover and liner systems, respectively. In order to quantify the variability of the shear strength for each GCL data set, the range of shear strength values was defined for each reference normal stress. Specifically, the lowest and highest shear strength values were defined using the individual failure envelopes (FE in Table 2) of each data set. Additional information is provided by McCartney et al. (2002). Inspection of the $\tau_{50}$ and $\tau_{300}$ values shown in Table 3, leads to the following observations regarding the internal peak shear strength of GCLs under low and high normal stresses:

- The peak internal shear strength of all GCLs in the database (Set SS1) can be characterized by a cohesion intercept of 38.9 kPa and a friction angle of 18.0°. However, there is a significant scatter in the results both under comparatively low normal stresses ($\tau_{50}$ ranges from 13 to 71 kPa) and comparatively high normal stresses ($\tau_{300}$ ranges from 36 to 241 kPa). The most frequently tested GCL in the GCLSS database is GCL *A* (Set SS2, 270 tests), which has peak internal shear strength that can be characterized by a cohesion intercept of 46.6 kPa and a friction angle of 18.7°. Less scatter is observed in the shear strength of GCL *A* than that observed for all GCLs both under comparatively low normal stresses ($\tau_{50}$ ranges from 48 to 66 kPa) and high normal stresses ($\tau_{300}$ ranges from 117 to 195 kPa).
- As expected, the peak internal shear strength of reinforced GCLs (Set SS3) in consistently higher than that of unreinforced GCLs (Set SS4) both under low normal stresses [$\tau_{50}$(Set SS3)=57 kPa and $\tau_{50}$(Set SS4)=10 kPa] and high normal stresses [$\tau_{300}$(Set SS3)=139 kPa and $\tau_{300}$(Set SS4)=35 kPa].
- The peak internal shear strength of needle-punched GCLs (Set SS5) is consistently higher than that of stitch-bonded GCLs (Set SS6) both under low normal stresses [$\tau_{50}$(Set SS5)=58 kPa and $\tau_{50}$(Set SS6)=33 kPa] and high normal stresses [$\tau_{300}$(Set SS5)=149 kPa and $\tau_{300}$(Set SS6)=58 kPa]. The difference is less significant under low normal stresses because stitch-bonded GCLs show some cohesion ($c_p$=28.5 kPa), but is more significant under high normal stresses due to the low friction angle ($\phi_p$=5.6°).
- The peak internal shear strength of needle-punched GCLs with woven-nonwoven (W-NW) carrier geotextile configurations (Set SS7) is similar to that of needle-punched GCLs with NW-NW carrier geotextiles (Set SS8) under low normal stresses [$\tau_{50}$(Set SS7)=58 kPa and $\tau_{50}$(Set SS8)=58 kPa].

**Table 3.** Geosynthetic Clay Liner (GCL) Data Sets for Overall Shear Strength Assessment

| GCL data set | GCL set description[a] | GCL label | Peak envelope | | Peak strength at $\sigma_n = 50$ kPa | Peak strength at $\sigma_n = 300$ kPa | Large-displacement envelope | |
|---|---|---|---|---|---|---|---|---|
| | | | $c_p$ (kpa) | $\phi_p$ (Degrees) | $\tau_{50}$[range][b,c] (kpa) | $\tau_{300}$[range][b,c] (kPa) | $c_{ld}$ (kPa) | $\phi_{ld}$ (Degrees) |
| SS1 | All GCLs | *A-J* | 38.9 | 18.0 | 55[13(FE24) to 71(FE23)] | 137[36(FE25) to 241(FE28)] | 17.2 | 7.8 |
| SS2 | GCL *A* | *A* | 46.6 | 18.7 | 63[48(FE7) to 66(FE1)] | 148[117(FE4) to 195(FE8)] | 17.2 | 7.6 |
| SS3 | All reinforced GCLs | *A-E*, *G-J* | 40.9 | 18.0 | 57[14(FE32) to 71(FE23)] | 139[48(FE13) to 241(FE28)] | 18.2 | 7.8 |
| SS4 | Unreinforced GCLs | F | 5.0 | 5.7 | 10[13(FE24) to 13(FE24)] | 35[36(FE25) to 36(FE25)] | 3.5 | 5.3 |
| SS5 | Needle-punched GCLs | *A*, *C-E*, *G-J* | 19.9 | 39.7 | 58[14(FE32) to 71(FE23)] | 149[107(FE19) to 241(FE28)] | 18.3 | 7.9 |
| SS6 | Stitch-bonded GCLs | *B* | 28.5 | 5.6 | 33[28(FE14) to 60(FE12)] | 58[48(FE13) to 92(FE12)] | N/A | N/A |
| SS7 | W-NW needle-punched GCLs | *A*, *C*, *G*, *I*, *J* | 19.1 | 40.9 | 58[14(FE32) to 66(FE1)] | 145[111(FE18) to 195(FE8)] | 19.1 | 7.8 |
| SS8 | NW-NW needle-punched GCLs | *D*, *E*, *H* | 35.0 | 24.5 | 58[23(FE19) to 71(FE23)] | 172[107(FE19) to 241(FE28)] | 11.3 | 8.7 |
| SS9 | Needle-punched GCLs without thermal-locking | *A*, *G-J* | 40.5 | 19.5 | 61[14(FE32) to 66(FE1)] | 149[117(FE4) to 195(FE8)] | 19.7 | 7.7 |
| SS10 | Needle-punched GCLs with thermal-locking | *C-E* | 33.2 | 22.7 | 54[23(FE19) to 71(FE23)] | 159[107(FE19) to 220(FE21)] | 11.8 | 9.0 |

[a]GCL sets do not consider the effect of specimen conditioning or SDR.
[b]The range includes the lowest shear strength and corresponding FE as well as the highest shear strength and corresponding FE.
[c]Upper and lower FE envelopes at the reference normal stresses were defined using the parameters presented in Table 2.

However, needle-punched GCLs with W-NW carrier geotextiles showed a lower peak shear strength than those with NW-NW carrier geotextile configurations under high normal stresses [$\tau_{300}$(Set SS7) = 145 kPa and $\tau_{300}$(Set SS8) = 172 kPa].

- Needle-punched GCLs that were not thermal-locked (Set SS9) showed higher peak internal shear strength under low normal stresses than those that were thermal-locked (Set SS10) [$\tau_{50}$(Set SS9) = 58 kPa and $\tau_{50}$(Set SS10) = 54 kPa]. However, the opposite trend is observed under high normal stress [$\tau_{300}$(Set SS9) = 146 kPa and $\tau_{300}$(Set SS10) = 159 kPa]. This finding suggests that thermal locking of the fiber reinforcements is more effective under high normal stresses.

Unlike comparisons of $\tau_p$ values, comparisons of $\tau_{ld}$ values among the 10 data sets can be conducted by direct comparison of the large-displacement friction angles. This is because the cohesion intercept of large-displacement shear strength envelopes is negligible (less than 20 kPa). Inspection of $\phi_{ld}$ values shown in Table 3 leads to the following observations regarding the internal large-displacement shear strength of GCLs:

- The large-displacement shear strength of unreinforced GCLs is consistently lower than that of reinforced GCLs [$\phi_{ld}$(Set SS4) = 5.3° and $\phi_{ld}$(Set SS3) = 7.8°].
- The range of large-displacement shear strength for the reinforced GCLs data sets in Table 3 is narrow ($\phi_{ld}$ ranging from 7.6° to 9.0°). However, the wider range of large-displacement shear strength observed for the individual failure envelopes of reinforced GCLs in Table 2 ($\phi_{ld}$ ranging from 4.0° to 13.7°) indicates that the variability in large-displacement shear strength should be considered.

### *Assessment of Shear Strength of GCLs Tested under the Same Conditioning Procedures*

The assessments using $\tau_{50}$ and $\tau_{300}$ allow direct comparison among the shear strength values of different GCL types under representative normal stresses. However, shear strength characterization for design purposes requires the definition of shear strength envelopes that account for the potential effect of GCL conditioning. Comparisons between GCLs tested under similar conditions are discussed below. Additional analyses are provided by McCartney et al. (2002).

Fig. 5(a) shows the $\tau_p$ envelopes for GCLs *A* (needle-punched), *B* (stitch-bonded), and *C* (thermal-locked) tested under the same $\sigma_n$ (34.5, 137.9, 310.3 kPa), $t_h$ (168 hs), $t_c$ (24 hs), and SDR (0.1 mm/min). Typical shear stress-displacement curves for some of these tests are shown in Fig. 2(a). Contrary to the observations made in the overall shear strength analysis, the needle-punched GCL *A* shows higher $\tau_p$ than the thermal-locked needle-punched GCL *C* for the full range of normal stresses (34.5 to 310.3 kPa). The thermal-locked GCL *C* appears to have been detrimentally affected by the long hydration time ($t_h$ = 168 hs) under the low hydration normal stress of ($\sigma_h$ = 20.7 kPa). Pullout of fibers may have occurred from the woven geotextile of GCL *C* during both hydration and shearing. The fibers in GCL *A* are typically left entangled on the surface of the woven geotextile, so significant swelling or shear displacement is required for pullout of the fibers from the carrier geotextile. On the other hand, the fibers in GCL *C* are melted together at the surfaces of the carrier geotextiles. This is consistent with the results reported by Lake and Rowe (2000), who observed that the melted fibers still pull out of the woven carrier geotextile despite thermal treatment during hydration and shearing. Consistent with trends observed using the overall shear strength assessment, the stitch-bonded GCL *B*

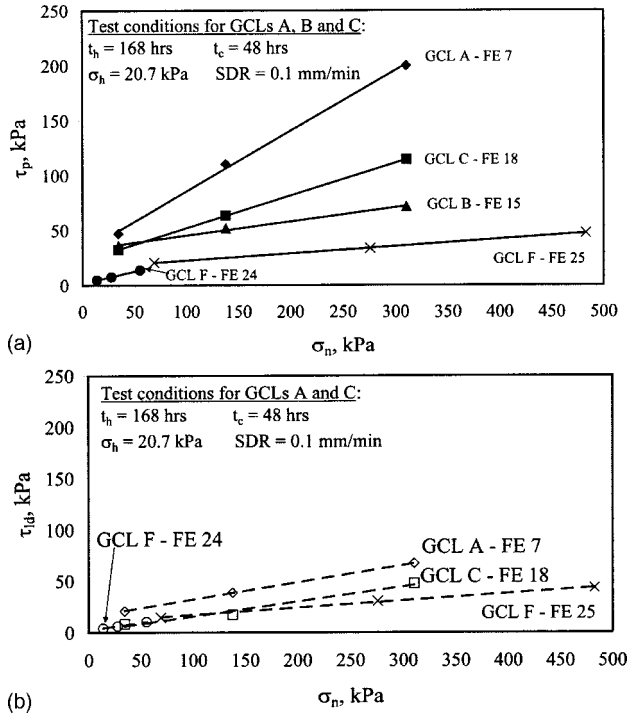


**Fig. 5.** Comparison of failure envelopes for needle-punched (GCL *A*), stitch-bonded (GCL *B*), thermal-locked (GCL *C*), and unreinforced (GCL *F*) GCLs: (a) peak shear strength; and (b) large-displacement shear strength. Note: When multiple shear strength results are available for a given $\sigma_n$, the data points in the figure correspond to the average shear strength value.

shows the lowest $\tau_p$ among the different reinforced GCLs. Further, consistent with observations reported by Fox et al. (1998), the continuous fiber reinforcements in GCL *B* did not break during shearing. Instead, the continuous fiber stitches tore the woven carrier geotextile while reaching comparatively large (post-peak) shear displacements. The relatively low reinforcement density (only three lines of stitching in a 305 mm wide specimen) as well as the transfer of shear stress from the stitches to the carrier geotextile during shearing probably contributed to the low $\tau_p$ of GCL *B*. Fig. 5(b) shows the $\tau_{ld}$ envelopes for the same cases. Similar to the observations for $\tau_p$, the needle-punched GCL *A* has higher $\tau_{ld}$ than the thermal-locked GCL *C*.

Also included in Figs. 5(a and b) are the $\tau_p$ and $\tau_{ld}$ envelopes for unreinforced GCL *F*. The hydration conditioning for tests conducted under comparatively low and high $\sigma_n$ (below and above approximately 60 kPa) are different. The GCL tested under low $\sigma_n$ is hydrated, but shows a higher friction angle than the unhydrated GCL tested under higher $\sigma_n$. Despite the differences in GCL conditioning between the tests on unreinforced specimens, both $\tau_p$ and $\tau_{ld}$ for GCL *F* are significantly below those obtained for reinforced GCLs.

## Indirect Evaluation of Pore Water Pressures Generated during Shearing

Direct measurement of pore water pressures generated during shearing poses significant experimental challenges and has not been successfully accomplished to date (Fox et al. 1998). While direct measurement of pore water pressures was beyond the scope of the commercial tests in the GCLSS database, some results provide indirect insight into the shear-induced pore water pressures. Such insight is provided by evaluation of direct shear tests conducted using different SDRs and of shear strength envelopes obtained for a wide range of $\sigma_n$. Although the behavior of GCLs under comparatively low $\sigma_n$ has been reported in the technical literature, the response of GCLs under comparatively high $\sigma_n$ has not been thoroughly investigated so far, probably due to experimental difficulties. Of particular interest in this study is the comparison between the behavior of GCLs tested under $\sigma_n$ below and above the swell pressure of the GCL. The swell pressure has been defined as the normal stress at which the sodium bentonite in the GCL does not swell beyond its initial thickness (Petrov et al. 1997). Petrov et al. (1997) reported swell pressures ranging from 100 to 160 kPa for thermal-locked GCLs, while lower values were reported by Stark (1997) for one test conducted using a needle-punched GCL. Pore water pressures generated during shearing are indirectly investigated herein by comparing the response of tests conducted under comparatively low and high $\sigma_n$.

### *Evaluation of the Effect of Shear Displacement Rate*

The effect of SDR on $\tau_p$ and $\tau_{ld}$ has been reported by Stark and Eid (1996), Gilbert et al. (1997), Eid and Stark (1997), Fox et al. (1998), and Eid et al. (1999). These studies, which primarily focused on the response of tests conducted under relatively low $\sigma_n$, reported an increasing $\tau_p$ with increasing SDR. The GCLSS database allows analysis of the effect of SDR on internal shear strength using tests conducted under $\sigma_n$ values beyond those reported in previous studies. Fig. 6(a) shows the results of tests on GCL *A* conducted under comparatively low $\sigma_n$ (50 kPa) using the same test conditions ($t_h$=24 hs, $\sigma_h$=$\sigma_n$, $t_c$=0 hs), but varying SDRs (0.01, 0.5, 1.0 mm/min). Consistent with the trend reported in past studies for tests conducted under low $\sigma_n$, the results show an increasing $\tau_p$ with increasing SDR. Fig. 6(b) shows the results of tests on GCL *A* conducted under high $\sigma_n$ (520 kPa) using the same test conditions ($t_h$=312 hs, $\sigma_h$=496.8 kPa, $t_c$=48 hs), but varying SDRs (0.0015, 0.01, 0.1, 1.0 mm/min). Unlike the trend shown in Fig. 6(a) for tests conducted under low $\sigma_n$, the results in Fig. 6(b) show a decreasing $\tau_p$ with increasing SDR. The results in Figs. 6(a and b) suggest that the large-displacement shear strength appears to approach residual conditions toward the end of the test conducted with high SDR (1.0 mm/min) test while the tests conducted at lower SDRs have not reached this condition at the end of testing.

Fig. 6(c) summarizes the peak shear strength results from Figs. 6(a and b), and includes additional tests conducted to verify the repeatability of results. The value of $\tau_p$ decreases at a rate of approximately 15 kPa per log cycle of SDR for tests conducted at $\sigma_n$=520 kPa, while it increases at a rate of approximately 12 kPa per log cycle of SDR for tests conducted at $\sigma_n$=50 kPa. Varying SDR appears to have a similar effect on $\tau_p$ for the $\sigma_n$ values shown in the figure (e.g., 10 to 15 kPa per log cycle). However, it should be noted that this corresponds to significant changes in $\tau_p$ for GCLs tested at $\sigma_n$=50 kPa (approximately 40% decrease per log cycle of SDR while it corresponds to smaller changes in $\tau_p$ for GCLs tested at $\sigma_n$=520 kPa (approximately 10% increase in shear strength per log cycle of SDR). Based on these observations, if design is governed by $\tau_p$, test specification involving comparatively high are acceptable if the $\sigma_n$ of interest is relatively high, as the test will lead to conservative (i.e., lower) shear

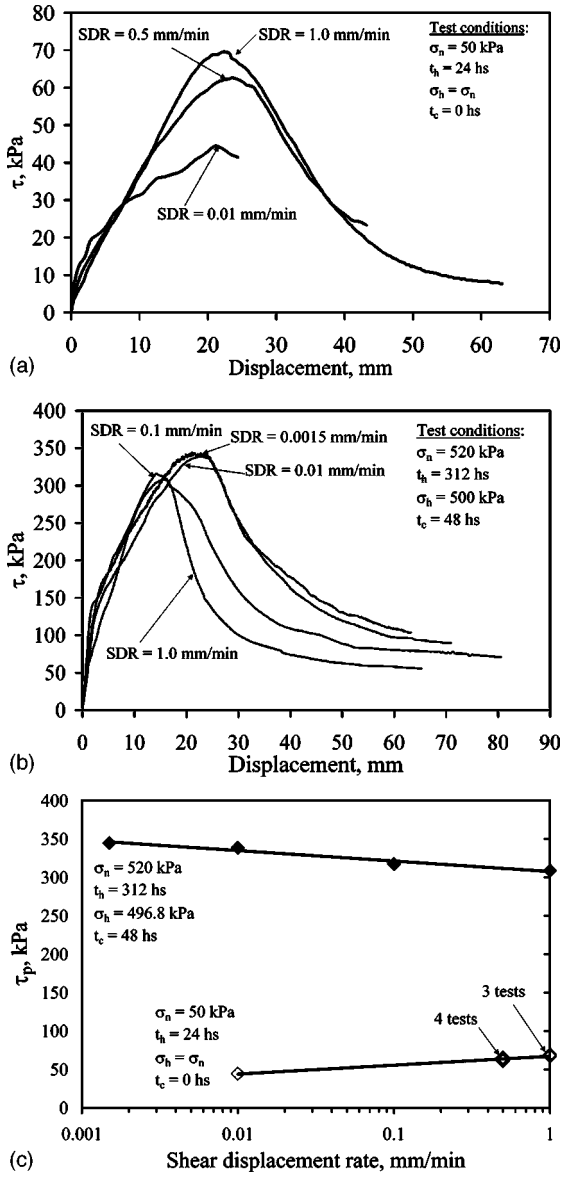


**Fig. 6.** Effect of shear displacement rate (SDR) on peak shear strength of needle-punched GCL *A*: (a) shear stress-displacement curves for tests under low $\sigma_n$ (50 kPa); (b) shear stress-displacement curves for tests under high $\sigma_n$ (520 kPa); and (c) summary trends of peak shear strength as a function of SDR

strength values. However, tests should still be specified with sufficiently low SDR (e.g., 0.1 mm/min) if the $\sigma_n$ of interest is relatively low.

Explanations proposed to justify the trend of increasing $\tau_p$ with increasing SDR observed in previous studies, conducted under relatively low $\sigma_n$, have included shear-induced pore water pressures, secondary creep, undrained frictional resistance of bentonite at low water content, and SDR-dependent pullout behavior of fibers during shearing. However, the results obtained from tests conducted under both low and high $\sigma_n$ suggest that the observed trends are consistent with the generation of shear-induced pore water pressures. Shear-induced pore water pressures are expected to be negative in tests conducted under low $\sigma_n$ (i.e., below the swell pressure of GCLs). Consequently, increasing SDR will lead to increasingly negative pore water pressures and thus higher $\tau_p$. This trend was also observed for tests conducted on unreinforced

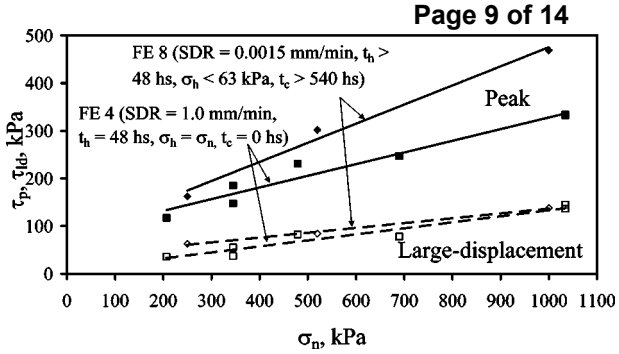


**Fig. 7.** Effect of shear displacement rate on the peak and large-displacement shear strength of needle-punched GCL *A*

GCLs (Gilbert et al. 1997). On the other hand, shear-induced pore water pressures are expected to be positive in tests conducted under high $\sigma_n$ (i.e., above the swell pressure of GCLs). In this case, increasing SDR will lead to increasingly positive pore water pressures and thus lower $\tau_p$.

Since no shear-induced pore water pressures are expected (positive or negative) for constant volume conditions, the same residual shear strength is anticipated for different SDRs. Eid and Stark (1999) reported that residual shear strength results were insensitive to SDRs, while Fox et al. (1998) found a slightly increasing strength with increasing SDR for a normal stress of 72.2 kPa. Although residual shear strength was not achieved for the tests reported in Figs. 6(a and b), the tests conducted using higher SDR showed post-peak shear strength loss at comparatively smaller shear displacement values. A consequence of this observation is that, if design is governed by large-displacement shear strength, direct shear tests conducted using high SDR should be adequate for preliminary internal shear strength characterization.

### *Indirect Evaluation of Pore Water Pressures from Shear Strength Envelopes*

Fig. 7 shows FE 8, which includes three tests that were hydrated under a constant low $\sigma_h$ for more than 48 hs. The normal stress was subsequently increased in stages from $\sigma_h$ to $\sigma_n$ during a period of over 540 hs. The specimens were finally sheared using a SDR of 0.0015 mm/min. Determination of the three data points for FE 8 required approximately one year of direct shear testing. For comparison, Fig. 7 also includes data from tests conducted using a SDR of 1.0 mm/min (FE 4). The results in this figure allow investigation of the cumulative effect of conditioning and SDR on the internal shear strength of GCL *A*. For instance, despite the different hydration and consolidation procedures of the three tests in FE 8, a well-defined linear failure envelope was obtained ($R^2$=0.988). Also, for the range of $\sigma_n$ shown in this figure (above the swell pressure of GCLs), the trends are consistent with those observed in Fig. 6. That is, the differences in $\tau_p$ between FE 4 (SDR=1.0 mm/min) and FE 8 (SDR=0.0015 mm/min) are more significant at higher $\sigma_n$ because of higher positive pore water pressures induced in FE 4. The direct shear tests corresponding to FE 4 and FE 8 appear to be approaching residual conditions toward the end of the test. The $\tau_{ld}$ envelopes suggest that the residual shear strength is approximately insensitive to the different conditioning procedures and different SDRs.

Additional insight on shear-induced pore water pressures can

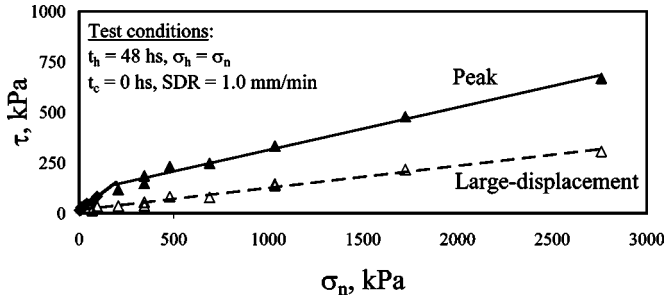


**Fig. 8.** Typical shear strength envelopes for needle-punched GCL *A* obtained using a wide range of $\sigma_n$

be obtained from evaluating shear strength envelopes in the GCLSS database that include tests conducted using $\sigma_n$ ranging from values below to values above the swell pressure of GCLs. Fig. 8 shows $\tau_p$ and $\tau_{ld}$ results for tests on GCL *A* (FE 4) conducted using $t_h$=48 hs, $\sigma_h=\sigma_n$, $t_c$=0 hs, and SDR=1.0 mm/min. The internal shear strength envelope shown in the figure was defined using 40 direct shear tests. Some tests were conducted using $\sigma_n$ as high as 2,759 kPa, which corresponds to stresses expected in bottom liners of high landfills or heap leach pads. Tests on GCLs under such high $\sigma_n$ have not been reported in previous investigations. A linear envelope does not provide a good representation of $\tau_p$ over the wide range of $\sigma_n$ encompassing the swell pressure of the GCL, which is consistent with nonlinear envelopes reported for GCLs (Gilbert et al. 1996; Fox et al. 1998), and for sodium montmorillonite (Mesri and Olson 1970). The GCL and unreinforced sodium bentonite are expected to be influenced by the same mechanisms when tested at normal stresses above and below the swell pressure. As shown in the figure, a bilinear FE provides a good representation of the $\tau_p$ data. Linear envelopes fit the $\tau_p$ data well for $\sigma_n$ below approximately 100 kPa ($c$=14.4 kPa, $\phi$=35.4°) and for $\sigma_n$ above approximately 200 kPa ($c$=102.4 kPa, $\phi$=11.9°). A transition zone appears to take place for $\sigma_n$ ranging from 100 to 200 kPa, which is within the reported range of GCL swell pressure. The bilinear trend is not caused by a change in fiber failure mechanisms (from pullout to breakage), as the normal stress needed to induce breakage of the polypropylene fibers is well above that of typical geotechnical projects (Zornberg 2002). The $\tau_{ld}$ envelope is well represented by a linear envelope characterized by a friction angle of 6.3° and negligible cohesion intercept ($c_p$=16.2 kPa). Other GCLs in the database, tested under a wide range of $\sigma_n$ (e.g., FE 16 and 21), show a similar bilinear $\tau_p$ response.

Consistent with the results obtained for varying SDR, the break in the bilinear trend in $\tau_p$ is in agreement with the generation of negative and positive excess pore water pressures in tests conducted using $\sigma_n$ below and above the swell pressure of GCLs, respectively. The linear trend obtained for $\tau_{ld}$ a wide range of $\sigma_n$ is also in agreement with the negligible pore water pressures expected under large-displacement conditions.

## Variability

The number of test results in the GCLSS database is large enough to provide a basis for assessment of internal shear strength variability. Considering the composite nature of GCLs, the analyses presented herein allow both identification and quantification of different sources of shear strength variability. This information may prove relevant for reliability-based limit equilibrium analyses (McCartney et al. 2004). Potential sources of GCL internal shear strength variability include: (1) Differences in material types (type of GCL reinforcement, carrier geosynthetic), (2) variation in test results from the same laboratory (repeatability), and (3) overall material variability. In turn, the overall material variability includes more specific sources such as: (3-*a*) Inherent variability of fiber reinforcements, and (3-*b*) inherent variability of sodium bentonite. The source of variability (1) listed above is not addressed in this study since only the variability of individual GCL types is evaluated. The sources of variability (2) and (3) are assessed in this study using data presented in Table 4. This table presents a total of seven sets identified for assessment of shear strength variability. Each data set includes tests conducted using the same GCL type, same conditioning procedures, and same $\sigma_n$.

### *Repeatability of Test Results Obtained from the Same Laboratory*

The source of variability (2) can be assessed by evaluating Sets V1 and V2 in Table 4, which includes the results of tests conducted by a single laboratory using specimens collected from a single manufacturing lot tested with the same conditioning procedures and same $\sigma_n$. Although the size of manufacturing lots is not standardized, it typically involves a set of rolls produced in a shift, day, or even week. Fig. 9 shows shear stress-displacement curves for GCL *A* specimens obtained from rolls of the same lot, which were tested by the same laboratory using the same $\sigma_n$. Although the number of tests is small, these results illustrate that good repeatability can be achieved in the stress-strain-strength response when tests are conducted in the same laboratory using same-lot specimens. As indicated by Table 4, the maximum relative difference between these tests is less than 6%, which is significantly smaller than the relative difference associated with different-lot GCLs presented in the next section.

### *Overall Material Variability*

The source of variability (3) may be assessed by evaluating Sets V3 through V7 in Table 4. Unlike the results for Sets V1 and V2 shown in Fig. 9, the GCL specimens in Sets V3 through V7 were obtained from different manufacturing lots. For each set, Table 4 indicates the mean values for $\tau_p$ and $\tau_{ld}$ [$E(\tau_p)$ and $E(\tau_{ld})$], their standard deviations [$s(\tau_p)$ and $s(\tau_{ld})$], their coefficient of variation c.o.v. values [$s(\tau)/E(\tau)$], and the maximum relative difference. Subsets of data sets V3, V4, and V5 (V3*a* though V3*e*, V4*a* through V4*e*, and V5*a* through V5*e*), in Table 4 include the shear strength variability data corresponding to the manufacturing year of each of the GCL specimens. The maximum relative differences for Sets V3 through V7 (approximately 55%) are significantly higher than those obtained for tests using same-lot GCL specimens (6%). Sets V3, V4, and V5 include data from 141 internal shear strength tests on GCL *A* conducted using the same test conditions ($t_h$=168 hs, $t_c$=48 hs, SDR=0.1 mm/min) and three different normal stresses ($\sigma_n$=34.5, 137.9, 310.3 kPa). Evaluation of statistical information on the $\tau_p$ results for these three sets shows an increasing $s(\tau_p)$ and a relatively constant c.o.v. with increasing $\sigma_n$, which indicates that peak shear strength variability increases linearly with $\sigma_n$. The c.o.v. and maximum relative difference values are approximately 0.25 and 55%, which are significantly high values for engineering materials. Fig. 10(a) shows the $\tau_p$ envelope defined using the mean values of the 141 direct shear test results (Sets V3, V4, and V5 in Table 4). This figure

**Table 4.** Geosynthetic Clay Liner (GCL) Data Sets for Assessment of Shear Strength Variability

| | | Test conditions | | | | | | Peak shear strength | | | | Large-displacement shear strength | | | |
|---|---|---|---|---|---|---|---|---|---|---|---|---|---|---|---|
| GCL data set | GCL label | $t_h$ (hs) | $t_c$ (hs) | SDR (mm/min) | $\sigma_n$ (kPa) | Year GCL manufactured | Number of tests | $E(\tau_p)$ (kPa) | $s(\tau_p)$ (kPa) | c.o.v. | Max. rel. difference[a] (%) | $E(\tau_{ld})$ (kPa) | $s(\tau_{ld})$ (kPa) | c.o.v. | Max. rel. difference[a] (%) |
| V1 | A | 24 | 0 | 0.5 | 48.3 | 1998 | 3 | 63.2 | 2.1 | 0.03 | 6 | 20.7 | 2.5 | 0.12 | 21 |
| V2 | A | 24 | 0 | 0.5 | 386.1 | 1998 | 3 | 210.7 | 6.4 | 0.03 | 6 | 79.3 | 4.8 | 0.06 | 11 |
| V3 | A | 168 | 48 | 0.1 | 34.5 | 1997–2003 | 47 | 35.6 | 10.4 | 0.29 | 64 | 20.6 | 6.27 | 0.30 | 79 |
| *V3a* | *A* | *168* | *48* | *0.1* | *34.5* | *1997* | *2* | *52.1* | *4.4* | *0.08* | *11* | *8.3* | *0.0* | *0.00* | *0* |
| *V3b* | *A* | *168* | *48* | *0.1* | *34.5* | *1998* | *8* | *44.6* | *3.6* | *0.08* | *24* | *16.5* | *3.1* | *0.19* | *45* |
| *V3c* | *A* | *168* | *48* | *0.1* | *34.5* | *1999* | *9* | *47.9* | *6.1* | *0.13* | *33* | *26.0* | *9.9* | *0.38* | *75* |
| *V3d* | *A* | *168* | *48* | *0.1* | *34.5* | *2002* | *15* | *28.5* | *2.9* | *0.10* | *32* | *19.9* | *2.9* | *0.15* | *41* |
| *V3e* | *A* | *168* | *48* | *0.1* | *34.5* | *2003* | *13* | *27.3* | *5.1* | *0.19* | *42* | *21.2* | *4.5* | *0.21* | *54* |
| V4 | A | 168 | 48 | 0.1 | 137.9 | 1997–2003 | 47 | 87.4 | 22.2 | 0.25 | 57 | 39.3 | 8.09 | 0.21 | 75 |
| *V4a* | *A* | *168* | *48* | *0.1* | *137.9* | *1997* | *2* | *114.1* | *32.7* | *0.29* | *34* | *13.8* | *0.00* | *0.00* | *0* |
| *V4b* | *A* | *168* | *48* | *0.1* | *137.9* | *1998* | *8* | *106.8* | *14.9* | *0.14* | *40* | *34.4* | *6.43* | *0.19* | *43* |
| *V4c* | *A* | *168* | *48* | *0.1* | *137.9* | *1999* | *9* | *112.7* | *15.8* | *0.14* | *34* | *43.6* | *9.16* | *0.21* | *48* |
| *V4d* | *A* | *168* | *48* | *0.1* | *137.9* | *2002* | *15* | *74.5* | *5.3* | *0.07* | *27* | *37.2* | *4.98* | *0.13* | *33* |
| *V4e* | *A* | *168* | *48* | *0.1* | *137.9* | *2003* | *13* | *68.7* | *6.0* | *0.09* | *25* | *43.9* | *4.82* | *0.11* | *29* |
| V5 | A | 168 | 48 | 0.1 | 310.3 | 1997–2003 | 47 | 166.0 | 33.4 | 0.20 | 51 | 66.6 | 11.75 | 0.18 | 56 |
| *V5a* | *A* | *168* | *48* | *0.1* | *310.3* | *1997* | *2* | *198.9* | *60.0* | *0.30* | *35* | *39.3* | *0.00* | *0.00* | *0* |
| *V5b* | *A* | *168* | *48* | *0.1* | *310.3* | *1998* | *8* | *203.0* | *21.0* | *0.10* | *27* | *63.9* | *10.06* | *0.16* | *43* |
| *V5c* | *A* | *168* | *48* | *0.1* | *310.3* | *1999* | *9* | *197.2* | *23.2* | *0.12* | *33* | *67.8* | *15.94* | *0.24* | *53* |
| *V5d* | *A* | *168* | *48* | *0.1* | *310.3* | *2002* | *15* | *146.5* | *12.8* | *0.09* | *29* | *61.5* | *7.99* | *0.13* | *34* |
| *V5e* | *A* | *168* | *48* | *0.1* | *310.3* | *2003* | *13* | *138.9* | *8.8* | *0.06* | *23* | *75.3* | *5.70* | *0.08* | *18* |
| V6 | A | 48 | 0 | 1.0 | 9.6 | 1997 | 18 | 31.1 | 5.8 | 0.19 | 55 | N/A | N/A | N/A | N/A |
| V7 | F | 24 | 0 | 1.0 | 9.6 | 1999 | 6 | 3.9 | 0.7 | 0.19 | 35 | 3.0 | 0.5 | 0.15 | 35 |

[a]Maximum relative difference=$[(\max \tau_p - \min \tau_p)/\max \tau_p] \times 100\%$.

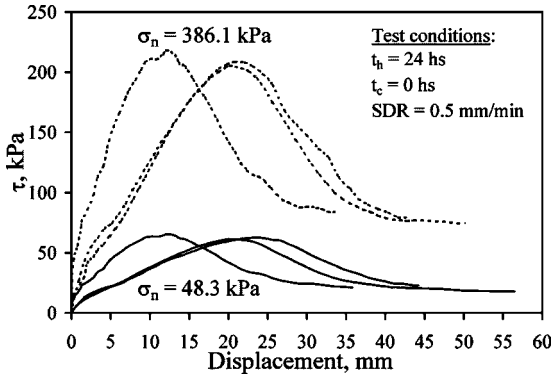


**Fig. 9.** Repeatability of test results on needle-punched GCL *A* specimens from rolls taken from the same lot

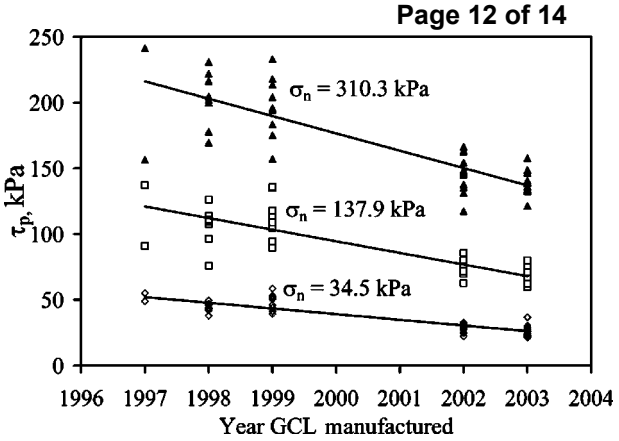


**Fig. 11.** Peak shear strength of GCL *A* for different manufacturing years

illustrates the significant scatter of results from tests conducted using the same GCL type and test conditions, but using specimens from different GCL *A* lots. Fig. 10(b) shows idealized normal probability density distributions for $\tau_p$ at each $\sigma_n$, obtained using the mean and standard deviation for the shear strength data of Sets V3, V4, and V5. These probability distributions quantify statistical information on $\tau_p$, which is useful for reliability-based design. Table 4 also includes statistical information regarding $\tau_{ld}$. Although $\tau_{ld}$ may not be fully representative of the residual shear strength, the c.o.v. of $\tau_{ld}$ is relatively high (up to 0.30), which indicates that the variability in large-displacement shear strength is not less significant than that of peak shear strength.

The 141 GCL specimens in Sets V3 through V5 were received between January 1997 and May 2003. The c.o.v. and maximum relative difference for each of the subsets of Sets V3 to V5 are typically lower each year than for the overall multiyear data sets. For example, the overall c.o.v. for Set V3 is 0.29 while the c.o.v. values for Subsets V3*a* through V3*d* range from 0.08 to 0.19. Fig. 11 shows the shear strength variability for each manufacturing year. A slight decreasing trend in the mean value of the peak shear strength is observed with each subsequent GCL manufacturing year. However, a decreasing trend in the standard deviation value of the peak shear strength is also observed with each subsequent GCL manufacturing year for high normal stresses (e.g., $\sigma_n$ =137.9 and 310.3 kPa), which may reflect an improvement over time of manufacturing quality assurance programs.

Set V6 in Table 4 includes variability data from a set of 19 direct shear tests conducted using the same GCL tested in Sets V3 through V5 (GCL *A*, manufactured in 1997), but different test conditions ($t_h$=48 hs, $t_c$=0 hs, SDR=1.0 mm/min, $\sigma_n$=9.6 kPa). The c.o.v. and maximum relative difference for Set V6 are similar to those for Sets V3 through V5 despite the shorter time allowed for conditioning ($t_h$=24 hs). This suggests that specimen conditioning is not a major source of inherent material variability.

### *Inherent Variability of Fiber Reinforcements*

Peel strength results have been reported to provide an index of the density (and possibly the contribution) of fiber reinforcements in needle-punched GCLs (Heerten et al. 1995, Eid and Stark 1997). Consequently, an assessment is made herein of the usefulness of peel strength as an indicator of the fiber contribution to GCL internal shear strength. If useful, the peel strength variability would be an indicator of the contribution of fibers to the variability of GCL shear strength [source of variability (3-*a*)]. The peel strength test (ASTM 1999) involves clamping the carrier geotextiles of a 100 mm wide unhydrated GCL specimen, and applying a force normal to the GCL plane until separating (or peeling) the geotextiles. It should be noted that the peel strength test mobilizes the fibers in a manner that may not be representative of the conditions in which the fibers are mobilized during shearing.

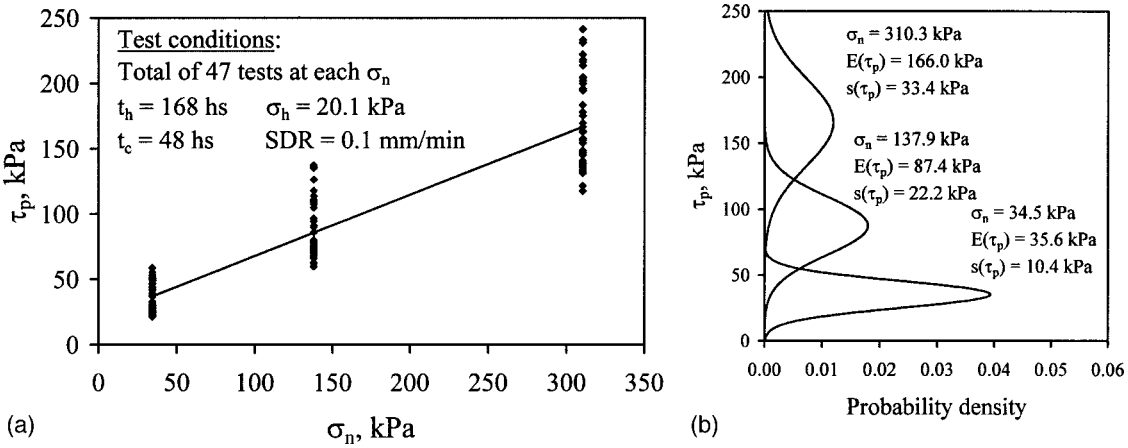


**Fig. 10.** Variability of peak shear strength results obtained using needle-punched GCL *A* specimens from different lots, tested using same conditioning procedures and $\sigma_n$: (a) $\tau_p$ envelope; and (b) normal distributions for $\tau_p$ at each $\sigma_n$

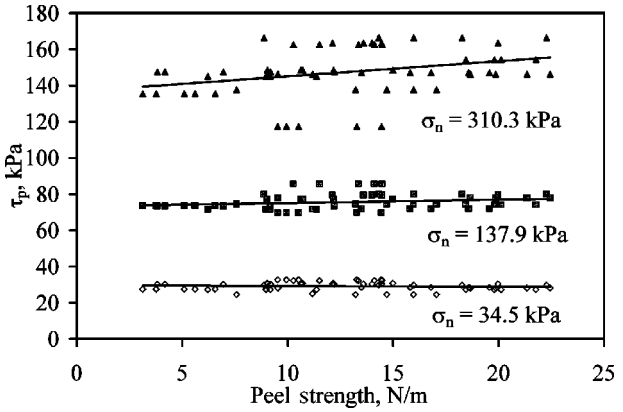


**Fig. 12.** Relationship between peel strength and $\tau_p$ for needle-punched GCL *A*

A total of 75 peel strength tests were conducted using GCL *A* specimens manufactured in 2002. Specifically, five tests were conducted using GCL *A* specimens from 15 rolls (different lots) manufactured in 2002 used for the test results presented in Fig. 10 (Sets V3 through V5 in Table 4). The peel strength specified by the GCL *A* manufacturer is 6.5 N/m. However, peel strength results varied significantly (from 4.3 to 22.5 N/m), with a mean of 12.5 N/m and a standard deviation of 5.51 N/m. The relationship between peel strength and $\tau_p$ obtained using GCL specimens collected from these 15 rolls is shown in Fig. 12. Although a slightly increasing trend of peel strength with increasing $\tau_p$ can be observed at high $\sigma_n$, the results suggest that $\tau_p$ is not very sensitive to the peel strength. This is consistent with results reported by Richardson (1997). Consequently, no conclusion can be drawn regarding the effect of the inherent variability of peel strength on the variability of the fiber contribution to GCL internal shear strength [source of variability (3-*a*)]. Instead, these results suggest that mobilization of fiber reinforcement in peel strength tests may not be representative of the mobilization of fibers in shear tests. Accordingly, the peel strength appears not to be a good indicator of the contribution of fibers to $\tau_p$.

### *Inherent Variability of Sodium Bentonite*

The source of variability (3-*b*) may be assessed by evaluating the internal shear strength variability of unreinforced GCLs. Set V7 (Table 4) includes variability data from six direct shear tests conducted using an unreinforced GCL (GCL *F*). The tests were conducted using a relatively low $\sigma_n$ (9.6 kPa) and the same test conditions ($t_h$=24 hs, $t_c$=48 hs, SDR=1.0 mm/min). The variability of direct shear test results for unreinforced GCLs is useful to assess the variability of the bentonite shear strength contribution to the shear strength of reinforced GCLs. It should be noted that adhesives are mixed with the sodium bentonite, but they have been reported to have little effect on the GCL internal shear strength once hydrated (Eid and Stark 1997). The c.o.v. and maximum relative difference of the $\tau_p$ obtained for Set V7 using unreinforced GCLs is similar to that obtained for Sets V3 through V6 using reinforced GCLs (c.o.v. of approximately 0.20). In particular, the reinforced GCLs (GCL *A*) in Set V6 were tested under the same $\sigma_n$ and similar conditioning procedures as the unreinforced GCLs in Set V7. Even though the internal shear strength variability has been attributed mainly to the fibers, the similar magnitude of variability observed in the unreinforced GCLs suggests that the variability of the sodium bentonite [source of variability (3-*b*)] is also relevant.

## Conclusions

A database of 414 GCL internal shear strength tests was analyzed in this study. The data were obtained from large-scale (305 mm by 305 mm) direct shear tests conducted by a single laboratory over a period of 12 years using procedures consistent with current testing standards. Shear strength parameters were defined to evaluate the effect of GCL type, indirectly quantify the effect of pore water pressures, and assess sources of internal shear strength variability. The following conclusions can be drawn from this study:

1. Comparisons were made between shear strength values obtained for normal stresses representative of cover and bottom liners (50 and 300 kPa, respectively). This evaluation indicates a high scatter in peak internal GCL shear strength. Reinforced GCLs were observed to have significantly higher peak shear strength than unreinforced GCLs. Stitch-bonded GCLs were observed to have lower peak shear strength than needle-punched GCLs. Needle-punched GCLs with NW-NW GCL carrier geotextile configurations were observed to have higher peak shear strength than those with W-NW GCL carrier geotextiles. Needle-punched GCLs without thermal locking were observed to have higher peak shear strength at low normal stresses than those with thermal locking, but the opposite trend was observed at high normal stresses.
2. Unreinforced GCLs were observed to have lower large-displacement shear strength than reinforced GCLs.
3. Stitch-bonded GCLs showed a higher displacement at peak than the other reinforced GCLs.
4. Thermal locking of needle-punched GCLs was detrimentally affected by long hydration periods under low hydration normal stresses. Thermal locking was observed to be effective at high normal stresses.
5. The peak shear strength of reinforced GCLs was observed to increase with increasing SDR for tests conducted under low $\sigma_n$, while the opposite trend was observed under high $\sigma_n$. This behavior is consistent with the generation of negative shear-induced pore water pressures under low $\sigma_n$ (below the swell pressure) and of positive pore water pressures under high $\sigma_n$. Consequently, if design is governed by $\tau_p$, test specification involving comparatively high SDR are acceptable if the $\sigma_n$ of interest is relatively high, as the test will lead to conservative (i.e., lower) shear strength values. However, tests should still be specified with sufficiently low SDR (e.g., 0.1 mm/min) if the $\sigma_n$ of interest is relatively low.
6. Large-displacement shear strength was achieved at smaller shear displacements in tests conducted using comparatively large SDRs. consequently, tests with high SDR should be adequate if design is governed by $\tau_{ld}$.
7. Peak shear strength results obtained over a wide range of $\sigma_n$ (up to 2,759 kPa) defined bilinear failure envelopes in which a break was defined for normal stresses consistent with the swell pressure of GCLs.
8. Good repeatability of results was observed for tests conducted by the same laboratory using GCL specimens from the same manufacturing lot. However, significant variability was observed for tests conducted using GCL specimens obtained from different lots over a period of 7 years. Nonetheless, the variability among GCLs manufactured in a single year is less than that observed over the 7 year period.
9. The shear strength variability, quantified by the c.o.v. and maximum relative difference, was observed to increase lin-

early with $\sigma_n$, but was found to be insensitive to specimen conditioning procedures.

10. Peel strength results showed a relatively high variability. However, the $\tau_p$ was found not to correlate well with the peel strength. Consequently, no conclusions can be drawn regarding the effect of the variability of peel strength on the variability of GCL internal shear strength.
11. The c.o.v. of unreinforced GCLs was observed to be similar to that of reinforced GCLs, indicating that the inherent variability of sodium bentonite is a relevant source of reinforced GCL shear strength variability.

## Acknowledgments

The writers thank SGI Testing Services and GeoSyntec Consultants for making available the experimental results analyzed in this study. Review provided by Dr. Paul Sabatini and Dr. Neven Matasovic of GeoSyntec Consultants is appreciated. The views expressed in this paper are solely those of the writers.

## References

American Society of Testing and Materials. (1998). "Standard test method for determining the internal and interface shear resistance of geosynthetic clay liner by the direct shear method." *ASTM D6243*, West Conshohocken, Pa.

American Society of Testing and Materials. (1999). "Standard test method for determining average bonding peel strength between the top and bottom layers of needle-punched geosynthetic clay liners." *ASTM D6496*, West Conshohocken, Pa.

Eid, H. T., and Stark, T. D. (1997). "Shear behavior of an unreinforced geosynthetic clay liner." *Geosynthet. Int.*, 4(6), 645–659.

Eid, H. T., Stark, T. D., and Doerfler, C. K. (1999). "Effect of shear displacement rate on internal shear strength of a reinforced geosynthetic clay liner." *Geosynthet. Int.*, 6(3), 219–239.

Fox, P. J., Rowland, M. G., and Scheithe, J. R. (1998). "Internal shear strength of three geosynthetic clay liners." *J. Geotech. Geoenviron. Eng.*, 124(10), 933–944.

Heerten, G., Saathoff, F., Scheu, C., von Maubeuge, K. P. (1995) "On the long-term shear behavior of geosynthetic clay liners (GCLs) in capping sealing systems." *Proc., Int. Symposium Geosynthetic Clay Liners*, 141–150.

Helsel, D. R., and Hirsh, R. M. (1991). *Statistical methods in water resources*, United States Geologic Survey.

Gilbert, R. B., Fernandez, F. F., and Horsfield, D. (1996). "Shear strength of a reinforced. clay liner." *J. Geotech. Eng.*, 122(4), 259–266.

Gilbert, R. B., Scranton, H. B., and Daniel, D. E. (1997). "Shear strength testing for geosynthetic clay liners." *Testing and acceptance criteria for geosynthetic clay liners, ASTM STP 1308*, L. W. Well, ed., ASTM, Philadelphia, 121–138.

Lake, C. G., and Rowe, R. K. (2000). "Swelling characteristics of needle-punched, thermal treated geosynthetic clay liners." *Geotext. Geomembr.*, 18, 77–101.

McCartney, J. S., Zornberg, J. G., and Swan, R. (2002). "Internal and interface shear strength of Geosynthetic Clay Liners (GCLs)." *Geotech. Research Rep.*, Dept. of Civil, Environmental, and Architectural Engineering, Univ. of Colorado at Boulder.

McCartney, J. S., Zornberg, J. G., Swan, R. H., Jr., and Gilbert, R. B. (2004). "Reliability-based stability analysis considering GCL shear strength variability." *Geosynthet. Int.* 11(3), 212-232.

Mesri, G., and Olson, R. E. (1970). "Shear strength of montmorillonite." *Geotechnique*, 20(3), 261–270.

Petrov, R. J., Rowe, R. K., and Quigley, R. M. (1997). "Selected factors influencing GCL hydraulic conductivity." *J. Geotech. Geoenviron. Eng.*, 123(8), 683–695.

Richardson, G. N. (1997). "GCL internal shear strength requirements." *Geosynth. Fabric Rep.*, March, 20–25.

Stark, T. D. (1997). "Effect of swell pressure on GCL cover stability." *Testing and Acceptance Criteria for Geosynthetic Clay Liners, ASTM STP 1308*, L. W. Well, ed., American Society for Testing and Materials, Philadelphia, 30–44.

Stark, T. D., and Eid, H. T. (1996). "Shear behavior of a reinforced geosynthetic clay liner." *Geosynthet. Int.*, 3(6), 771–785.

Stoewahse, C., Nixon, N., Jones, D. R. V., Blumel, W., and Kamugisha, P. (2002). "Geosynthetic interface shear behavior." *Ground Eng.*, February, 35–41.

Zornberg, J. G. (2002). "Discrete framework for limit equilibrium analysis of fiber-reinforced soil." *Geotechnique*, 52(8), 593–604.

**SOAH DOCKET NO. 582-22-0844**
**TCEQ DOCKET NO: 2021-1000-MSW**

| | | |
|---|---|---|
| **IN THE MATTER OF THE** | **§** | **BEFORE THE STATE OFFICE** |
| **APPLICATION BY DIAMOND BACK** | **§** | |
| **RECYCLING AND SANITARY** | **§** | **OF** |
| **LANDFILL, LP FOR NEW MSW** | **§** | |
| **PERMIT NO. 2404** | **§** | **ADMINISTRATIVE HEARINGS** |

# EXHIBIT KNOX-117

# Analysis of a Large Database of GCL-Geomembrane Interface Shear Strength Results

John S. McCartney, A.M.ASCE[1]; Jorge G. Zornberg, M.ASCE[2]; and Robert H. Swan Jr.[3]

**Abstract:** A database of 534 large-scale direct shear test results was assembled in this study to evaluate the interface shear strength between geosynthetic clay liners (GCLs) and geomembranes (GMs). The tests were conducted between 1992 and 2003 by a single independent laboratory using procedures consistent with current testing standards. The number of results in the database allowed quantification of the impact of GCL type, GM type, normal stress, and procedures for specimen hydration and consolidation on the shear strength of GCL-GM interfaces, as well as identification of sources of shear strength variability. The interface shear strength was found to be sensitive to the type of GCL internal reinforcement, GM polymer, and GM texturing, but not to the GM thickness or manufacturer. On average, the GCL internal shear strength was observed to be higher than the GCL-GM interface shear strength when tested using the same procedures. GCLs sheared internally show similar stress-displacement responses and friction angles to GCL-GM interfaces that incorporate a GCL with the same reinforcement type. Hydration under normal stresses below those used during shearing (followed by a consolidation period) led to higher GCL internal shear strength, but lower GCL-GM interface shear strength, than when hydration was conducted under the shearing normal stress. Such different responses are attributed to bentonite extrusion from the GCL into the interface. Good repeatability of test results was obtained using GCL and GM specimens from the same manufacturing lot, while high variability was obtained using specimens from different lots. GCL-GM interface peak shear strength variability was found to increase linearly with normal stress.

**DOI:** 10.1061/(ASCE)1090-0241(2009)135:2(209)

**CE Database subject headings:** Database; Geomembranes; Shear strength; Clay liners.

## Introduction

Use of geomembranes (GMs) directly above a clay layer (i.e., a composite lining system) in hydraulic barrier systems such as landfill covers or bottom liners have been shown to perform better than single GMs or single compacted clay layers. Geosynthetic clay liners (GCLs) have often replaced the compacted clay layer in composite liners since they may offer equivalent or superior hydraulic performance while having limited thickness, good compliance with differential settlements of underlying soil or waste, easy installation, and low cost. GCLs are prefabricated geocomposite materials manufactured by bonding sodium bentonite clay to one or two geosynthetic backing materials (carrier geosynthetics). Stability is a major concern for side slopes in liners that include GCLs and GMs because of the very low shear strength of hydrated sodium bentonite, which has been reported to extrude from the GCL leading to weakening of the interface (Triplett and Fox 2001). Accordingly, proper shear strength characterization is needed for the different liner materials and interfaces. In particular, a failure surface is likely to develop at the interface between a GCL and a GM. The shear strength of GCL-GM interfaces is the focus of the study presented herein.

Previous investigations have evaluated the GCL-GM interface shear strength using direct shear and ring shear tests (Gilbert et al. 1996, 1997; Hewitt et al.1997; Triplett and Fox 2001). While these experimental studies have provided good insight into shear strength testing issues and variables affecting GCL-GM interface shear strength, available information on GCL-GM interface shear strength is still limited to specific ranges of normal stresses, GCL and GM types, and conditioning procedures. A GCL shear strength (GCLSS) database of results from 534 direct shear tests on the interface between different GCLs and GMs, conducted by a single laboratory, was assembled and evaluated in this study to identify and quantify the variables governing GCL-GM interface shear strength. Analysis of the results in the GCLSS database allows evaluation of: (i) the influence of different GCL and GM types on the GCL-GM interface shear strength; (ii) differences between GCL internal and GCL-GM interface shear strength; (iii) the effect of GCL conditioning on GCL-GM interface shear strength; and (iv) the variability in GCL-GM interface shear strength. This database also includes 414 direct shear tests conducted by the same laboratory used to quantify variables affecting the internal shear strength of GCLs, which were reported elsewhere (Zornberg et al. 2005). The results in the GCLSS database complement those presented in other databases (Chiu and Fox 2004) by providing more information specifically focused toward variables governing GCL-GM interface shear strength and inter-

[1]Barry Faculty Fellow and Assistant Professor, Univ. of Colorado at Boulder, Dept. of Civil, Environmental, and Architectural Engineering, 428 UCB, Boulder, CO 80309. E-mail: john.mccartney@colorado.edu

[2]Associate Professor, Univ. of Texas at Austin, 1 University Station C1792, Austin, TX 78712.

[3]Faculty Associate, Univ. of North Carolina at Charlotte Dept. of Engineering Technology, The William States Lee College of Engineering, 9201 University City Blvd, Smith 244 Charlotte, NC 28223-0001. E-mail: rswan1@uncc.edu

Note. Discussion open until July 1, 2009. Separate discussions must be submitted for individual papers. The manuscript for this paper was submitted for review and possible publication on October 18, 2007; approved on April 9, 2008. This paper is part of the ***Journal of Geotechnical and Geoenvironmental Engineering***, Vol. 135, No. 2, February 1, 2009. ©ASCE, ISSN 1090-0241/2009/2-209–223/$25.00.

**Table 1.** Different GCLs in the Database

| GCL product | GCL description | Product label[a] | GCL reinforcement label[b] | Upper carrier geotextile[c] | Lower carrier geotextile[c] |
|---|---|---|---|---|---|
| Bentomat (Arlington, IL) ST | Needle-punched, granular bentonite | *A* | np | W | NW |
| Claymax (Arlington, IL) 500SP | Stitch-bonded, granular bentonite | *B* | sb | W | W |
| Bentofix (Houston, TX) NS | Thermally locked, needle-punched, powdered bentonite | *C* | tl | W | NW |
| Bentofix NW | Thermally locked, needle-punched, powdered bentonite | *D* | tl | NW | NW |
| Bentofix NWL | GCL *D* with lower bentonite mass per unit area | *E* | tl | NW | NW |
| Claymax 200R | Unreinforced, granular bentonite | *F* | u | W | W |
| Bentomat DN | Needle-punched, granular bentonite | *H* | np | NW | NW |

[a]Product label is consistent with Zomberg et al. (2005).

[b]np=needle punched, tl=thermally locked needle punched, sb=stitch bonded, *u*=unreinforced.

[c]W=woven carrier geotextile, NW=nonwoven carrier geotexile.

relationships between GCL internal and GCL-GM interface shear strength.

## Database

### Data Source

The large-scale direct shear tests in the GCLSS database were performed between 1992 and 2003 by the Soil-Geosynthetic Interaction laboratory, currently operated by SGI Testing Services (SGI). It should be noted that procedures used for all GCL direct shear tests conducted by SGI over the period 1992 to 2003 are consistent with ASTM D6243 and has been approved in 2008 (ASTM 2008), even though this standard was and originally between only and approved (and originally approved in 1998). Most tests in the GCLSS database were conducted for commercial purposes and, consequently, the test characteristics and scope were defined by project-specific requirements. Test conditions reported for each series in the GCLSS database include hydration time ($t_h$), consolidation time ($t_c$), normal stress during hydration ($\sigma_h$), normal stress during shearing ($\sigma_n$), and shear displacement rate (SDR).

### Materials

Direct shear test results in the GCLSS database include 40 GCL-GM interfaces between eight GCL products (seven reinforced and one unreinforced) and seven GM types (from nine manufacturers). Table 1 summarizes the GCLs used in this study and provides a short description of the reinforcement characteristics, bentonite characteristics (powdered or granular), and carrier geotextiles. The unreinforced GCL investigated in this study (GCL *F*) consists of an adhesive-bonded bentonite core attached to two woven polypropylene geotextiles. The stitch-bonded GCL investigated in this study (GCL *B*) consists of a bentonite layer stitched using synthetic yarns between two woven polypropylene carrier geotextiles. This GCL is no longer produced in the U.S. The needle-punched GCLs investigated in this study (GCLs *A*, *G*, and *H*) consist of a bentonite layer between two (woven or nonwoven) carrier geotextiles, reinforced by pulling fibers through using a needling board. The fiber reinforcements are typically left entangled on the surface of the top carrier geotextile. Other needle-punched GCL products (GCLs *C*, *D*, and *E*) were thermal locked, which involves heating the GCL surface (Lake and Rowe 2000). For simplicity, thermal-locked needle-punched GCLs are referred to as thermal-locked GCLs in this paper. This study also evaluates the interface behavior of GCLs with either woven or nonwoven carrier geotextiles. A labeling system was developed to distinguish between the different GCL products, reinforcement alternatives, and the carrier geotextile under investigation in interface testing. The GCL product label is used as a prefix (e.g., *A*, *B*, *C*, *D*, *E*, *F*, or *H*), and a reinforcement label (e.g., u for unreinforced, np for needle punched, sb for stitch bonded, or tl for thermally locked needle punched) and a label for the carrier geotextile being sheared against the geomembrane to the right of a dash (e.g., NW or W) are included in parenthesis. For example, if the woven carrier geotextile side of GCL *A* were under investigation, it would be labeled as GCL *A*(npW), while if its nonwoven carrier geotextile side were under investigation, it would be labeled as GCL *A*(npNW).

**Table 2.** Different GMs in the Database

| GM manufacturer | Manufacturing approach | Texturing approaches | GM manufacturer label | GM polymers evaluated from each manufacturer[a] |
|---|---|---|---|---|
| Oxychem (Dallas, TX) | Sheet calend. | Smooth | *r* | S/PVC |
| GSE (Houston, TX) | Blown film | Smooth and coextruded | *s* | T/HDPE, T/LLDPE, S/VLDPE |
| NSC (Galesburg, IL) | Blown film | Smooth and coextruded | *t* | T/HDPE, T/VLDPE, T/LLDPE, S/HDPE |
| Polyflex (Grand Prairie, TX) | Blown film | Smooth and coextruded | *u* | T/HDPE, T/VLDPE, T/LLDPE, S/VLDPE, S/LDPE, S/HDPE |
| Serrot (Huntington Beach, CA) | Blown film | Coextruded | *v* | T/HDPE |
| SLT (Woodlands, TX) | Die extrusion | Coextruded | *w* | T/HDPE |
| Watersaver (Denver, CO) | Sheet calend. | Smooth | *x* | S/PVC |
| EL (Tolleson, AZ) | Sheet calend. | Faille finish | *y* | T/PVC |
| EPI (Mancelona, MI) | Sheet calend. | Smooth | *z* | S/PVC |

[a]Prefix "T" is for a textured surface, prefix "S" is for a smooth surface.

Table 2 summarizes the products from different GM manufacturers used in this study, and shows the GM polymer types and texture (textured or smooth surfaces) investigated in this study. Polyethylene (PE) is the most common polymer, as it is predominantly used in landfill applications. This study includes, in order of increasing flexibility, high density polyethylene (HDPE), linear low density polyethylene (LLDPE), and very-low density polyethylene (VLDPE) polymers. In addition, polyvinyl chloride (PVC) GMs, which are comparatively more flexible than PE GMs, were also evaluated in this study. The asperity heights of the textured GMs were not measured consistently in the database, as the tests were conducted for commercial purposes. Nonetheless, some studies (Triplett and Fox 2001; Ivy 2003; McCartney et al. 2005) indicate that asperity height can have an important influence on interface shear strength. A labeling system was also developed to distinguish between the GM manufacturers, textured and smooth surfaces, and polymer types. The manufacturing label is used as a prefix (e.g., r through z), while a texturing label (e.g., T for textured and S for smooth) and a polymer label are included in parenthesis. For example, if the textured side of an HDPE GM s was under investigation, it would be labeled as GM s(T/HDPE).

The direct shear equipment used in this study is similar to that reported by Zornberg et al. (2005). The bottom half of the shear box was filled with concrete sand, which provided a level surface for placement of the GM. The GM was secured with clamps to the bottom shear box. The GCL specimen was attached to a porous rigid substrate by wrapping extensions of the upper carrier geotextile (and occasionally lower carrier geotextile) around the rigid porous substrate, then placing another rigid porous substrate to provide a frictional connection. This assembly was placed in the upper half of the shear box. The rigid porous substrates have steel gripping teeth that allow shear stress transfer to the GCL by minimizing slippage between the carrier geotextiles and the substrates. Conditioning of specimens for GCL-GM shear strength testing involves hydration and (in some cases) subsequent consolidation of the bentonite core of the GCL while in contact with the GM. The specimen and rigid substrates were placed outside the direct shear device under the specified normal stress $\sigma_h$ and soaked in tap water during the specified $t_h$. This assembly was then transferred to the direct shear device. The shearing normal stress ($\sigma_n$), which was often equal to $\sigma_h$, was subsequently applied. When $\sigma_h$ was less than $\sigma_n$ (i.e., to simulate field conditions representative of bottom liners), the normal stress was slowly ramped up from $\sigma_h$ to $\sigma_n$, and pore pressures were allowed to dissipate during a consolidation period ($t_c$).

Shearing was conducted after GCL conditioning by applying a shear load to maintain a constant displacement rate. The maximum shear stress $\tau_p$ and the shear stress at large displacement $\tau_{ld}$ were defined for each test from the measured shear stress-displacement curve. The SDR used for most tests in the GCLSS database was 1.0 mm/min. While relatively fast for guaranteeing drained conditions as anticipated in the field, a SDR of 1.0 mm/min is typically used in engineering practice because of time and cost considerations (Triplett and Fox 2001; Fox and Stark 2004). Interface tests were also conducted using slower displacement rates (as low as 0.025 mm/min), but unlike GCL internal tests (Zornberg et al. 2005), the SDR showed little effect on the GCL-GM interface shear strength values. This is consistent with observations by Triplett and Fox (2001). Shearing was typically terminated when either a displacement of 75 mm or a constant $\tau_{ld}$ value was reached. In the tests reported in this database, failure was always observed along the GCL-GM interface. Although this test forced failure to occur along this interface, the GCL internal shear strength may be greater than the GCL-GM interface shear strength as shown by some results in the database. Testing was conducted under room temperature conditions, so shear strength values should be used carefully if extrapolated to high or low temperature environments.

## Analysis of Results from Tests on Different GCL and GM Materials

This section summarizes the analyses conducted to evaluate the effect of GCL type, GM type, and testing procedures on GCL-GM interface shear strength. Specifically, these analyses provide: (i) comparison of the shear stress-displacement behavior of different interfaces; (ii) a simplified representation of GCL-GM interface shear strength suitable for comparison among different interfaces; and (iii) conventional representation of GCL-GM interface shear strength.

### *Shear Stress-Displacement Behavior*

Typical shear stress-displacement curves for the interfaces between an 80-mil textured HDPE GM s and the woven carrier geotextiles of GCLs *A* (needle punched), and *B* (stitch bonded), and *C* (thermal locked) are shown in Figs. 1(a–c), respectively. The three interfaces shown in these figures were tested using the same $\sigma_n$ (310.3 kPa), same $t_h$ (168 hrs), same $t_c$ (48 hrs), and same SDR (1.0 mm/min). For comparison, the figures also show internal shear stress-displacement curves for GCLs *A*, *B*, and *C* tested under the same conditions (Zornberg et al. 2005). Although the three interface direct shear tests involve the same combination of geosynthetics in contact (woven carrier geotextile of a GCL and a GM), the interface shear-displacement responses are significantly different. Indeed, the curves follow patterns similar to the corresponding internal shear-displacement curves. Specifically, the GCL *A*-GM interface shows a well defined peak (the highest $\tau_p$) and a clear postpeak shear strength loss. This pattern is similar to that for GCL *A* when sheared internally, although it should be noted that the GCL *A*-GM internal $\tau_{ld}$ is lower than the GCL *A*-GM interface $\tau_{ld}$. The GCL *B*-GM interface shows a rapid initial mobilization of shear strength until reaching a "yield" stress level, beyond which less pronounced hardening takes place until reaching $\tau_p$. The displacement at peak for the GCL *B*-GM interface is larger than that observed for the GCL *A-GM* interface and only a little postpeak shear strength loss is observed for larger displacements. This observation may not be the same if GCL *B* were sheared in the cross-machine direction (opposite the direction of the stitches). In this case, the GCL *B*-GM interface also shows a similar shear displacement pattern as the GCL *B* internal curve. The GCL *C*-GM interface shows lower $\tau_p$ than the GCL *A*-GM interface, but both interfaces show a similar $\tau_{ld}$. The GCL *C* internal shear-displacement curve also shows a similar response as the GCL *C*-GM interface curve. It should be noted that GCLs *A* and *C* are reinforced using similar needle-punching techniques and have the same specified peel strength [650 N/m obtained using ASTM D6496, (ASTM 2004)]. Consequently, the differences in behavior can be attributed to the effects of the thermal-locking process of GCL *C*. Although a similar pattern could have been expected among all interface shear-displacement curves (all interfaces involved a woven carrier geotextile and the same textured GM), the GCL-GM interface results show different patterns. However, the pattern of each GCL-GM interface shear displacement curve corresponds with that of the GCL sheared internally.

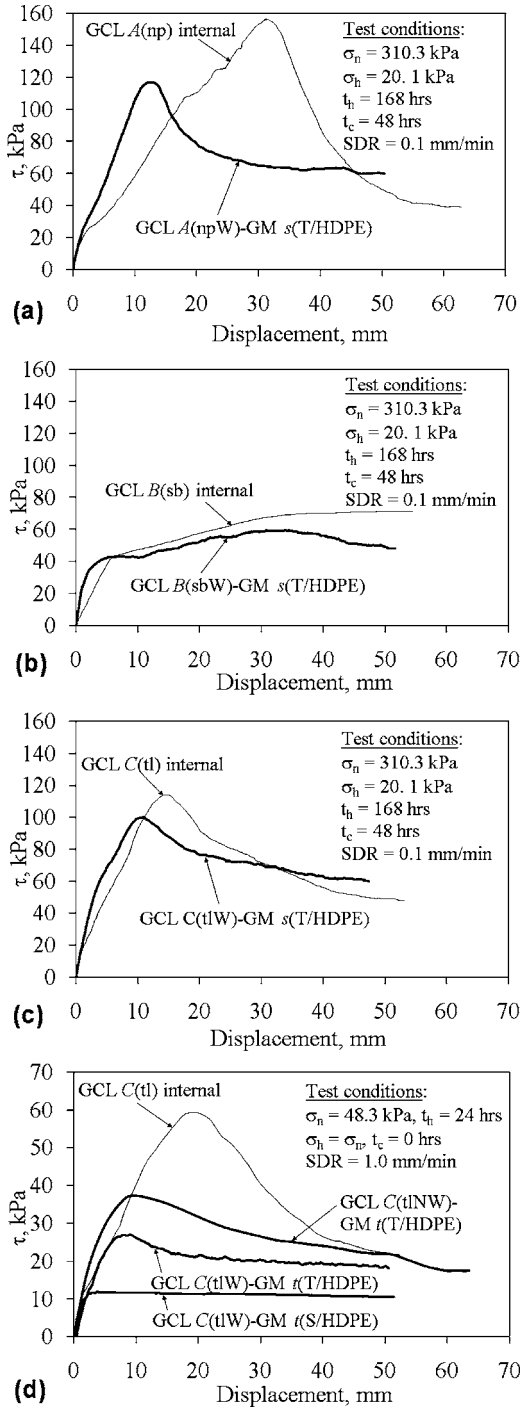


**Fig. 1.** Comparison between shear stress-displacement curves from GCL internal tests and GCL-GM interface tests involving: (a) woven side of GCL *A* (needle punched) with textured HDPE GM *s*, (b) woven side of GCL *B* (stitch bonded) with textured HDPE GM *s*; (c) woven side of GCL *C* (thermally locked) with textured HDPE GM *s*; and (d) nonwoven and woven sides of GCL *C* with textured and smooth HDPE GM *t*

As in the case of internal shear strength (Zornberg et al. 2005), the GCL fiber reinforcement influences the behavior of GCL-GM interfaces.

A comparison between the GCL internal and the GCL-GM interface shear stress-displacement curves is shown in Fig. 1(d) for tests conducted using the same GCL and different GM types.

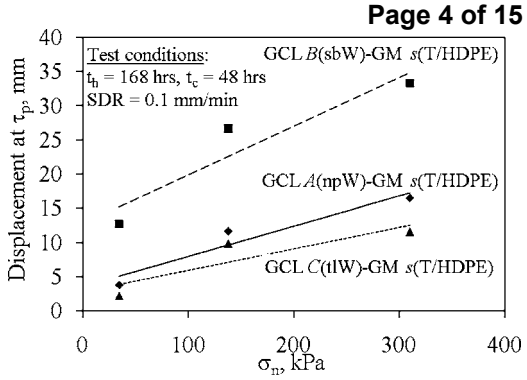


**Fig. 2.** Displacement at peak shear strength as a function of $\sigma_n$ for interfaces between a textured HDPE GM and the woven sides of GCLs *A*, *B*, and *C*

The interface shear-displacement curves were obtained for both the woven and nonwoven sides of GCL *C* and HDPE GM *t* with textured and smooth finishes. The tests were conducted using the same $\sigma_n$ (48.3 kPa), same $t_h$ (24 hrs), same $t_c$ (0 hrs), and same SDR (1.0 mm/min). Consistent with previous observations regarding the responses of interfaces between different GCLs and a textured GM [Fig. 1(a)], the GCL-GM interfaces in Fig. 1(d) show a similar pattern in the shear-displacement curves to that of the corresponding GCL internal test (although lower $\tau_p$). The $\tau_p$ obtained using the woven side of the GCL is below that obtained using the nonwoven side of the GCL. The $\tau_p$ obtained using a smooth GM is significantly lower than the $\tau_p$ obtained using a textured GM. The curve obtained using a smooth GM showed a negligible postpeak shear strength loss (i.e., $\tau_p$ was similar to $\tau_{ld}$).

The displacements at peak shear strength are shown in Fig. 2 for the interface shear tests shown in Figs. 1(a–c), along with the results from additional tests on these interfaces conducted using two other $\sigma_n$ (34.5 and 137.9 kPa). The test results show increasing displacement at peak with increasing $\sigma_n$. Consistent with observations by Triplett and Fox (2001), GCL *B* shows much larger displacement at peak than the other GCL types, a characteristic that may be relevant for displacement-based stability analyses. The trends of the displacement at peak shear strength for the different GCLs are similar to those observed in internal shear tests on the same GCLs (Zornberg et al. 2005).

### *Overall GCL-GM Interface Shear Strength Assessment*

The $\tau_p$ results for all GCL-GM interfaces in the GCLSS database are shown in Fig. 3(a). The wide range of normal stresses at which the interfaces were tested and the scatter in the data are apparent in this figure. The $\tau_{ld}$ data for all GCL-GM interfaces in the GCLSS database are shown in Fig. 3(b). Less scatter is observed in the $\tau_{ld}$ data than that observed in the $\tau_p$ data. As most data points shown in Figs. 3(a and b) correspond to comparatively low $\sigma_n$, Figs. 3(c and d) show a detail of the test results for $\sigma_n$ values below 100 kPa. The results shown in Fig. 3(c) indicate that, unlike GCL internal shear strength results (Zornberg et al. 2005), the interface $\tau_p$ at low normal stress follows a trend approaching zero shear strength at zero normal stress. Consistent with findings of Triplett and Fox (2001), this indicates that cohesion intercept plays a less relevant role than in GCL internal shear strength. Only a slight nonlinearity is observed at low $\sigma_n$. Table 3 summarizes the shear strength parameters ($c_p$, $\phi_p$, $c_{ld}$, $\phi_{ld}$) for the 67 peak ($\tau_p$) and large-displacement ($\tau_{ld}$) failure envelopes (FEs).

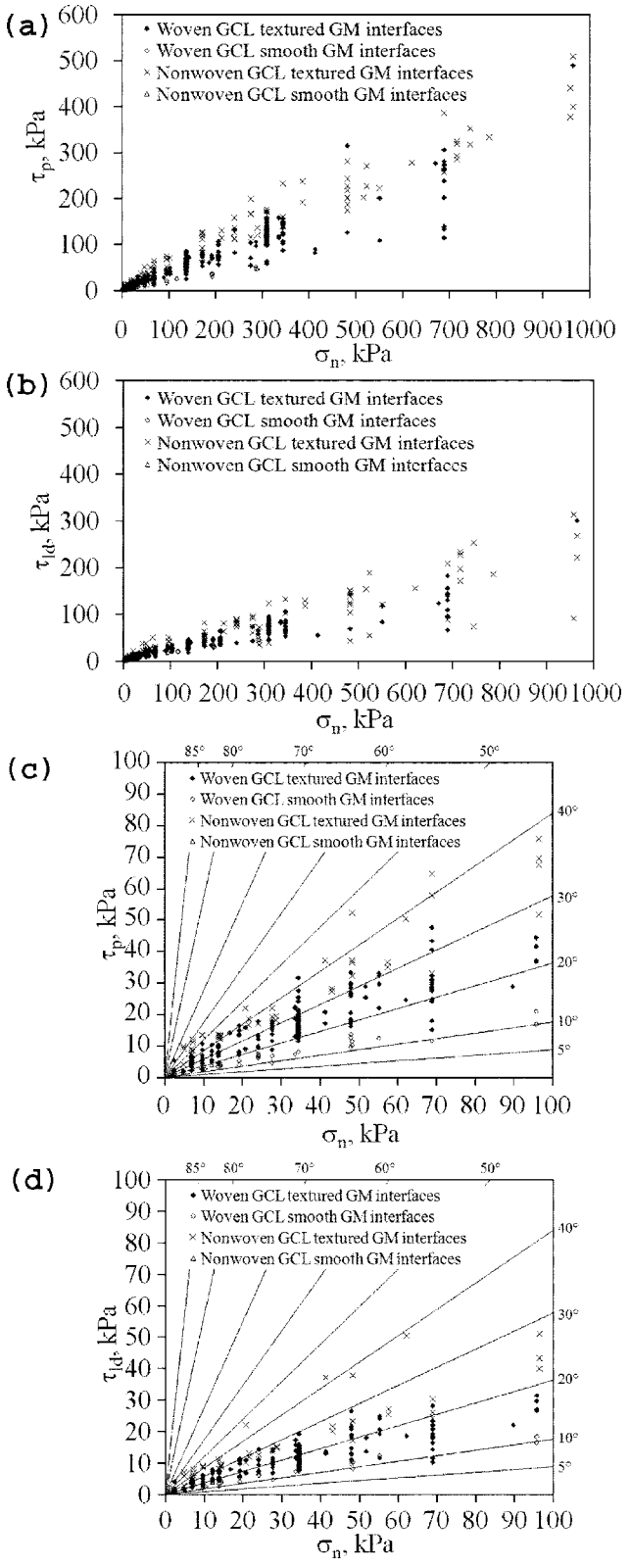


**Fig. 3.** Shear strength results for all GCL-GM interfaces: (a) peak shear strength; (b) large-displacement shear strength; (c) peak shear strength (scaled); and (d) large-displacement shear strength (scaled)

The shear strength parameters were defined using linear regression of $\tau_p$ versus. $\sigma_n$, with the $R^2$ values in the regression exceeding 0.95.

The test results for all GCL-GM interfaces were grouped into 36 data sets defined according to the GM and GCL types as well as the GCL carrier geotextile type tested (woven or nonwoven). Table 4 summarizes the information about each data set, and provides the shear strength parameters for the peak and large-displacement envelopes ($c_p$, $\phi_p$, $c_{ld}$, $\phi_{ld}$). These GCL-GM interface data sets define preliminary shear strength values, as they do not account for the effect of GCL conditioning or GM asperity height. Comparison among the 36 GCL sets is aided by calculating the peak shear strength at a reference normal stress of 50 kPa ($\tau_{50}$) using the GCL-GM interface data set envelopes. The $\tau_{50}$ peak shear strength is used to provide a single value with which to compare different data sets. A reference stress of 50 kPa is used to be consistent with that reported by Zornberg et al. (2005), who found that there were different trends in GCL internal shear strength under normal stresses above and below the swell pressure of GCLs. Although Zornberg et al. (2005) chose reference normal stresses of 50 and 300 kPa to bracket the approximate value of the swell pressure (~150 kPa), a single reference stress of 50 kPa is used in this study because the GCL-GM interface shear strength data can be well represented by a linear envelope. In order to quantify the variability of the shear strength for each GCL data set, the range of shear strength values was defined for this reference normal stress. Specifically, the lowest and highest shear strength values were defined using the individual failure envelopes (FE in Table 3) of each data set. Because of the small cohesion values of the interface shear strength envelopes, the general trends in the database can also be inferred from inspection of the $\phi$ values in Table 4. The following observations can be made regarding the peak shear strength of GCL-GM interfaces at a reference stress of 50 kPa:

- Consistent with the results of previous studies, woven GCL-textured GM interfaces generally have lower peak shear strength than nonwoven GCL-textured GM interfaces (Triplett and Fox 2001). The peak shear strength of all woven GCL-textured GM interfaces in the database (Set SS1) is characterized by $c_p$=5.9 kPa and $\phi_p$=19.5° ($\tau_{50}$=24 kPa), while the peak shear strength of all nonwoven GCL-textured GM interfaces in the database (Set SS2) is characterized by $c_p$ =16.5 Kpa and $\phi_p$=23.2° ($\tau_{50}$=38 kPa). The peak shear strength involving textured GM interfaces show significant scatter [$\tau_{50}$ (Set SS1) ranges from 15 to 69 kPa and $\tau_{50}$ (Set SS2) ranges from 26 to 79 kPa].
- Woven GCL-smooth GM interfaces generally have lower peak shear strength than nonwoven GCL-smooth GM interfaces. The peak shear strength of all woven GCL-smooth GM interfaces in the database (Set SS3) is characterized by $c_p$ =2.3 kPa and $\phi_p$=9.3° ($\tau_{50}$=10 kPa), while the peak shear strength of all nonwoven GCL-textured GM interfaces in the database (Set SS4) is characterized by $c_p$=0.4 kPa and $\phi_p$ =16.8° ($\tau_{50}$=16 kPa). Less scatter is observed in the peak strength of interfaces involving smooth GMs than in those involving textured GMs [$\tau_{50}$ (Set SS3) ranges from 9 to 17 kPa; $\tau_{50}$ (Set SS4) ranges from 14 to 17 kPa].
- Comparison of the values for Sets SS1, SS2, SS3, and SS4 indicates that peak shear strength of interfaces involving textured GMs is higher than that of interfaces involving smooth GMs (for both woven and nonwoven GCLs), similar to observations by Triplett and Fox (2001). Further, based on results reported by Zornberg et al. (2005), the average peak GCL internal shear strength ($\tau_{50}$=55 kPa) is higher than the average shear strength of the interface between GCLs and textured or smooth GMs. However, the GCL internal shear strength variability observed by Zornberg et al. (2005) is consistent with

**Table 3.** Summary of GCL-GM Interface Shear Envelopes in the Database

| | Interface details | | | | Text conditions | | | | | Peak | | | Large displacement | | |
|---|---|---|---|---|---|---|---|---|---|---|---|---|---|---|---|
| Failure envelope | GCL tested | GM tested | GM thickness (mil) | Number of tests | SDR (mm/min) | $t_h$ (hrs) | $\sigma_h$[a] (kPa) | $t_c$ (hrs) | $\sigma_s$ range (kPa) | $c_p$ (kPa) | $\phi_p$ (°) | $s_p$[b] (kPa) | $c_{ld}$ (kPa) | $\phi_{ld}$ (°) | $s_{ld}$[b] (kPa) |
| FE 1 | *A*(npW) | *s*(T/HDPE) | 80 | 3 | 1.0 | 0 | 0.0 | 0 | 241–965 | 45.5 | 25.3 | 49.8 | 6.6 | 16.8 | 11.6 |
| FE 2 | *A*(npW) | *v*(T/HDPE) | 60 and 80 | 36 | 1.0 | 24 | $\sigma_n$ | 0 | 6.9–689 | 5.8 | 20.7 | 15.9 | 6.7 | 11.0 | 9.0 |
| FE 3 | *A*(npW) | *s*(T/HDPE) | 60 and 80 | 18 | 1.0 | 24 | $\sigma_n$ | 0 | 6.9–483 | 4.1 | 21.4 | 15.2 | 3.5 | 11.9 | 12.9 |
| FE 4 | *A*(npW) | *w*(T/HDPE) | 80 | 3 | 1.0 | 24 | $\sigma_n$ | 0 | 38–345 | 22.4 | 20.2 | 10.4 | 14.0 | 9.1 | 3.9 |
| FF.5 | *A*(npW) | *u*(T/HDPE) | 60 | 3 | 1.0 | 48 | $\sigma_n$ | 0 | 51–103 | 8.3 | 18.2 | 28.7 | 3.1 | 16.7 | 10.8 |
| FE 6 | *A*(npW) | *w*(TMDPE) | 80 | 3 | 1.0 | 48 | 4.8 | 0 | 89–276 | 11.8 | 12.8 | 41.6 | 12.8 | 6.4 | 44.5 |
| FE 7 | *A*(npW) | *s*(T/HDPE) | 60 | 6 | 1.0 | 48 | $\sigma_n$ | 0 | 51–345 | 16.4 | 12.2 | 41.6 | 6.7 | 8.4 | 17.6 |
| FE 8 | *A*(npW) | *u*(T/HDPE) | 60 | 10 | 0.2 | 24 | 57.5 | 0 | 9.6–287 | 2.6 | 19.4 | 3.5 | 4.4 | 11.7 | 3.1 |
| FE 9 | *A*(npW) | *s*(T/HDPE) | 60 | 3 | 0.1 | 48 | $\sigma_n$ | 0 | 68–345 | 0.0 | 19.3 | 1.7 | 6.7 | 9.6 | 0.5 |
| FE 10 | *A*(npW) | *t*(T/HDPE) | 60 | 3 | 1.0 | 72 | 6.9 | 24 | 172–690 | 23.8 | 9.4 | 3.3 | 23.1 | 3.8 | 4.9 |
| FE 11 | *A*(npW) | *v*(T/HDPE) | 80 | 3 | 1.0 | 24 | 68.9 | 12 | 138–552 | 3.1 | 19.7 | 2.8 | 12.1 | 11.1 | 8.7 |
| FE 12 | *A*(npW) | *s*(T/HDPE) | 80 | 162 | 0.1 | 168 | 20.7 | 48 | 34–310 | 6.0 | 20.5 | 10.5 | 5.2 | 12.7 | 6.0 |
| FE 13 | *B*(sbW) | *s*(T/HDPE) | 60 | 6 | 1.0 | 0 | 0.0 | 0 | 12–48 | 1.6 | 23.3 | 3.4 | 2.0 | 17.7 | 3.3 |
| FE 14 | *B*(sbW) | *t*(T/HDPE) | 60 | 5 | 1.0 | 0 | 0.0 | 0 | 2.4–48 | 1.3 | 31.2 | 0.9 | 1.7 | 22.5 | 1.1 |
| FE 15 | *B*(sbW) | *t*(T/HDPE) | 40 and 60 | 18 | 1.0 | 24 | 13.8 | 0 | 2.4–103 | 3.9 | 17.9 | 3.2 | 4.1 | 9.8 | 2.8 |
| FE 16 | *B*(sbW) | *s*(T/HDPE) | 60 | 9 | 1.0 | 24 | $\sigma_n$ | 0 | 68–690 | 12.3 | 10.4 | 15.6 | 6.7 | 7.7 | 6.2 |
| FE 17 | *B*(sbW) | *s*(T/HDPE) | 40 and 60 | 6 | 1.0 | 48 | 12.0 | 0 | 6.9–48 | 0.4 | 19.3 | 1.0 | 1.8 | 12.0 | 0.9 |
| FE 18 | *B*(sbW) | *s*(T/HDPE) | 80 | 6 | 0.1 | 168 | 20.7 | 48 | 34–310 | 9.2 | 9.8 | 4.9 | 8.7 | 7.3 | 3.5 |
| FE 19 | *C*(tlW) | *t*(T/HDPE) | 40 | 4 | 1.0 | 0 | 0.0 | 0 | 16–670 | 13.9 | 21.8 | 9.8 | 12.8 | 9.9 | 10.4 |
| FE 20 | *C*(tlW) | *t*(T/HDPE) | 60 | 3 | 1.0 | 1 | $\sigma_n$ | 0 | 20–62 | 1.2 | 20.9 | 0.3 | 1.1 | 15.8 | 0.3 |
| FE 21 | *C*(tlW) | *t*(T/HDPE) | 60 | 3 | 1.0 | 24 | 13.8 | 0 | 34–138 | 0.0 | 23.3 | 0.7 | 1.0 | 16.2 | 1.3 |
| FE 22 | *C*(tlW) | *t*(T/HDPE) | 60 | 10 | 0.2 | 24 | 57.5 | 0 | 9.6–335 | 7.9 | 18.3 | 4.6 | 4.9 | 13.1 | 3.3 |
| FE 23 | *C*(tlW) | *t*(T/HDPE) | 60 | 3 | 0.025 | 24 | 13.8 | 0 | 34–138 | 0.0 | 22.6 | 1.5 | 0.0 | 18.2 | 0.7 |
| FE 24 | *C*(tlW) | *s*(T/HDPE) | 80 | 6 | 0.1 | 168 | 20.7 | 48 | 34–310 | 3.7 | 17.9 | 3.8 | 3.3 | 10.4 | 3.7 |
| FE 25 | *B*(sbW) | *u*(T/VLDPE) | 60 | 6 | 1.0 | 0 | 0.0 | 0 | 12–48 | 0.8 | 31.9 | 1.7 | 0.5 | 26.1 | 0.9 |
| FE 26 | *B*(sbW) | *t*(T/VLDPE) | 60 | 5 | 1.0 | 24 | 4.8 | 0 | 2.4–48 | 2.5 | 30.3 | 0.4 | 1.7 | 23.5 | 0.8 |
| FE 27 | *B*(sbW) | *u*(T/VLDPE) | 60 | 3 | 1.0 | 48 | 12.0 | 0 | 12–48 | 4.7 | 18.6 | 1.3 | 5.5 | 11.3 | 1.1 |
| FE 28 | *A*(npW) | *u*(T/VLDPE) | 40 | 3 | 1.0 | 24 | $\sigma_n$ | 0 | 2.4–19.2 | 4.1 | 33.2 | 0.2 | 2.6 | 24.2 | 0.2 |
| FE 29 | *A*(npW) | *u*(T/LLDPE) | 40 | 4 | 1.0 | 72 | $\sigma_n$ | 0 | 6.9–55.2 | 2.2 | 28.8 | 0.3 | 1.2 | 23.5 | 0.8 |
| FE 30 | *A*(npW) | *t*(T/LLDPE) | 40 | 4 | 1.0 | 72 | $\sigma_n$ | 0 | 6.9–55.2 | 2.5 | 26.3 | 0.5 | 1.6 | 19.3 | 0.8 |
| FE 31 | *A*(npW) | *s*(T/LLDPE) | 40 | 3 | 1.0 | 72 | 0.0 | 48 | 4.8–19.2 | 0.2 | 20.6 | 0.8 | 0.6 | 15.8 | 0.1 |
| FE 32 | *C*(tlW) | *u*(T/LLDPE) | 40 | 4 | 1.0 | 72 | $\sigma_n$ | 0 | 6.9–55.2 | 2.2 | 29.3 | 0.5 | 2.4 | 21.9 | 0.6 |
| FE 33 | *C*(tlW) | *t*(T/LLDPE) | 40 | 4 | 1.0 | 72 | $\sigma_n$ | 0 | 6.9–55.2 | 0.1 | 27.9 | 0.2 | 1.1 | 18.3 | 0.4 |
| FE 34 | *B*(sbW) | *t*(S/HDPE) | 60 | 5 | 1.0 | 24 | 4.8 | 0 | 2.4–48 | 0.5 | 11.1 | 0.2 | 0.5 | 11.1 | 0.2 |
| FE 35 | *B*(sbW) | *u*(S/HDPE) | 60 | 10 | 0.2 | 24 | 57.5 | 0 | 9.6–287 | 3.9 | 9.2 | 0.5 | 2.9 | 9.2 | 0.5 |
| FE 36 | *C*(tlW) | *t*(S/HDPE) | 60 | 3 | 1.0 | 48 | 10.3 | 0 | 10–69 | 0.9 | 8.8 | 2.1 | 0.9 | 8.8 | 2.1 |
| FE 37 | *C*(tlW) | *t*(S/HDPE) | 60 | 10 | 0.2 | 24 | 55.2 | 0 | 9.7–290 | 3.6 | 8.6 | 2.6 | 2.4 | 8.0 | 2.1 |
| FE 38 | *A*(npW) | *s*(S/VLDPE) | 40 | 2 | 1.0 | 24 | 4.8 | 0 | 14.4–23.9 | 0.2 | 14.0 | 0.0 | 0.2 | 14.0 | 0.0 |
| FE 39 | *A*(npW) | *u*(S/VLDPE) | 40 | 3 | 1.0 | 24 | $\sigma_n$ | 0 | 2.4–19.2 | 0.4 | 14.1 | 0.4 | 0.4 | 14.1 | 0.4 |
| FE 40 | *A*(npW) | *u*(S/VLDPE) | 60 | 3 | 1.0 | 24 | $\sigma_n$ | 0 | 13.8–34.5 | 0.6 | 13.1 | N/A | 0.0 | 13.1 | N/A |
| FE 41 | *F*(uW) | *u*(S/VLDPE) | 40 | 3 | 1.0 | 168 | $\sigma_n$ | 0 | 13.8–55.2 | 0.7 | 12.1 | 0.8 | 0.7 | 12.1 | 0.8 |
| FE 42 | *A*(npW) | *y*(T/PVC) | 40 | 3 | 1.0 | 48 | $\sigma_n$ | 0 | 4.8–24 | 0.2 | 18.5 | 0.6 | 0.2 | 18.5 | 0.6 |
| FE 43 | *A*(npW) | *x*(S/PVC) | 30 | 3 | 1.0 | 24 | 4.8 | 0 | 13.8–41 | 1.7 | 16.7 | 0.2 | 1.7 | 16.7 | 0.2 |
| FE 44 | *A*(npW) | *z*(S/PVC) | 40 | 3 | 0.05 | 24 | 0.0 | 48 | 2.4–36 | 0.6 | 15.9 | 0.1 | 0.6 | 15.9 | 0.1 |
| FE 45 | *A*(npNW) | *s*(T/HDPE) | 80 | 3 | 1.0 | 0 | 0 | 0 | 241–965 | 44.8 | 25.7 | 4.4 | 3.1 | 15.1 | 10.1 |
| FE 46 | *A*(npNW) | *w*(T/HDPE) | 80 | 3 | 1.0 | 0 | 0 | 0 | 69–276 | 18.5 | 33.0 | 3.7 | 7.4 | 16.7 | 5.6 |
| FE 47 | *A*(npNW) | *t*(T/HDPE) | 80 | 3 | 1.0 | 24 | $\sigma_n$ | 0 | 48–386 | 22.1 | 28.6 | 9.4 | 24.3 | 15.1 | 1.5 |
| FE 48 | *A*(npNW) | *w*(T/HDPE) | 80 | 3 | 1.0 | 24 | 172 | 0 | 69–276 | 24.0 | 27.6 | 5.3 | 7.2 | 13.3 | 1.4 |
| FE 49 | *A*(npNW) | *v*(T/HDPE) | 80 | 5 | 1.0 | 48 | 4.8 | 0 | 14–276 | 8.0 | 30.3 | 3.1 | 5.4 | 18.2 | 3.6 |
| FE 50 | *A*(npNW) | *t*(T/HDPE) | 60 | 4 | 1.0 | 72 | $\sigma_n$ | 0 | 69–517 | 7.4 | 20.8 | 1.9 | 1.9 | 16.3 | 4.9 |
| FE 51 | *A*(npNW) | *v*(T/HDPE) | 80 | 3 | 1.0 | 24 | 345 | 14 | 621–965 | 61.4 | 19.2 | 2.5 | 34.3 | 11.0 | 0.9 |
| FE 52 | *A*(npNW) | *v*(T/HDPE) | 80 | 3 | 1.0 | 24 | 68.9 | 12 | 138–552 | 11.7 | 20.8 | 1.1 | 3.1 | 12.0 | 2.4 |
| FE 53 | *A*(npNW) | *v*(T/HDPE) | 60 | 3 | 1.0 | 24 | 0 | 24 | 4.8–23.9 | 1.1 | 33.8 | 0.1 | 0.4 | 27.1 | 0.1 |

**Table 3.** (*Continued.*)

| | Interface details | | | | Text conditions | | | | | Peak | | | Large displacement | | |
|---|---|---|---|---|---|---|---|---|---|---|---|---|---|---|---|
| Failure envelope | GCL tested | GM tested | GM thickness (mil) | Number of tests | SDR (mm/min) | $t_h$ (hrs) | $\sigma_h$[a] (kPa) | $t_c$ (hrs) | $\sigma_s$ range (kPa) | $c_p$ (kPa) | $\phi_p$ (°) | $s_p$[b] (kPa) | $c_{ld}$ (kPa) | $\phi_{ld}$ (°) | $s_{ld}$[b] (kPa) |
| FE 54 | *C*(tlNW) | *t*(T/HDPE) | 60 | 3 | 1.0 | 1 | 21 | 0 | 21–62 | 8.3 | 34.3 | 0.8 | 8.3 | 34.3 | 0.8 |
| FE 55 | *C*(tlNW) | *t*(T/HDPE) | 40 and 80 | 9 | 1.0 | 24 | $\sigma_n$ | 0 | 7.2–386 | 7.4 | 25.9 | 3.4 | 4.6 | 16.2 | 1.6 |
| FE 56 | *C*(tlNW) | *v*(T/HDPE) | 60 | 3 | 1.0 | 24 | $\sigma_n$ | 0 | 6.9–35 | 3.0 | 32.2 | 0.2 | 2.2 | 20.8 | 0.2 |
| FE 57 | *D*(tlNW) | *v*(T/HDPE) | 80 | 5 | 1.0 | 24 | $\sigma_n$ | 0 | 97–958 | 53.7 | 19.0 | 14.0 | 34.0 | 3.0 | 10.9 |
| FE 58 | *D*(tlNW) | *t*(T/HDPE) | 60 | 6 | 1.0 | 24 | 0.0 | 24 | 97–482 | 33.5 | 17.2 | 10.7 | 32.3 | 4.7 | 25.2 |
| FE 59 | *D*(tlNW) | *t*(T/HDPE) | 80 | 6 | 1.0 | 24 | 69 | 24 | 6.9–690 | 14.1 | 20.3 | 14.4 | 13.1 | 6.9 | 11.8 |
| FE 60 | *E*(tlNW) | *t*(T/HDPE) | 40 | 8 | 1.0 | 336 | $\sigma_n$ | 0 | 14–58 | 4.2 | 28.6 | 1.0 | 3.6 | 21.7 | 0.7 |
| FE 61 | *H*(tlNW) | *x*(T/HDPE) | 60 and 80 | 20 | 1.0 | 24 | $\sigma_n$ | 0 | 48–958 | 22.1 | 22.6 | 18.4 | 12.4 | 16.2 | 19.2 |
| FE 62 | *H*(tlNW) | *t*(T/HDPE) | 80 | 3 | 1.0 | 24 | 3.4 | 24 | 172–690 | 4.8 | 32.2 | 0.4 | 43.8 | 24.9 | 72.8 |
| FE 63 | *H*(tlNW) | *s*(T/HDPE) | 80 | 3 | 1.0 | 24 | 3.4 | 24 | 6.9–28 | 48.6 | 26.3 | 17.1 | 43.8 | 13.6 | 6.4 |
| FE 64 | *H*(tlNW) | *s*(T/HDPE) | 40 | 6 | 0.25 | 96 | 0 | 24 | 4.8–9.6 | 5.7 | 39.4 | 0.4 | 4.4 | 24.5 | 0.5 |
| FE 65 | *H*(tlNW) | *z*(S/PVC) | 40 | 2 | 1 | 24 | 4.8 | 0 | 14–24 | 0.3 | 18.0 | N/A | 0.1 | 17.8 | N/A |
| FE 66 | *H*(tlNW) | *r*(S/PVC) | 40 | 3 | 1 | 24 | $\sigma_n$ | 0 | 4.8–24 | 0.8 | 15.1 | 0.0 | 0.8 | 15.1 | 0.1 |

[a]$\sigma_h=\sigma_a$ means that the hydration stress used for each specimen equals the normals tress to be used during shearing.

[b]$s_p$ and $s_{kl}$=standard deviationsof the lienar regressions for the peak and large displacement shear strength data, respectively.

that of GCL-textured GM interfaces ($\tau_{50}$ ranging from 13 to 71 kPa), and it is possible that the GCL internal shear strength may be lower than the GCL-GM interface shear strength.

- Comparison of Sets SS5–SS12 in Table 4 indicates that interfaces involving flexible GMs lead to higher shear strength than those involving rigid GMs. Specifically, interfaces involving the relatively flexible VLDPE GMs (Set SS5, $\tau_{50}=29$ kPa show higher strength than interfaces involving the relatively rigid HDPE GMs (Set SS7, $\tau_{50}=24$ kPa. The interfaces involving textured LLDPE GMs (Set SS6), $\tau_{50}=28$ kPa show intermediate strength values while the faille-finish PVC GMs (Set SS8, $\tau_{50}=17$ kPa) show the lowest shear strength due to their smaller asperity height. Although the textured HDPE GM interfaces in this comparison were tested over a much wider range of normal stresses, investigations considering only those tests conducted at normal stresses less than 50 kPa led to similar conclusions. Nonetheless, these conclusions should only be considered for low normal stress applications. Among the tests involving smooth GMs, interfaces with flexible PVC GMs (Set SS12) have the highest strength ($\tau_{50}=16$ kPa), while interfaces involving the more rigid smooth HDPE GMs (Set SS11) have the lowest strength ($\tau_{50}=11$ kPa).
- The effect of GCL reinforcement types is evaluated by comparing the results of Sets SS13–SS15 for woven GCL interfaces and the results of Sets SS24–SS28 for nonwoven GCL interfaces. The peak shear strength of the interfaces involving woven needle-punched GCL *A* (Set SS13, $\tau_{50}=23$ kPa) is similar to that of interfaces involving woven thermal-locked GCL *C* (Set SS15, $\tau_{50}=21$ kPa) but higher than that of interfaces involving woven stitch-bonded GCL *B* (Set SS14, $\tau_{50}=17$ kPa). This trend is consistent with that observed for the internal shear strength of the same GCLs (Zornberg et al. 2005). The peak shear strength of interfaces involving nonwoven GCLs (Sets SS24–SS28) is consistently higher than that of interfaces involving woven GCLs.
- For the textured HDPE GMs tested, the interface shear strength results are reasonably independent of the GM manufacturer. This can be evaluated by comparing the results of Sets SS16–SS20 for woven GCL interfaces and of Sets SS29–SS32 for nonwoven GCL interfaces. The interfaces involving a woven GCL and textured HDPE GMs from multiple manufacturers have similar shear strength ($\tau_{50}\approx 23$ kPa). It should be noted that the GMs evaluated in this study were all blown-film geomembranes with texturing consisting of coextruded asperities, so this observation should not be extrapolated to interfaces involving GMs that use structured or calendared texturing. The interfaces involving nonwoven GCL and textured HDPE GMs from multiple manufacturers have similar strength ($\tau_{50}\approx 36$ kPa). Although it appears that the nonwoven interfaces with GM manufacturer *w* were higher, it should be noted that this interface was sheared under unhydrated conditions (FE 46), a feature not captured by this analysis.
- Interface shear strength results are independent of GM thickness. This can be evaluated by comparing Sets SS21–SS23 for woven GCL interfaces and Sets SS34–SS36 for nonwoven GCL interfaces (thicknesses of 40, 60, and 80 mil). Sets SS21–SS23 show a similar $\tau_{50}$ of 23 kPa while Sets SS34–SS36 have a similar $\tau_{50}$ of 31 kPa.

In summary, the results in Table 4 indicate that the peak shear strength values of the GCL-GM interfaces are sensitive to the type of GCL carrier geotextile, the flexibility of different GM polymer types, and the GCL reinforcement type. However, the peak shear strength was not sensitive to the GM manufacturer or GM thickness.

Inspection of $\phi_{ld}$ values shown in Table 4 leads to the following observations regarding the large-displacement shear strength of GCL-GM interfaces:

- The large-displacement friction angles of woven and nonwoven GCL-textured GM interfaces [$\phi_{ld}$ (Set SS1)=11.3° and $\phi_{ld}$ (Set SS2)=13.0°] are lower than the corresponding peak friction angles, indicating substantial postpeak shear strength loss. Instead, the large-displacement friction angles of woven and nonwoven GCL-smooth GM interfaces [$\phi_{ld}$ (Set SS3)=8.8° and $\phi_{ld}$ (Set SS4)=16.9°] are similar to the corresponding peak friction angles indicating little postpeak shear strength loss for interfaces involving smooth GMs. The $\phi_{ld}$ for the smooth GM interfaces in Set SS4 is higher than that in the

**Table 4.** GCL-GM Interface Data Sets for Overall Shear Strength Assessment

| | Set description[a] | | | Peak | | | Large displacement | |
|---|---|---|---|---|---|---|---|---|
| GCL-GM data set | GCL grouping | — | GM grouping | $c_p$ (kPa) | $\phi_p$ (°) | $\tau_{50}$ [Range][b] (kPa) | $c_{ld}$ (kPa) | $\phi_{ld}$ (°) |
| SS1 | Woven (W) | — | Textured (T) | 5.9 | 19.5 | 24 [15 (FE 44) to 69 (FE 1)] | 6.0 | 11.3 |
| SS2 | Nonwoven (NW) | — | T | 16.5 | 23.2 | 38 [26 (FE 50) to 79 (FE 51)] | 12.2 | 13.0 |
| SS3 | W | — | Smooth (S) | 2.3 | 9.3 | 10 [9(FE 36) to 17 (FE 42)] | 2.1 | 8.8 |
| SS4 | NW | — | S | 0.4 | 16.8 | 16 [14 (FE 66) to 17 (FE 65)] | 0.3 | 16.9 |
| SS5 | W | — | T/VLDPE | 3.4 | 27.4 | 29 [21 (FE 27) to 37 (FE 28)] | 2.4 | 21.7 |
| SS6 | W | — | T/LLDPE | 0.8 | 28.8 | 28 [19 (FE 32) to 30 (FE 33)] | 1.0 | 21.3 |
| SS7 | W | — | T/HDPE | 5.9 | 19.4 | 24 [18 (FE 9) to 69 (FE 1)] | 6.0 | 11.3 |
| SS8 | W | — | T/PVC | 1.6 | 16.7 | 17 [17 (FE 43) to 17 (FE 43)] | 1.6 | 16.7 |
| SS9 | W | — | S/VLDPE | 0.4 | 14.1 | 13 [13 (FE 38) to 13 (FE 39)] | 0.4 | 14.1 |
| SS10 | W | — | S/LLDPE | 0.9 | 12.1 | 12 [11 (FE 41) to 11 (FE 40)] | 0.3 | 12.5 |
| SS11 | W | — | S/HDPE | 2.5 | 9.2 | 11 [9 (FE 36) to 11 (FE 35)] | 2.0 | 8.8 |
| SS12 | W | — | S/PVC | 0.8 | 16.4 | 16 [15 (FE 44) to 17 (FE 43)] | 0.8 | 16.4 |
| SS13 | *A*(npW) | — | T/HDPE | 4.4 | 20.9 | 23 [19 (FE 9) to 69 (FE 1)] | 5.8 | 11.8 |
| SS14 | *B*(sbW) | — | T/HDPE | 6.6 | 12.1 | 17 [18 (FE 18) to 23 (FE 13)] | 4.6 | 9.2 |
| SS15 | *C*(tlW) | — | T/HDPE | 2.0 | 21.0 | 21 [20 (FE 24) to 34 (FE 19)] | 7.4 | 11.0 |
| SS16 | W | — | *s*(T/HDPE) | 4.4 | 20.1 | 23 [18 (FE 9) to 69 (FE 1)] | 4.0 | 12.2 |
| SS17 | W | — | *t*(T/HDPE) | 9.2 | 15.6 | 23 [20 (FE 15) to 34 (FE 19)] | 7.6 | 9.6 |
| SS18 | W | — | *u*(T/HDPE) | 3.7 | 19.3 | 21 [20 (FE 8) to 25 (FE 5)] | 5.6 | 12.2 |
| SS19 | W | — | *v*(T/HDPE) | 5.5 | 20.6 | 24 [21 (FE 11) to 25 (FE 2)] | 7.0 | 11.1 |
| SS20 | W | — | *w*(T/HDPE) | 6.6 | 19.5 | 24 [23 (FE 6) to 41 (FE 4)] | 5.4 | 11.2 |
| SS21 | W | — | T/HDPE 40-mil | 2.3 | 22.8 | 23 [18 (FE 17) to 34 (FE 19)] | 4.5 | 10.7 |
| SS22 | W | — | T/HDPE 60-mil | 6.0 | 17.9 | 22 [18 (FE 9) to 32 (FE 14)] | 7.3 | 10.0 |
| SS23 | W | — | T/HDPE 80-mil | 3.9 | 21.0 | 23 [18 (FE 18) to 69 (FE 1)] | 2.9 | 13.0 |
| SS24 | *A*(npNW) | — | T/HDPE | 23.7 | 23.5 | 45 [31 (FE 52) to 79 (FE 51)] | 12.1 | 13.5 |
| SS25 | *C*(tlNW) | — | T/HDPE | 9.0 | 25.8 | 33 [32 (FE 55) to 42 (FE 54)] | 8.8 | 15.9 |
| SS26 | *D*(tlNW) | — | T/HDPE | 21.4 | 20.5 | 40 [33 (FE 59) to 71 (FE 57)] | 25.7 | 4.5 |
| SS27 | *E*(tlNW) | — | T/HDPE | 4.2 | 28.6 | 31 [31 (FE 60) to 31 (FE 60)] | 3.6 | 21.7 |
| SS28 | *H*(npNW) | — | T/HDPE | 15.7 | 23.8 | 38 [36 (FE 62) to 73 (FE 63)] | 9.4 | 16.5 |
| SS29 | NW | — | *s*(T/HDPE) | 14.3 | 23.6 | 36 [43 (FE 61) to 73 (FE 63)] | 11.3 | 15.2 |
| SS30 | NW | — | *t*(T/HDPE) | 12.7 | 23.5 | 34 [31 (FE 60) to 49 (FE 47)] | 14.1 | 11.8 |
| SS31 | NW | — | *v*(T/HDPE) | 18.1 | 21.6 | 38 [31 (FE 52) to 79 (FE 51)] | 20.0 | 5.6 |
| SS32 | NW | — | *w*(T/HDPE) | 21.3 | 30.4 | 51 [50 (FE 48) to 51 (FE 46)] | 7.3 | 15.0 |
| SS34 | NW | — | T/HDPE 40-mil | 7.0 | 25.8 | 31 [31 (FE 60) to 47 (FE 64)] | 4.4 | 20.8 |
| SS35 | NW | — | T/HDPE 60-mil | 12.0 | 21.9 | 32 [26 (FE 50) to 49 (FE 58)] | 9.4 | 14.5 |
| SS36 | NW | — | T/HDPE 80-mil | 10.0 | 23.2 | 31 [31 (FE 52) to 79 (FE 51)] | 15.6 | 12.2 |

[a]Sets do not capture the effect of specimen conditioning and SDR and should not be used for design.

[b]Range defined by the lowest $\tau_p$ (and corresponding FE) and the highest $\tau_p$ (and corresponding FE), defined at a reference stress of $\sigma_n$=50 kPa using the shear strength parameters from Table 4.

other interface sets due to the low normal stresses under which the tests in this set were performed.

- The range of large-displacement shear strength for the GCL-GM interface data sets in Table 4 ($\phi_{ld}$ ranging from 4.5–21.7°), as well as that presented for the individual failure envelopes in Table 3 ($\phi_{ld}$ ranging from 3.0–34.3°), indicates that the variability in large-displacement shear strength is not-negligible. This is consistent with observations made from large-displacement GCL internal shear strength (Zornberg et al. 2005).

### *Assessment of Shear Strength of GCL-GM Interfaces Tested under Similar Conditioning Procedures*

Shear strength characterization for design purposes requires an accurate representation of shear strength envelopes and assessment of the effect of GCL conditioning. Some comparisons between the shear strength of GCL-GM interfaces prepared using similar conditioning procedures are discussed below.

The GCL-GM interface peak failure envelopes obtained for different GCL types (FE 12 for GCL *A*, FE 18 for GCL *B*, FE 24 for GCL *C*) and the same GM *s* tested under the same conditions ($t_h$=168 hrs, $t_c$=48 hrs, SDR=0.1 mm/min) are shown in Fig. 4(a). The shear stress-displacement curves of the tests conducted under $\sigma_n$=310.3 kPa are shown in Fig. 1. Fig. 4(a) also shows the GCL internal failure envelopes obtained using the same GCL conditions (Zornberg et al. 2005). The results in Fig. 4(a) indicate that interfaces including GCL *A*, *C*, and *B* show the highest, intermediate, and lowest $\tau_p$, respectively. This is the same trend shown by the internal peak shear strength of GCLs *A*, *B*, and *C*. The internal peak shear strength envelope of each GCL is consis-

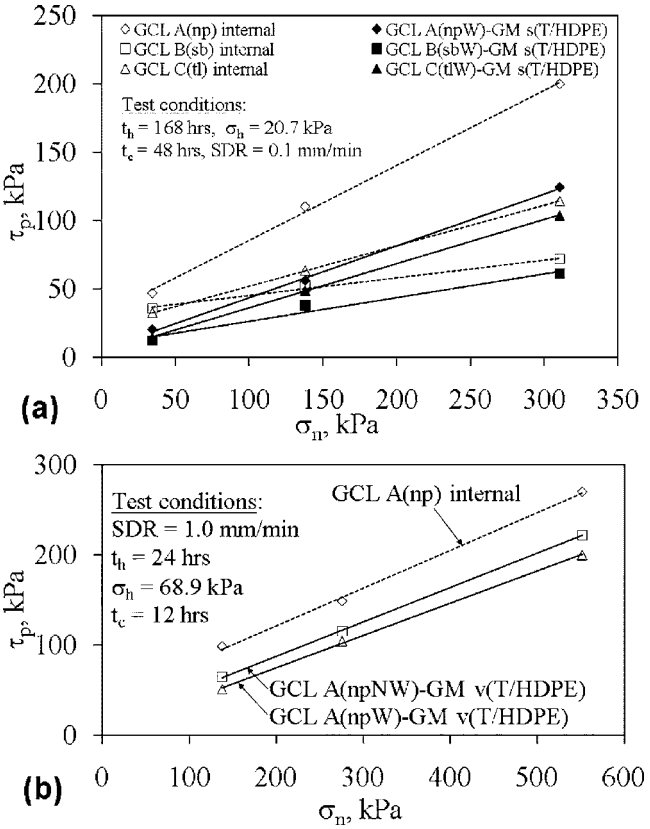


**Fig. 4.** Shear strength envelopes for same conditioning procedures: (a) peak shear strength values for different GCLs sheared internally and along the interface between the woven geotextile of the GCL and a textured HDPE GM; (b) peak shear strength values for GCL *A* sheared internally and along the interface between the woven and nonwoven geotextiles of the GCL and a textured HDPE GM

tently higher than (and approximately parallel to) the corresponding GCL-GM interface shear strength. That is, internal and interface shear strength envelopes involving the same GCLs had similar friction angles. Since the internal shear strength is consistently higher than the interface shear strength, the stability of a GCL-GM composite liner is expected to be governed by the interface shear strength properties if design is based on peak strength. Unlike the peak failure envelopes, the GCL internal and GCL-GM interface large-displacement failure envelopes were found to be similar in both trend and magnitude (see FE 12, 18, and 24 in Table 3). Consequently, the stability of a GCL-GM composite liner could be governed by either the internal or interface shear strength properties if design is based on large-displacement conditions.

As the test conditions and geomembrane were the same in each of the three interfaces whose strengths are shown in Fig. 4(a), the differences in the shear strength results for these three interfaces can be attributed to the characteristics of the GCL. Specifically, the primary differences between the woven carrier geotextile side of GCLs *A*, *B*, and *C* are the surface roughness and the tendency for different amounts of bentonite extrusion during hydration and shearing. With respect to the surfaces of the three GCLs, GCL *A* has fibers from the needle-punching process entangled on the woven carrier geotextile of the GCL, the woven carrier geotextile of GCL *B* is relatively smooth due to the continuous stitched reinforcements, and the woven carrier geotextile of GCL *C* has a burnished surface with small balls of melted fibers from the thermal-locking process. It is possible that the textured asperities of the GM may interact in different ways with the entangled fibers on GCL *A* (i.e., the "Velcro effect") than the smoother surfaces of GCLs *B* and *C* (McCartney et al. 2005). This may be evidenced by the greater postpeak drop in shear stress observed in GCL *A* interface tests than in the other GCL interfaces. Nonetheless, it is also likely that different amounts of bentonite were extruded from the three GCLs into the GCL-GM interface during hydration. Posttest observations of the interfaces after shearing indicates that hydration and subsequent shearing of the GCL-GM interface led to extrusion of bentonite from the GCL into the GCL-GM interface, consistent with observations by Triplett and Fox (2001). Although quantitative measurements of the volume of bentonite extrusion were not made for the tests shown in Fig. 4(a), visual observations from free swell tests indicate that the different reinforcement approaches led to different resistances to swelling. Specifically, the relatively rigid stitches in GCL *B* provided the most resistance to swelling (at least in the vicinity of the stitches), the thermal-locking of GCL *C* was found to provide a relatively uniform, rigid connection between the reinforcing fibers and the woven carrier geotextile, while the loose fiber reinforcements of GCL *A* were found to provide the least resistance to swelling [consistent with observations by Lake and Rowe (2000)]. A higher tendency of the bentonite to extrude through the woven carrier geotextiles is expected in cases where the reinforcement connections are rigid (i.e., more resistant to swelling). Additional research is needed on the quantification of bentonite extrusion from GCLs.

Dry migration of bentonite through the carrier geotextiles of the GCL during shipping and handling also plays a role in GCL-GM interface shear strength. The amount of dry bentonite on the surfaces of the GCL is difficult to quantify and depends on different variables. Nonetheless, greater amounts of dry bentonite were visible on the surface of GCLs with woven carrier geotextiles than on those with nonwoven carrier geotextiles. Further, greater amounts of dry migration were observed for GCLs with powdered bentonite (GCLs) *C*, *D*, *E* than for GCLs with granular bentonite (GCLs *A*, *B*, *F*, *H*, *G*).

The internal peak envelope for GCL *A*, as well as the interface peak envelopes for interfaces involving the textured HDPE GM *v* and the woven and nonwoven sides of GCL *A* (FE 11 and 52 in Table 3), are shown in Fig. 4(b). Consistent with the results shown in Fig. 4(a), the peak shear strength envelopes in Fig. 4(b) show a similar slope (i.e., similar friction angle). Although lower than the internal GCL shear strength, the nonwoven GCL-GM interface shear strength is slightly higher than that of the woven GCL-GM interface. The internal GCL large-displacement envelopes are similar in trend and magnitude to the woven and nonwoven GCL-GM interface large-displacement envelopes (see FE 11 and 52 in Table 3).

## Effect of Conditioning on Interface Shear Strength

Conditioning of GCL specimens involves hydration of the bentonite component, which usually has an initial gravimetric water content of approximately 10%. Hydration of the bentonite leads to an increase in volume (swelling) that depends on the applied normal stress. As hydration of the GCL in the field occasionally occurs under normal stresses below the final expected values, specimen conditioning also includes subsequent consolidation under the normal stress to be used during shearing. Results from GCL internal and GCL-GM interface direct shear tests using dif-

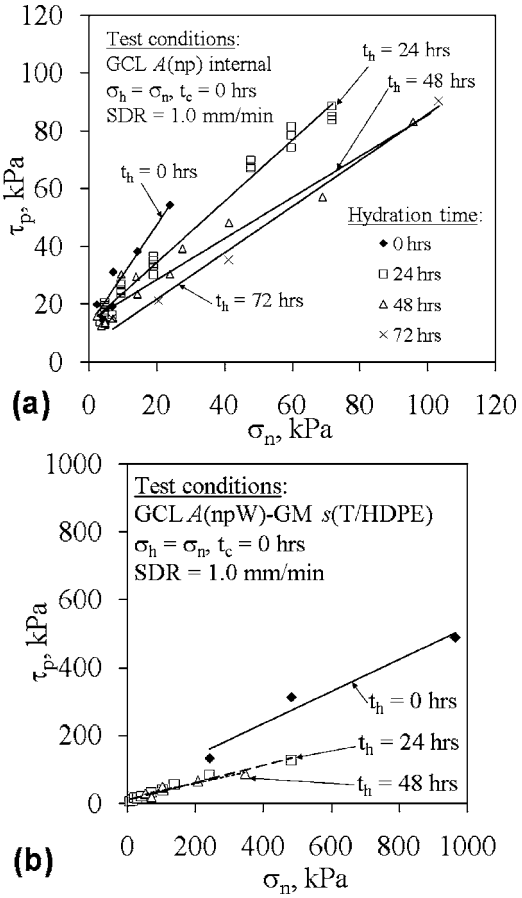


**Fig. 5.** Effect of hydration under $\sigma_h=\sigma_n$ on: (a) internal GCL peak shear strength; (b) woven GCL-GM interface peak shear strength

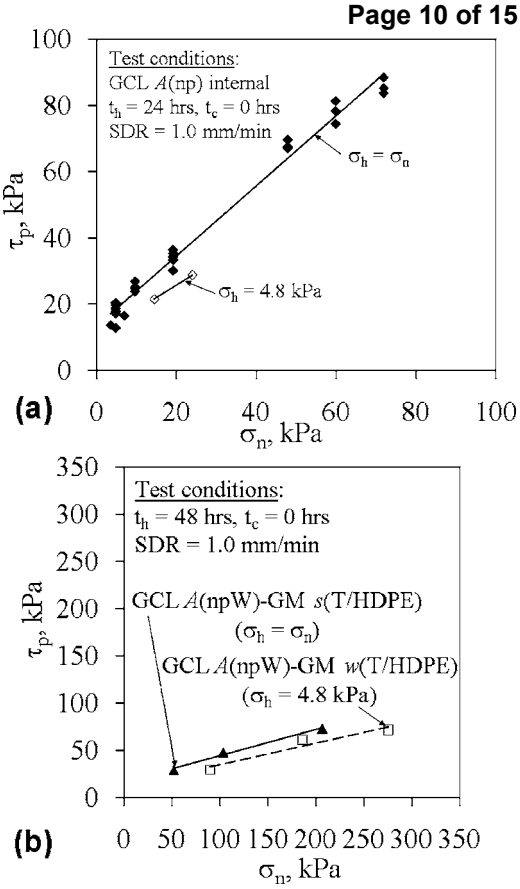


**Fig. 6.** Effect of hydration under $\sigma_h<\sigma_n$ with $t_c=0$ hrs on: (a) internal GCL peak shear strength; (b) woven GCL-GM interface peak shear strength

ferent conditioning procedures were used to evaluate the effects of hydration and consolidation on the GCL internal and GCL-GM interface peak shear strength. This evaluation extends the discussion of McCartney et al. (2004a), although the trends in the datasets have been reinterpreted. The effect of conditioning on large-displacement shear strength (from GCL internal and GCL-GM interface tests) was also investigated. However, large-displacement envelopes were found to be insensitive to conditioning procedures, so they are not discussed in this section.

The effect of $t_h$ on the peak internal shear strength of GCL *A* (needle punched) tested using $\sigma_n$ ranging from 2.4 to 100 kPa is shown in Fig. 5(a). The specimens were conditioned using the same normal stress during hydration and shearing (i.e., $\sigma_h=\sigma_n$). The results show a decreasing $\tau_p$ with increasing $t_h$. However, no further changes in $\tau_p$ are observed for $t_h$ beyond 48 hrs. The results in Fig. 5(b) for woven GCL-GM interfaces (needle-punched GCL *A* and a textured HDPE geomembrane *s*) indicate that hydration time has a similar effect on the GCL-GM interface $\tau_p$ as on the GCL internal $\tau_p$. While the range of $\sigma_n$ used for the interface envelopes is different, the interfaces with no hydration show a higher $\tau_p$ than the other interfaces. The interfaces with times of hydration of 24 and 48 hrs show essentially the same $\tau_p$ envelopes. The results in Fig. 5(b) indicate that, while interfaces will continue to hydrate beyond $t_h$=24 hrs, little further decrease in shear strength is expected to occur. A similar effect of $t_h$ was noted for nonwoven GCL-GM interfaces (see FE 46, 47, 50).

The effect of $\sigma_h$ on the peak shear strength of GCL *A* specimens hydrated during 24 hrs then sheared internally is shown in Fig. 6(a). The normal stress used for first failure envelope during hydration was $\sigma_h=\sigma_n$, while a constant, relatively low $\sigma_h$ (4.8 kPa) was used in the other failure envelope. The normal stress in the latter failure envelope was increased from $\sigma_h$ to $\sigma_n$ without allowing consolidation of the bentonite before shearing ($t_c$=0 hrs). Despite some scatter in the data, the $\tau_p$ obtained when $\sigma_h=\sigma_n$ is consistently higher than that obtained when hydration is conducted using a relatively low $\sigma_h$. The effect of $\sigma_h$ on the peak shear strength of woven GCL *A*-GM *s* interfaces hydrated during 48 hrs is shown in Fig. 6(b). The normal stress used for first failure envelope during hydration was $\sigma_h=\sigma_n$, while a constant, relatively low $\sigma_h$ (4.8 kPa) was used in the other failure envelope. Similar to the GCL internal results, the $\tau_p$ obtained for the GCLs hydrated under $\sigma_h=\sigma_n$ is consistently higher than that obtained for the GCL-GM interfaces hydrated under a relatively low $\sigma_h$. Nonwoven GCL-GM interfaces were not sensitive to the hydration normal stress (see FE 47 and 48).

When GCLs are hydrated under a $\sigma_h$ that is below $\sigma_n$, testing procedures often specify that the GCL be subsequently consolidated under the normal stress to be used during shearing. The effect of $\sigma_h$ on $\tau_p$ and $\tau_{ld}$ for needle-punched GCL *A* specimens hydrated during 60 and 24 hrs then sheared internally is shown in Fig. 7(a). This figure includes data for GCL that were hydrated under $\sigma_h=\sigma_n$ (not consolidated) and subsequently sheared, and GCLs for which a constant, relatively low $\sigma_h$ (6.9 kPa) was used. For the GCLs in which $\sigma_h<\sigma_n$, the normal stress was increased after hydration from $\sigma_h$ to $\sigma_n$ and 24 hrs was permitted for consolidation before shearing. While McCartney et al. (2004a) re-

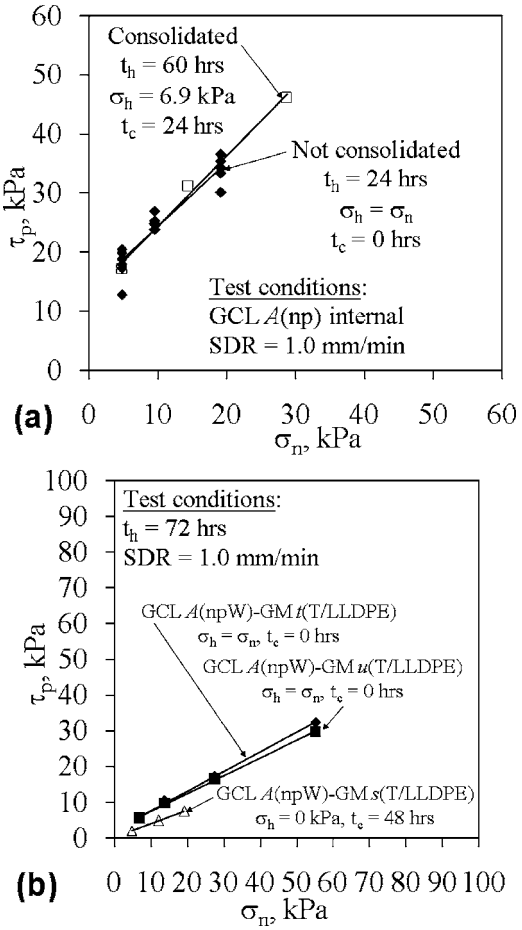


**Fig. 7.** Effect of consolidation when $\sigma_h < \sigma_n$ with $t_c > 0$ hrs on: (a) internal GCL peak shear strength; (b) woven GCL-GM interface peak shear strength

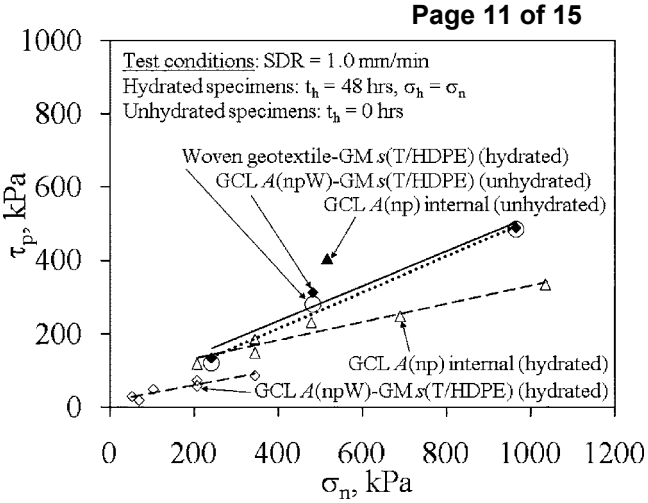


**Fig. 8.** Comparison of peak shear strength values from wetted geotextile-textured GM interface shear tests with those from GCL internal and GCL-textured GM interface shear tests using hydrated and unhydrated GCLs

ported that consolidation of GCLs led to a lower shear strength than specimens hydrated under $\sigma_h = \sigma_n$, reinterpretation of the data as shown in Fig. 7(a) indicates that the $\tau_p$ envelope obtained using $\sigma_h = \sigma_n$ is essentially the same as that obtained when the specimen is consolidated under $\sigma_n$ after hydration using a relatively low $\sigma_h$. This observation contradicts results presented by other studies (Eid and Stark 1997; McCartney et al. 2004a). The effect of $\sigma_h$ on the peak shear strength of the interface between the woven carrier geotextile side of GCL *A* and textured HDPE GMs is shown in Fig. 7(b). This figure includes results from tests on GCL-GM interfaces that were hydrated for 72 hrs under $\sigma_h = \sigma_n$ (not consolidated), and from tests on GCL-GM interfaces that were hydrated for 72 hrs under $\sigma_h = 0$ and consolidated under $\sigma_n$ for 48 hrs. The shear strength of the GCL-GM interfaces that were hydrated using $\sigma_h < \sigma_n$ have lower shear strength after consolidation. This is inconsistent with the observations from GCL internal test results shown in Fig. 7(a). This investigation was also performed for nonwoven GCL-GM interfaces. While it appears that similar observations can be made from GCL-GM interfaces (see FE 47 and 52), the database did not include sufficient tests to evaluate the sensitivity of the peak shear strength of nonwoven GCL-GM interfaces to consolidation.

To better understand the role of GCLs in GCL-GM interface shear strength, the peak shear strength values obtained from GCL internal and GCL-GM interface shear tests with different hydration conditions are shown in Fig. 8, along with those from woven geotextile-GM interface shear tests. The interface tests include the same textured HDPE GM *s* and GCL *A*, and were sheared under both unhydrated and hydrated conditions. As expected, the highest $\tau_p$ was obtained for the unhydrated GCL sheared internally, due to the fiber reinforcements. The $\tau_p$ values from the wetted geotextile-GM interface and the unhydrated GCL-GM interfaces were slightly lower than the unhydrated GCL sheared internally, but were very similar. The $\tau_p$ values from the hydrated GCL sheared internally were found to not only be lower than that for the unhydrated GCL sheared internally, but also lower than those for the unhydrated GCL-GM interface. The lowest $\tau_p$ values were obtained for the hydrated GCL-GM interface. If the GCL did not play a role in the GCL-GM interface shear strength, the $\tau_p$ for the hydrated GCL-GM interface and the wetted geotextile-GM interface should have been similar. As this is not the case, it may be concluded that extrusion of bentonite from the GCL affected the shear behavior of the woven carrier geotextile side of the GCL-GM interface.

The observations from Fig. 8 allow interpretation of the similarity between the trends in GCL internal and GCL-GM interface shear strength with hydration (Figs. 5 and 6), and the lack of similarity between the trends in GCL internal and GCL-GM interface shear strength with consolidation (Fig. 7). The decrease in GCL-GM interface shear strength with $t_h$ and $\sigma_h$ observed in Figs. 5(a) and 6(b) occur because of extrusion of sodium bentonite from the GCL during hydration. Extruded bentonite: (i) lubricates connections between needle-punched fibers and the GM asperities; and (ii) acts as a plane of weakness with shear strength less than that of an internally reinforced GCL and a GM-geotextile interface (Gilbert et al. 1997; Triplett and Fox 2001). Further, subsequent consolidation of the GCL-GM interface was found from analysis of the data in Fig. 7(b) not to result in an increase in shear strength due to the weakening of the GCL-GM interface with bentonite extruded from the GCL during hydration and consolidation. If $\sigma_h$ is below the swelling pressure of the bentonite (100 to 200 kPa), bentonite extrusion is expected to occur during hydration. If higher $\sigma_h$ is used, extrusion is less likely. The volume of extruded bentonite is expected to increase with hydration time and probably also depends on the normal stress used during hydration ($\sigma_h$). Further, if a GCL-GM interface is consolidated

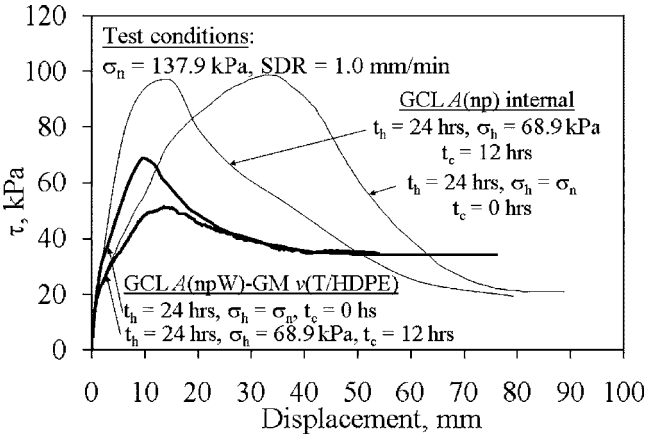


**Fig. 9.** Comparison between GCL-GM interface shear stress-displacement curves for different conditioning procedures

after having been hydrated under a low $\sigma_h$, additional extrusion is expected during consolidation due to the high hydraulic gradients caused by the increase in load.

A comparison between GCL internal and woven GCL-textured GM interface shear stress-displacement curves is shown in Fig. 9, for tests involving hydration under $\sigma_n$=68.9 kPa followed by consolidation for 12 hrs under $\sigma_n$=137.9 kPa before shearing. In addition, GCL internal and woven GCL-textured GM interface shear stress-displacement curves are presented for tests involving hydration and shearing under $\sigma_h$=$\sigma_n$=137.9 kPa. Consistent with the results observed in Fig. 1, the internal and interface curves have a similar initial response for comparatively small shear displacements. This suggests that shearing develops initially within the GCL but shearing subsequently develops along the GCL-GM interface. Further, the shear displacement curve for the unconsolidated GCL-GM interface matches the curve for the consolidated GCL-GM interface (as well as the GCL internal curve) at small displacements. However, the curve for the unconsolidated GCL-GM interface shows a steep increase to a peak value of 69 kPa while that for the consolidated GCL-GM interface shows a more gradual increase to a peak value of 51 kPa. The curves for both GCL-GM interfaces show similar shear stress at larger shear displacements (beyond 25 mm). The difference in shear displacement response with conditioning procedures suggests that more bentonite extrusion, and a corresponding decrease in shear stress, occurred along the consolidated GCL-GM interface before shearing. However, all of the interfaces had similar GCL-GM interface large-displacement shear strength likely equal to the shear strength of the extruded bentonite. Although not a general trend, the GCLs sheared internally show higher peak shear strength (99 kPa) yet their large-displacement shear strength (20 kPa) is lower than that of the GCL-GM interfaces (34 kPa).

## Variability

An evaluation of the variability in GCL internal shear strength is provided by Zornberg et al. (2005). The number of interface shear strength test results in the GCLSS database is large enough for assessment of GCL-GM interface shear strength variability. The different sources of interface shear strength variability can be quantified for use in reliability-based limit equilibrium analyses (McCartney et al. 2004a, b). Potential sources of variability in GCL-GM interface shear strength include: (i) differences in material types (GCL reinforcement, carrier geotextile type, GM polymer, GM surface texturing); (ii) variation in test results from the same laboratory (repeatability); and (iii) overall material variability. In turn, the overall material variability includes more specific sources such as: (iii-a) inherent variability of fiber reinforcement and their interaction on the GCL surface with GM textured asperities; and (iii-b) inherent variability in the volume of extruded bentonite. Source of variability (i) is not addressed in this study since only the variability of individual GCL-GM interfaces is evaluated. The potential sources of variabilities (ii) and (iii) are assessed in this study using data presented in Table 5. This table presents nine sets of tests conducted using the same GCL and GM types, conditioning procedures, and $\sigma_n$.

### Repeatability of Test Results Obtained from the Same Laboratory

The source of variability (ii) can be assessed by evaluating Sets V1, V2, and V3 in Table 5, which includes the results of tests conducted by a single laboratory using specimens collected from a single GCL and GM manufacturing lot, tested using the same conditioning procedures and same $\sigma_n$. For each set, Table 5 indicates the mean $\tau_p$ and $\tau_{ld}$ [$E(\tau_p)$ and $E(\tau_{ld})$], their standard deviations [$s(\tau_p)$ and $s(\tau_{ld})$], their COV values [$s(\tau)/E(\tau)$], and the maximum relative difference. Shear stress-displacement curves for woven GCL *A*-textured HDPE GM u interfaces are shown in Fig. 10 for interfaces with GM and GCL specimens from the same manufacturing lots, tested by the same laboratory, and using the same $\sigma_n$. These results illustrate that a very good repeatability can be achieved in the stress-displacement-strength response when tests are conducted by the same laboratory using same-lot specimens. The maximum relative difference in GCL-GM interface $\tau_p$ for specimens from the same manufacturing lots is less than 10%, which is well below the relative difference associated with different-lot specimens discussed next.

### Overall Material Variability

The source of variability (iii) may be assessed by evaluating Sets V4–V9 in Table 5. Unlike the results for Sets V1–V3 (Fig. 10), the GCL and GM specimens in Sets V4–V9 were obtained from different manufacturing lots. Each set of tests was conducted using the same GCL type, same GM (type, manufacturer, thickness), same conditioning procedures, and same $\sigma_n$. The maximum relative differences for Sets V4–V9 (approximately 50%) are significantly higher than those obtained for tests using GCL and GM specimens from rolls of the same lot (10%). Sets V4, V5, and V6 include data from 162 GCL-GM interface shear strength tests on GCL *A* and GM *s* conducted using the same conditioning procedures ($t_h$=168 hrs, $t_c$=48 hrs, SDR=0.1 mm/min) and three different normal stresses ($\sigma_n$=34.5, 137.9, 310.3 kPa). Subsets V4*a* to V4*e*, V5*a* to V5*e*, and V6*a* to V6*e* in Table 5 include the data from Sets V4, V5, and V6, respectively, grouped by the corresponding manufacturing year. Evaluation of statistical information on $\tau_p$ for V4–V6 shows an increasing $s(\tau_p)$ and a relatively constant COV with increasing $\sigma_n$, which indicates that $\tau_p$ variability increases linearly with $\sigma_n$. Fig. 11(a) shows the $\tau_p$ envelope obtained using the mean values of the 162 direct shear test results (Sets V4, V5, and V6 in Table 5). Significant scatter is noted in the results for tests conducted using the same GCL and GM types and conditioning procedures, but using specimens from different lots. The scatter likely arises due to differences in the surface roughness of the GCLs (reflected in variations in the

**Table 5.** GCL-GM Interface Data Sets for Assessment of Interface Shear Strength Variability

| | | GM | | Test conditions | | | | | | Peak strength[a] | | | | Large-displacement strength[a] | | | |
|---|---|---|---|---|---|---|---|---|---|---|---|---|---|---|---|---|---|
| GCL-GM data set | GCL descrip. | Description | Thickness (mils) | $t_h$ (hrs) | $t_c$ (hrs) | SDR (mm/min) | $\sigma_a$ (kPa) | Year GCL manufac. | Num. of tests | $E(\tau_p)$ (kPa) | $s(\tau_p)$ (kPa) | COV | Max. rel. diff. (%) | $E(\tau_{ld})$ (kPa) | $s(\tau_{ld})$ (kPa) | COV | Max. rel. diff. (%) |
| V1 | *A*(npW) | *u*(T/HPDE) | 60 | 24 | 0 | 0.2 | 9.6 | 1996 | 2 | 5.8 | 0.4 | N/A | 9 | 4.9 | 0.1 | N/A | 4 |
| V2 | *A*(npW) | *u*(T/HPDE) | 60 | 24 | 0 | 0.2 | 47.9 | 1996 | 2 | 18.1 | 0.4 | N/A | 3 | 12.9 | 0.0 | N/A | 0 |
| V3 | *A*(npW) | *u*(T/HPDE) | 60 | 24 | 0 | 0.2 | 95.8 | 1996 | 2 | 37.0 | 0.4 | N/A | 2 | 27.0 | 0.4 | N/A | 2 |
| V4 | *A*(npW) | *s*(T/HPDE) | 80 | 168 | 48 | 0.1 | 34.5 | 1997–2003 | 54 | 17.7 | 3.5 | 0.20 | 58 | 12.1 | 2.32 | 0.19 | 59 |
| V4a | *A*(npW) | *s*(T/HPDE) | *80* | *168* | *48* | *0.1* | *34.5* | *1997* | *3* | *20.5* | *3.2* | *0.16* | *23* | *13.1* | *1.38* | *0.11* | *19* |
| V4b | *A*(npW) | *s*(T/HPDE) | *80* | *168* | *48* | *0.1* | *34.5* | *1998* | *8* | *22.2* | *5.5* | *0.25* | *48* | *14.6* | *2.34* | *0.16* | *39* |
| V4c | *A*(npW) | *s*(T/HPDE) | *80* | *168* | *48* | *0.1* | *34.5* | *1999* | *9* | *18.1* | *1.8* | *0.10* | *28* | *11.9* | *1.61* | *0.14* | *30* |
| V4d | *A*(npW) | *s*(T/HPDE) | *80* | *168* | *48* | *0.1* | *34.5* | *2002* | *21* | *16.1* | *2.2* | *0.14* | *37* | *11.6* | *2.45* | *0.21* | *49* |
| V4e | *A*(npW) | *s*(T/HPDE) | *80* | *168* | *48* | *0.1* | *34.5* | *2003* | *13* | *16.8* | *2.1* | *0.13* | *33* | *11.5* | *1.82* | *0.16* | *38* |
| V5 | *A*(npW) | *s*(T/HPDE) | 80 | 168 | 48 | 0.1 | 137.9 | 1997–2003 | 54 | 59.7 | 8.9 | 0.15 | 50 | 37.9 | 5.30 | 0.14 | 47 |
| V5a | *A*(npW) | *s*(T/HPDE) | *80* | *168* | *48* | *0.1* | *137.9* | *1997* | *3* | *53.1* | *6.9* | *0.13* | *23* | *31.5* | *6.22* | *0.20* | *33* |
| V5b | *A*(npW) | *s*(T/HPDE) | *80* | *168* | *48* | *0.1* | *137.9* | *1998* | *8* | *65.9* | *14.6* | *0.22* | *45* | *36.9* | *7.00* | *0.19* | *40* |
| V5c | *A*(npW) | *s*(T/HPDE) | *80* | *168* | *48* | *0.1* | *137.9* | *1999* | *9* | *57.0* | *11.3* | *0.20* | *45* | *33.6* | *5.88* | *0.18* | *43* |
| V5d | *A*(npW) | *s*(T/HPDE) | *80* | *168* | *48* | *0.1* | *137.9* | *2002* | *21* | *61.5* | *5.0* | *0.08* | *31* | *40.9* | *3.20* | *0.08* | *25* |
| V5e | *A*(npW) | *s*(T/HPDE) | *80* | *168* | *48* | *0.1* | *137.9* | *2003* | *13* | *56.1* | *5.2* | *0.09* | *24* | *38.1* | *2.82* | *0.07* | *22* |
| V6 | *A*(npW) | *s*(T/HPDE) | 80 | 168 | 48 | 0.1 | 310.3 | 1997–2003 | 54 | 121.5 | 15.4 | 0.13 | 42 | 74.9 | 8.55 | 0.11 | 39 |
| V6a | *A*(npW) | *s*(T/HPDE) | *80* | *168* | *48* | *0.1* | *310.3* | *1997* | *3* | *117.2* | *15.5* | *0.13* | *23* | *61.6* | *2.22* | *0.04* | *6* |
| V6b | *A*(npW) | *s*(T/HPDE) | *80* | *168* | *48* | *0.1* | *310.3* | *1998* | *8* | *138.2* | *17.3* | *0.13* | *29* | *80.2* | *10.17* | *0.13* | *33* |
| V6c | *A*(npW) | *s*(T/HPDE) | *80* | *168* | *48* | *0.1* | *310.3* | *1999* | *9* | *114.3* | *18.6* | *0.16* | *36* | *71.2* | *6.88* | *0.10* | *28* |
| V6d | *A*(npW) | *s*(T/HPDE) | *80* | *168* | *48* | *0.1* | *310.3* | *2002* | *21* | *121.5* | *12.3* | *0.10* | *35* | *73.5* | *7.0S* | *0.10* | *31* |
| V6e | *A*(npW) | *s*(T/HPDE) | *80* | *168* | *48* | *0.1* | *310.3* | *2003* | *13* | *117.2* | *10.0* | *0.09* | *20* | *79.4* | *7.00* | *0.09* | *24* |
| V7 | *A*(npW) | *s*(T/HPDE) | 80 | 24 | 0 | 1.0 | 172.4 | 1999 | 7 | 73.5 | 8.1 | 0.11 | 27 | 43.8 | 7.9 | 0.18 | 40 |
| V8 | *A*(npW) | *s*(T/HPDE) | 80 | 24 | 0 | 1.0 | 344.7 | 1999 | 1 | 138.5 | 16.5 | 0.12 | 31 | 75.1 | 5.6 | 0.07 | 30 |
| V9 | *A*(npW) | *s*(T/HPDE) | 80 | 24 | 0 | 1.0 | 689.5 | 1999 | 7 | 264.6 | 31.8 | 0.12 | 34 | 139.9 | 6.8 | 0.05 | 31 |

[a] $E(\tau)$=mean of $\tau$, $s(\tau)$=standard deviation of COV=coefficient of variation of $\tau$, maximum relative difference=$|\max(\tau)-\min(\tau)|/\max(\tau)\times 100\%$.

needle-punching process), the surface roughness of the GMs (reflected in variations in the asperity height), and the amount of bentonite extrusion during hydration and consolidation. The scatter in this figure has important implications on the selection of shear strength parameters for use in the design of slopes. McCartney et al. (2004b) summarizes the implications of project-specific and product-specific testing on relationships between the factor of safety and the probability of failure for infinite slopes.

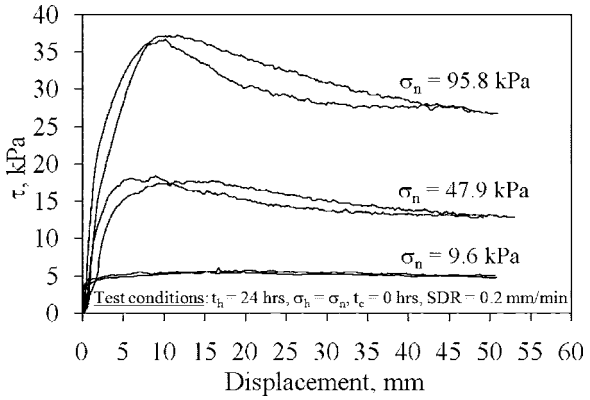


**Fig. 10.** Shear stress-displacement curves for GCL *A*(npW)-GM *u*(*T*/HDPE) interfaces with GCL and GM specimens obtained from the same manufacturing lots

Fig. 11(b) shows idealized normal probability density distributions for $\tau_p$ at each $\sigma_n$ obtained using the same mean and standard deviation as the shear strength data for Sets V4, V5, and V6 in Table 5. These probability distributions quantify the statistical information on $\tau_p$, which is useful for reliability-based design. Table 5 also includes statistical information regarding $\tau_{ld}$. Although $\tau_{ld}$ may not be fully representative of the residual shear strength, the high COV of $\tau_{ld}$ indicates that GCL-GM interface large-displacement shear strength cannot be treated as a deterministic value.

Although comparisons between GCL internal and GCL-GM interface direct shear test results made in this study indicate that the average peak GCL internal shear strength is higher than the average peak GCL-GM interface shear strength, this observation should not be generalized. The ranges of GCL internal shear strength reported by Zornberg et al. (2005) are shown in Fig. 11(a). These data show that although the maximum GCL internal shear strength is significantly higher than the maximum GCL-GM interface shear strength, the minimum GCL internal shear strength is approximately the same as the average GCL-GM interface shear strength. This may have wide reaching impacts on the design of slopes incorporating a GCL and a GM. Further, as illustrated by the shear stress-displacement curves shown in Fig. 1, the large-displacement GCL-GM interface shear strength is often similar to that of GCLs sheared internally.

The 162 GCL specimens in Sets V4–V6 were received between Jan. 1997 and May 2003. In each subset, the COV and

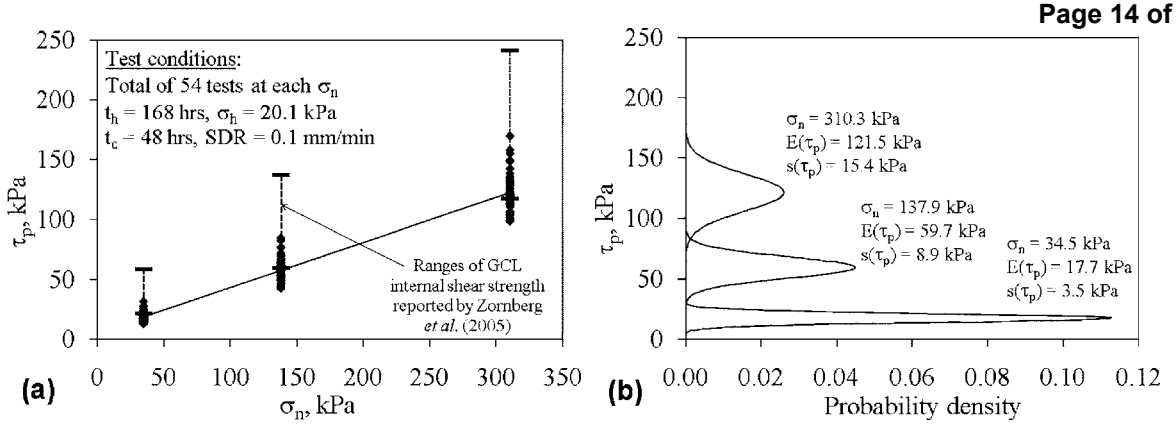


**Fig. 11.** Variability of the GCL *A*(npW)-GM *s*(*T*/HDPE) interface peak shear strength: (a) $\tau_p$ envelope; (b) normal probability distributions for $\tau_p$ at each $\sigma_n$

maximum relative difference is generally lower than for the overall multiyear data sets. The results in Table 5 indicate that the mean and the standard deviation values of the peak shear strength under the same normal stress are practically the same for the various GCL manufacturing years. The slight differences observed in variability from year to year are likely due to improvements in texturing of the GMs produced over time.

Sets V7–V9 in Table 5 include variability data from a set of 21 direct shear tests conducted using the same GCL tested in Sets V4, V5 and V6 (GCL *A*), but a different GM (GM *v*) and different conditioning procedures ($t_h$=24 hrs, $t_c$=0 hrs, SDR =1.0 mm/min). Three different $\sigma_n$ (172.4, 344.7, and 689.5 kPa) were used in this program. The different GM and conditioning procedures led to a maximum relative difference in $\tau_p$ of approximately 30%. This maximum relative difference is smaller than that obtained for Sets V4, V5, and V6 using different conditioning procedures (~30%), suggesting that conditioning procedures may have some effect on the variability of interface GCL-GM test results.

## Conclusions

A database of 534 GCL-GM interface shear strength tests was analyzed in this study. The data were obtained from large-scale (305 by 305 mm) direct shear tests conducted by a single laboratory over a period of 12 years using procedures consistent with current testing standards. Shear strength parameters were obtained to evaluate the effect of GCL and GM type, compare the shear strength of woven and nonwoven GCL interfaces, compare GCL internal and GCL-GM shear strength, evaluate the effect of GCL conditioning, and assess sources of GCL-GM interface shear strength variability. The following conclusions are drawn from this study:

1. The GCL-GM interface peak and large displacement shear strength values were found to be generally lower than the GCL internal peak and large-displacement shear strengths tested under normal stresses between 2.5 and 1,000 kPa, although both showed significant variability. However, comparison of the variability of GCL internal peak shear strength and the GCL-GM interface peak shear strength indicates that the GCL internal shear strength may potentially be lower than the GCL-GM interface shear strength if products from different manufacturing lots are used on a project. The large-displacement GCL-GM interface shear strength was often found to be similar to that of GCLs sheared internally.
2. Analysis of the GCL-GM interface shear strength data indicates that the peak shear strength of nonwoven GCL-textured GM interface is higher than that of woven GCL-textured GM interface (for normal stresses between 2.4 and 1,000 kPa), and higher than that of woven GCL-smooth GM interfaces and nonwoven GCL-smooth GM interfaces. GCL internal shear strength envelopes are higher than those for woven and nonwoven GCL-GM interfaces, but have a similar friction angle.
3. The woven and nonwoven GCL-textured HDPE GM interface shear strengths are sensitive to the GCL type. Specifically, the woven needle-punched GCL interfaces were found to have higher interface shear strength than woven thermal-locked and stitch-bonded GCL interfaces.
4. Textured GM interfaces showed large postpeak shear strength loss, while smooth GM interfaces experienced essentially no postpeak shear strength loss.
5. The woven and nonwoven GCL-textured GM interface shear strengths were found to be sensitive to the GM flexibility for the set of interfaces tested in this study under normal stresses less than 50 kPa. Specifically, flexible GMs (e.g., VLDPE GMs) were found to have higher interface shear strength than stiffer GMs (e.g., HDPE GMs). The GCL-textured GM interfaces shear strengths were found not to be sensitive to the GM manufacturer or GM thickness.
6. Unlike results for GCLs sheared internally, the peak shear strength envelopes for woven and nonwoven GCL-GM interfaces showed a comparatively small cohesion intercept and remained linear for a wide range of $\sigma_n$. Similar large-displacement shear strength envelopes were found for GCL internal and woven and nonwoven GCL-GM interfaces.
7. Hydration was found to lead to a decrease in both GCL internal peak shear strength and woven GCL-GM interface peak shear strength. Hydration using a normal stress less than that used during shearing without allowing time for subsequent consolidation was found to lead to further decrease in GCL internal and woven GCL-GM interface peak shear strength. Subsequent consolidation of GCLs hydrated under a normal stress less than that used during shearing was found to lead to an increase in GCL internal shear strength, but a decrease in woven GCL-GM interface shear strength. Hydration and consolidation had a negligible effect on the peak shear strength of nonwoven GCL-GM interfaces.
8. The inconsistencies in the trends in GCL internal and woven

GCL-GM interface shear strength with hydration and consolidation were proposed to be due to bentonite extrusion. Hydrated GCL-GM interfaces were found to have lower peak shear strength than wetted geotextile-GM interfaces, indicating that the bentonite extrusion from the GCL plays an important role in the GCL-GM interface shear behavior. Interfaces involving nonwoven GCLs were found to be less affected by bentonite extrusion than interfaces involving woven GCLs.

9. Good repeatability was obtained for duplicate tests on GCLs and GMs from the same manufacturing lots (maximum relative difference of 10%). However, significant variability was obtained for GCL-textured GM interface with materials from different lots (maximum relative difference of 50%). The variability of GCL-GM interface shear strength was less than that for GCL internal shear strength, and normal stress, interface conditioning, GM manufacturer were found to impact the peak shear strength variability.

## Acknowledgments

The writers thank SGI Testing Services and GeoSyntec Consultants for making available the experimental results analyzed in this study. Comments by John Allen during the review stage of the manuscript are much appreciated. The writers also would like to thank the reviewers of this paper for their many helpful suggestions. The views expressed in this paper are solely those of the writers.

## References

American Society of Testing and Materials. (2004). "Standard test method for determining average bonding peel strength between the top and bottom layers of needle-punched geosynthetic clay liners." *ASTM D6496*, West Conshohocken, Pa.

American Society of Testing and Materials. (2008). "Standard test method for determining the internal and interface shear resistance of geosynthetic clay liner by the direct shear method." *ASTM D6243*, West Conshohocken, Pa.

Chiu, P., and Fox, P. J. (2004). "Internal and interface shear strengths of unreinforced and needle-punched geosynthetic clay liners." *Geosynthet. Int.*, 11(3), 176–199.

Eid, H. T., and Stark, T. D. (1997). "Shear behavior of an unreinforced geosynthetic clay liner." *Geosynthet. Int.*, 4(6), 645–659.

Fox, P. J., and Stark, T. (2004). "State of the art report: GCL shear strength and its measurement." *Geosynthetics Int.*

Gilbert, R. B., Fernandez, F. F., and Horsfield, D. (1996). "Shear strength of a reinforced clay liner." *J. Geotech. Geoenviron. Eng.*, 122(4), 259–266.

Gilbert, R. B., Scranton, H. B., and Daniel, D. E. (1997). "Shear strength testing for geosynthetic clay liners." *Testing and acceptance criteria for geosynthetic clay liners*, L. Well, ed., American Society for Testing and Materials, Philadelphia, 121–138.

Hewitt, R. D., Soydemir, C., Stulgis, R. P., and Coombs, M. T. (1997). "Effect of normal stress during hydration and shear on the shear strength of GCL/textured geomembrane interfaces." *Testing and acceptance criteria for geosynthetic clay liners*, L. Well, ed., American Society for Testing and Materials, Philadelphia, 55–71.

Ivy, N. (2003). "Asperity height variability and effects." *GFR. Oct.*, 28–29.

Lake, C. G., and Rowe, R. K. (2000). "Swelling characteristics of needle-punched, thermal treated geosynthetic clay liners." *Geotext. Geomembr.*, 18, 77–101.

McCartney, J. S., Zornberg, J. G., and Swan, R. H., Jr. (2004a). "Effect of specimen conditioning on gcl shear strength." *Proc. Geoasia 2004: 3rd Asian Regional Conf. on Geosynthetics*, J. G. Shim, C. Yoo, and H.-Y. Jeon, eds., Korean Geosynthetics Society, Seoul, Korea, 631–643.

McCartney, J. S., Zornberg, J. G., and Swan, R. H., Jr. (2005). "Effect of geomembrane texturing on geosynthetic clay liner—Geomembrane interface shear strength." *Proc., GeoFrontiers 2005* (CD-ROM), ASCE.

McCartney, J. S., Zornberg, J. G., Swan, R. H., Jr., and Gilbert, R. B. (2004b). "Reliability-based stability analysis considering GCL shear strength variability." *Geosynthet. Int.*, 11(3), 212–232.

Triplett, E. J., and Fox, P. J. (2001). "Shear strength of HDPE geomembrane/geosynthetic clay liner interfaces." *J. Geotech. Geoenviron. Eng.*, 127(6), 543–552.

Zornberg, J. G., and McCartney, J. S., Swan, R. H. (2005). "Internal shear strength of geosynthetic clay liners." *J. Geotech. Geoenviron. Eng.*, 131(3), 1–14.

**SOAH DOCKET NO. 582-22-0844**
**TCEQ DOCKET NO: 2021-1000-MSW**

| | | |
|---|---|---|
| **IN THE MATTER OF THE APPLICATION BY DIAMOND BACK RECYCLING AND SANITARY LANDFILL, LP FOR NEW MSW PERMIT NO. 2404** | **§** | **BEFORE THE STATE OFFICE OF ADMINISTRATIVE HEARINGS** |

# EXHIBIT KNOX-118

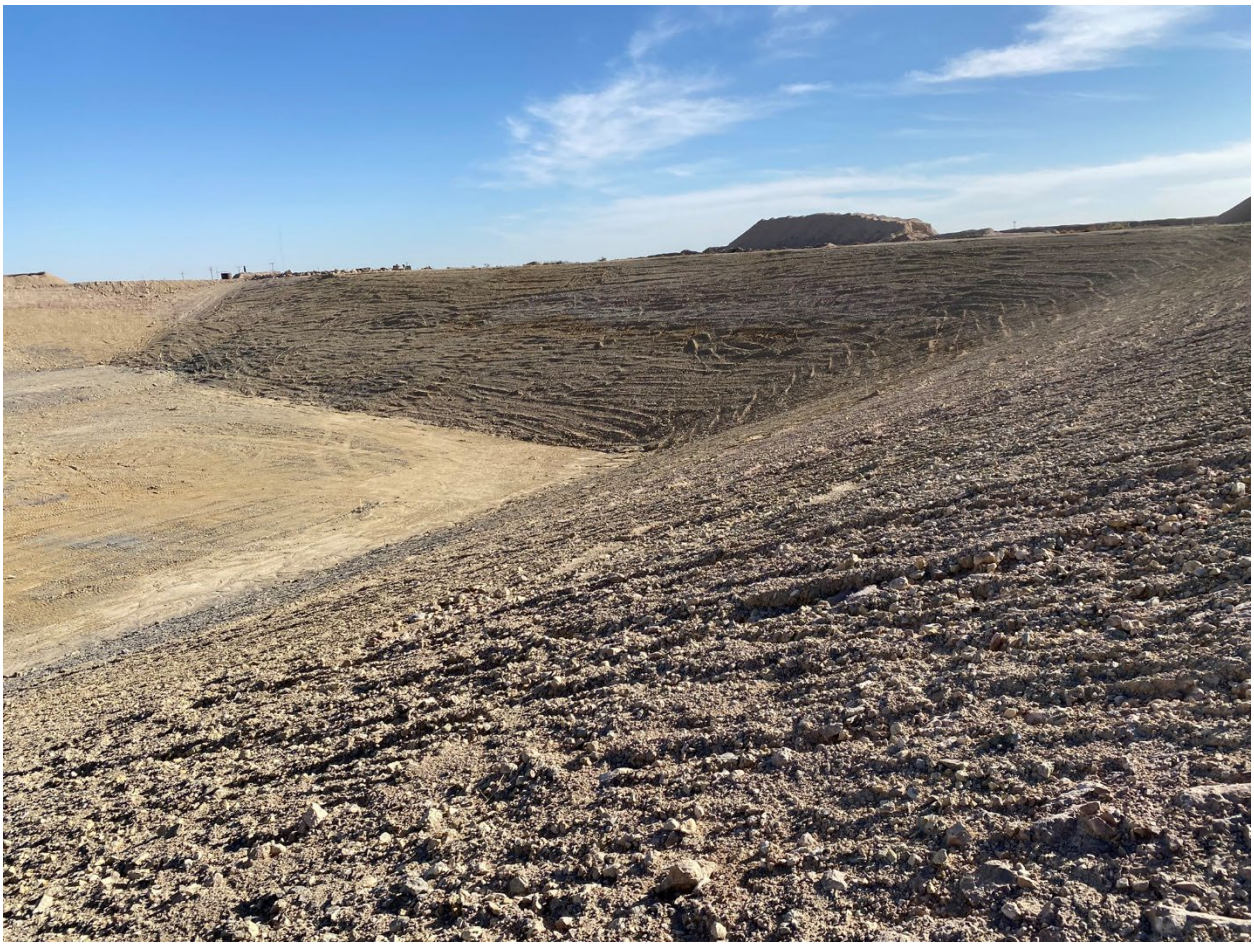

Photo 1 – IMG_3338

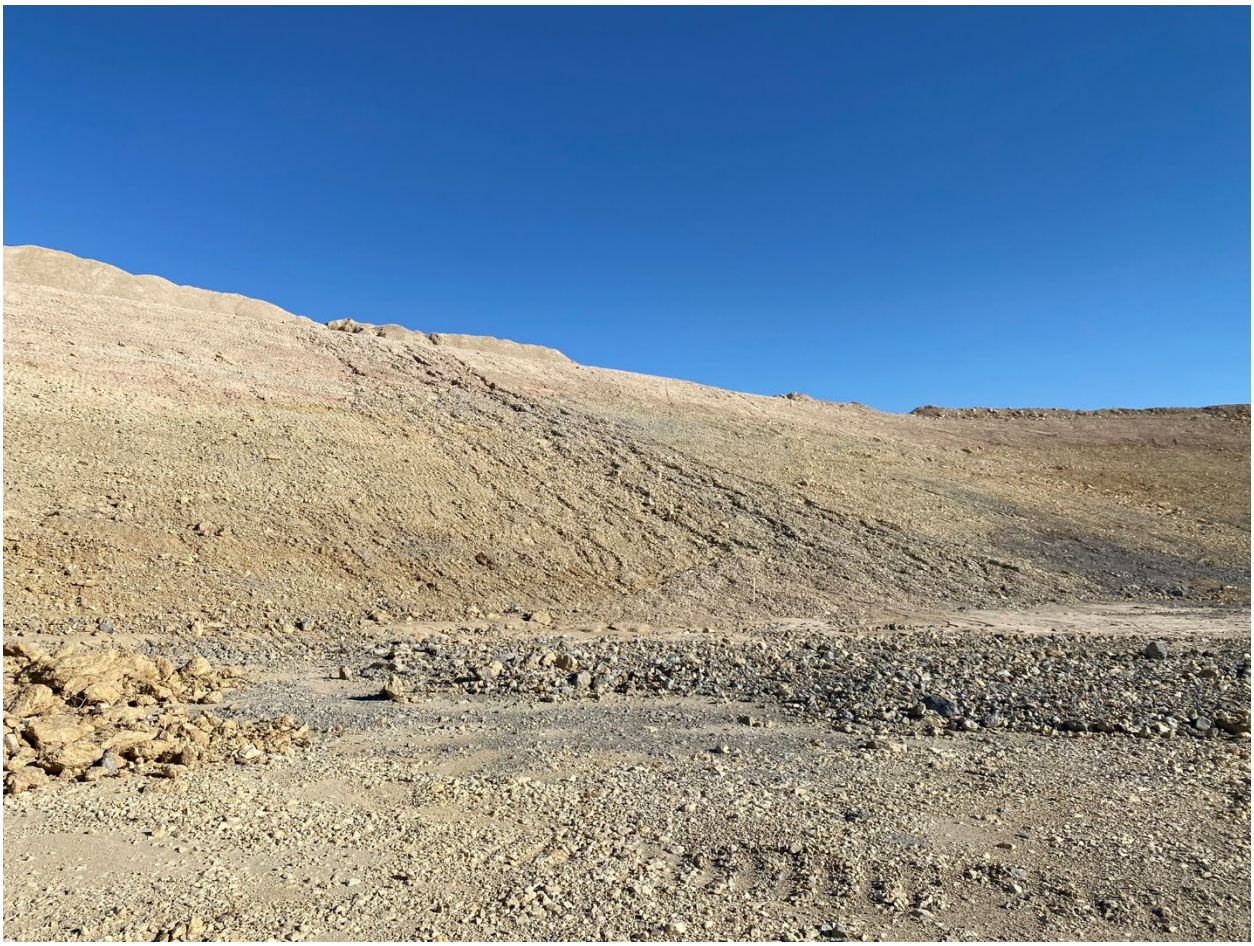

Photo 2 – IMG_3354

Photo 3 – IMG_3364

Photo 4 – IMG_3345

Photo 5 – IMG_3356

Photo 6 – IMG_3377

Photo 7 – IMG_3339

Photo 8 – IMG_3334

**SOAH DOCKET NO. 582-22-0844**
**TCEQ DOCKET NO: 2021-1000-MSW**

| | | |
|---|---|---|
| **IN THE MATTER OF THE APPLICATION BY DIAMOND BACK RECYCLING AND SANITARY LANDFILL, LP FOR NEW MSW PERMIT NO. 2404** | **§** | **BEFORE THE STATE OFFICE OF ADMINISTRATIVE HEARINGS** |

# EXHIBIT KNOX-119

Photo 1 - IMG_3314

Photo 2 - IMG_3315